TECHNISCHE UNIVERSITÄT WIEN

VIENNA UNIVERSITY OF TECHNOLOGY

DIPLOMARBEIT

In-Vivo-Writing

Using Two-Photon-Lithography

ausgeführt zum Zwecke der Erlangung des akademischen Grades eines

Diplom-Ingenieurs unter der Leitung von

Ao.Univ.-Prof. Dr. Jürgen STAMPFL

Institut für Werkstoffwissenschaften und Werkstofftechnologie

Bereich Nichtmetallische Werkstoffe

eingereicht an der Technischen Universität Wien

Fakultät für Maschinenwesen und Betriebswissenschaften

von

Jan Torgersen

0425694 (E740)

Meiselstrasse 8/2/16

1150 Wien

Wien, im März 2010

_____

Jan Torgersen

Abstract

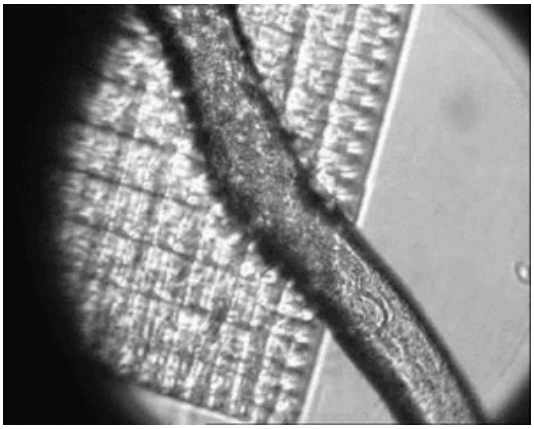

Two-Photon-Lithography is a fast developing application used for the micro- and nanostructuring of three-dimensional parts. The manufacturing of biocompatible structures using this technique is a promising field as it fulfils the demand for high resolution parts. This paper describes the fabrication of scaffolds inside photopolymer based resins with embedded living organisms (Caenorhabditis elegans). The structuring was performed with a pulsed near-infrared laser with a wavelength of 810nm and adjustable power up to 160mW. The intensities applied do not cause damage at the cellular level for the model organism since biological tissue is very transparent to red and infrared light. Since environmental stress is of chemical origin only, the limiting factor is the toxicity of the resin, so the polymerisation time had to be kept short. Using a Carl Zeiss objective with a 20 times magnification and a numerical aperture of 0.4, a high resolution scaffold with a base area of 300x300µm and a height of 80µm could be fabricated (see figure). As considerably high laser intensities were possible, a writing speed set to 250µm/s permitted a short structuring process of 12 minutes, which the animal survived in the resin. As toxicity increases with the reactivity of the resin there is a trade-off between the two parameters in the *in vivo* writing process. To advance this method, water-based resins have to be developed. This work holds out the prospect of structuring high-resolution scaffolds inside living organisms.

Kurzfassung

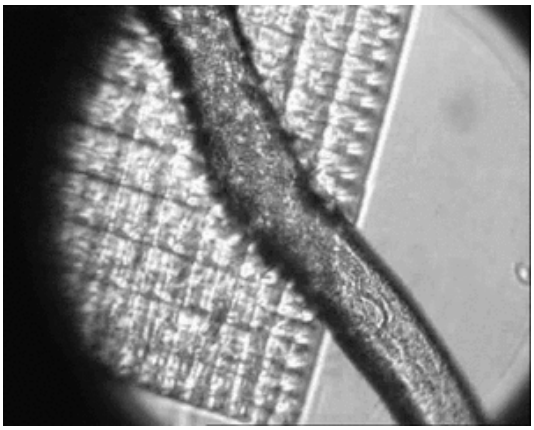

Zwei-Photonen-Lithographie ist eine Methode zur Herstellung von Strukturen mit Abmessungen im Nano- und Mikrometerbereich, die sich in den letzten Jahren wachsender Beliebtheit erfreut. Für die Erzeugung von biokompatiblen Strukturen scheint sich dieses neue additive Fertigungsverfahren besonders gut zu eignen, da die hergestellten Teile dem Anspruch höchster Fertigungsgenauigkeit entsprechen. Diese Arbeit beschreibt eine Methode zur Herstellung von einfachen Strukturen innerhalb von fotosensitiven Harzen, in denen lebende Organismen eingeschlossen wurden (Rundwurm Caenorhabditis elegans). Der Bauprozess wurde mit einem gepulsten Laser mit einer Lichtwellenlänge im nahen Infrarotbereich (810nm) bewerkstelligt. Die Leistung konnte eingestellt werden und betrug maximal 160mW. Da biologisches Gewebe transparent für rotes und infrarotes Licht ist, verursachten die Laserintensitäten in den Experimenten dieser Arbeit keinen zellulären Schaden am Modellorganismus. Schädliche Umwelteinflüsse waren chemischer Art und durch die Reaktivität des Harzes bedingt. Die Polymerisationszeit musste daher kurz gehalten werden. Mit einem Carl Zeiss Objektiv mit einer 20 fachen Vergrößerung und einer numerischen Apertur von 0.4 wurde ein Würfel mit einer quadratischen Grundfläche von 300x300 µm und einer Höhe von 80 µm hergestellt (siehe Bild). Da relativ hohe Laserintensitäten verwendet werden konnten, wurde die Schreibgeschwindigkeit auf 250 µm/s eingestellt. Eine Herstellungszeit von 12 Minuten war dadurch möglich. Wie die Ergebnisse dieser Arbeit zeigen, überlebte das Versuchstier den Strukturierungsprozess. Da jedoch die Toxizität des Harzes mit der Reaktivität steigt, gibt es immer einen Zielkonflikt zwischen diesen beiden Parametern. Um diese Methode zu verbessern und in Zukunft für Applikationen innerhalb von Organismen anzuwenden, bedarf es wasserbasierter Harze. Aufbauend auf dieser Arbeit kann langfristig eine Möglichkeit zur Strukturierung hochauflösender Bauteile innerhalb lebender Organismen entwickelt werden.

Table of Contents

1. Acknowledgement

This work arose from an idea of ao. Prof. DI Dr. Jürgen Stampfl. In the first place I have to thank him for his great support in every respect. No matter whether I needed financial aid for the realization of an experiment, whether I suffered from a lack of technical knowledge or I needed personal advice, Prof. Stampfl always had a sympathetic ear each and every time I confronted him with my matters.

Secondly, I have to thank my adviser, Dipl.-Ing. Klaus Stadlmann. He was really patient with my initial disability to handle the 2PP setup M3DL. He certainly had a lot of extra work, instructing and tutoring his "thesis student". Most of the findings of this work were achieved as the both of us worked together and brought our knowledge to a collective consensus. I have profited from him a lot and I hope this is based on mutuality, at least to a small extend. I hope we can stay in contact throughout the future.

Thirdly, I have to express my admiration to Dipl.-Ing. Klaus Cicha. He was the third student to work with the 2PP setup M3DL. We, too, spend a lot of time together working with the –sometimes very wilful- machine. I really enjoyed the fruitful and humorous discussions with him.

Fourthly, I have to particularly express my thanks to all employees of the department of Chromosome biology from the Vienna Biocenter under the leadership of Mag[a]. Verena Jantsch-Plunger PhD. Especially Antoine Baudrimont (Ma) supported me very much. He showed real interest for my affairs and told me how to perform biological experiments, where I might get information about C. elegans and which chemical substances I could use without harming the model organism. He provided me in excess of 400 specimens of C. elegans, a variety of agar plates in different sizes, M9 buffer, tools to handle the worms and many other things I would never had access to. Moreover, he gave me the possibility to perform the toxicity tests described in this work at his personal working area in the Vienna Biocenter. All this is, of course, not self-evident. I really owe Antoine Baudrimont a lot and I hope we can stay in contact.

Fifthly, I expressively like to thank Dipl.-Ing. Christian Heller and Dipl.-Ing. Niklas Pucher as well as ao. Univ. Prof. Dipl.-Ing. Dr. Robert Liska for their great support. All chemical compounds and resins were provided by them. Without the resins and the development methods evolved at the institute of Synthetic Chemistry I would have had no chance to gain any findings. I really enjoyed the little insight into synthetic chemistry the above mentioned people provided to me.

I also have to thank the whole staff of the Institute of Material Science. I have never worked in such a friendly and personal surrounding. The atmosphere provided an ideal balance of comfort, on the one hand, and focused work, on the other. Moreover, all people of the institute took their time whenever I needed help.

This, in particular, is of fundamental importance in scientific work, at least to my point of view.

Last, I have to thank my family and my friends for their patience and their support. Especially my father, Dr. Helge Torgersen, helped me a lot during the work on my thesis. Furthermore, he introduced me to Mag. Verena Jantsch-Plunger, he gave me biological insight and got me in touch with colleagues of the Institute of Technology Assessment of the Austrian Academy of Sciences. My biological understanding brought into this work derived more or less from the explanation provided by him and his colleagues at the beginning of my thesis.

The quite elaborate acknowledgement illustrates that this work originated from the cooperation of many people from very different fields. Thus I hesitate to attribute the findings reported in this thesis solely to myself. The reader will notice that wherever the active mode is used in describing experiments this is done using the plural form, indicating the involvement of our entire research group. I hope this shows my appreciation for all my supporters in an appropriate way.

2. Polymerisation

Polymerisation is a chemical process in which monomer-molecules convert into a polymer, a new composition with a molecular mass that is an integral multiple of that of the monomer (Wissenmedia GesmbH, 2000-2009). Polymerisates, the products of this process can be classified into homo-polymers and co-polymers. The first group consists of one type of monomer only, whereas the other's structure integrates two or more types of basic molecules that can vary in their complexity.

Polymerisation always proceeds following the same order. Under the influence of a catalyst the monomer molecules break up their multiple bonds and connect to each other via these freed bonds. The type of chain growth can be classified into step-wise and chain-wise growth. In the first case, already existing chain segments can grow together whereas in the second case, only the reactive end of the polymer molecule reacts with a further monomer. Another classification distinguishes *Polyaddition:* from *Polycondensation. Polyaddition* is often used synonymously to polymers built up step-wise, whereas *polycondenstation* describes the type of macromolecules derived from a chain-wise reaction type. Yet this is not always the case, so one should be cautious using these terms as synonyms (Odian, 2004).

2.1. The process of radical polymerisation

This work is primarily concerned with the radical type of polymerisation as two-photon-lithography uses this process to structure three dimensional objects. For the better understanding of the investigations presented in the following chapters, an explanation of the basics of radical polymerisation is given below.

The radical polymerisation is a member of the chain-growth type of polymerisation. This reaction type uses the so called Ziegler-Natta-Catalysts, which are metal-organic mixed catalysts, consisting of metal-organic and transition metal compositions (e.g.: Triethylaluminium and Titantetrachlorid). The process of radical polymerisation can be divided into 3 major steps (Matyjaszewski & Davis, 2002).

1. Initiation: Production of radicals
2. Propagation: Radicals react to give a radical product
3. Termination: Radicals are lost

2.1.1. Initiation

A radical breaks the double-bond of a monomer molecule and creates a primary radical which is capable of growth. This radical is called the initiator. The formation of an initiator radical is mostly affected by *Homolytic cleavage*. The most important factor for the formation is the stability of the radicals and the energy used for dissociation. Methods to initiate the reaction can be divided into thermolysis, electron transfer and photolysis (Matyjaszewski & Davis, 2002). Thermolysis reactions require an initiator with a weak bond, especially an *azo* or *peroxy* compound. Electron transfer reactions are involved in many reactions of metals with organic substrates, where it is necessary to reduce radicals to anions or organo-metallic species. This method is used with insufficiently strong reducing agents only as they can take over the same function to a certain extend (Matyjaszewski & Davis, 2002). Photolysis is of special interest in this work as we will deal with photosensitive initiators, reacting to the exposure of near-infrared light. Matyjaszewski and Davis (2002) distinguished photo-chemical initiation from photoinduced electron transfer.

2.1.1.1. Thermolysis

This initiation method is favoured by the existence of a reactive state or the *Homolytic cleavage* of a weak bond. The process may be best explained by the example of polyethene. The ethene monomers of excitation energy will already dissociate benzoylperoxide into radicals. Benzoylperoxide already dissociates into radicals at slight energy expenditures, for example with an increase in temperature[1].

Figure 1 shows the structural formula of the molecule before and after its dissociation into radicals (University of Berlin, 2001).

Breaking up a weak bond of benzoylperoxide (homolytic cleavage)

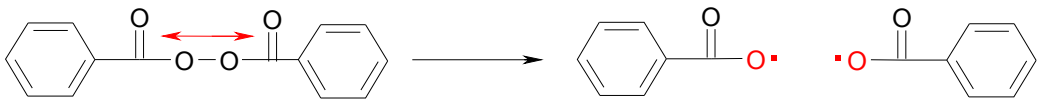

Figure 1: Step 1 of Initiation

In a further reaction, carbon dioxide is separated from the molecules resulting from step 1. The final result of the dissociation is a phenyl radical (Figure 2).

[1] The type of radical dissociation is dependent on the medium in which the substance is dissolved. In our case, benzoylperoxide is surrounded by an inert medium. That's why the initiation occurs with the dissociation of carbon dioxide. With styrol, for example, the reaction products are solely benzoyl radicals and no carbon dioxide is shed off (Hahn & Taton, 2006).

Dissociation of carbondioxide and phenylradicals

Figure 2: Step 2 of Initiation

The resulting radicals react with electrons from ethene C=C double bonds and create a bond with the monomer. Another unpaired electron remains, which becomes the connector for further monomers. In our example, the phenyl radicals originating from Step 2 react with ethene (Figure 3).

Reaction of a Phenylradical with Ethen

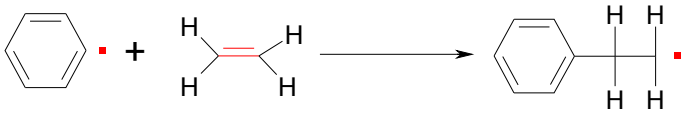

Figure 3: Step 3 of initiation in radical polymerisation

Phenyl radical induced polymerisation is one of the most common types of radical polymerisation. As the dissociation is dependent on the operating temperature, the initiators are selected by the temperature of 10 hours half-value period (T_{10h}) (Gruber, 2008).

2.1.1.2. Electron transfer

Initiator molecules reach an excited energy level that renders them either strongly oxidant or reductant. They react with other molecules (Matyjaszewski & Davis, 2002). In other words, the activation energy of the dissociation of the initiator is decreased by a redox reaction. Polymerisation can occur at low temperatures (from 0°C). The most important initiator in this field is azobisisobutyronitrile (AIBN) (Gruber, 2008). It is used to polymerize vinyl monomers and has a convenient polymerisation temperature between 60 and 70°C. Figure 4 shows the dissociation of AIBN into the isobutyronitrile radicals as well as nitrogen gas (Burke, 2008).

Dissociation of AIBN

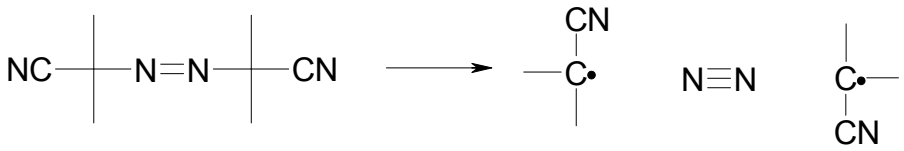

Figure 4: Initiation via electron transfer by the example of AIBN

2.1.2. Propagation

The chain-growth process requires lower activation energy. New monomers are attached constantly. As seen in Figure 3, one radical remains during the initiation, which now acts as an anchor point for further monomers. In this example, additional ethene molecules connect to the reactive end of the chain (Figure 5).

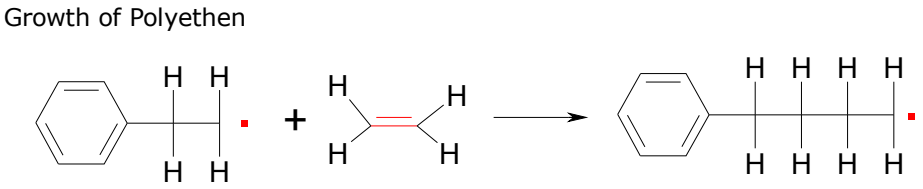

Figure 5: Propagation of radical polymerisation

As long as reactive elements are available, this chain will grow endlessly long. The reaction can only be terminated by a chain termination reaction.

2.1.3. Termination

Either recombination[2] or *Disproportionation* can terminate up the polymerisation process. In recombination, the unpaired electrons bond together and build up an electron pair. One non-reactive molecule emerges out of two reactive ones (Figure 6).

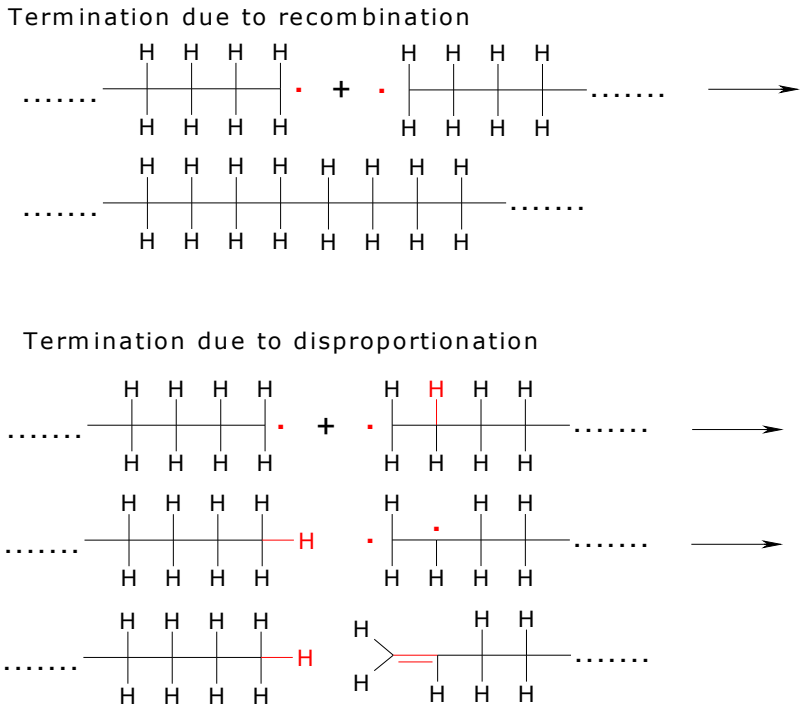

Figure 6: Recombination and disproportionation

[2] The coincidence of two radicals

Instead of the unpaired electron, the radical can also attach to a single C-H bond from another molecule. This is called *disproportionation*. As this reaction renders another reactive electron in the reaction partner, the partner itself can now bond its two unpaired electrons together to form a non-reactive C-H group. The radical usually reacts with the hydrogen and its additional electron from the carbon atom nearest to the C-H bond on the reactive end. This can be seen in Figure 6. In the example given above, an alkane and an alkene result, without reactive ends both. Chain growth is terminated.

Chain termination might also occur accidentally due to random incidentally existent inhibitors such as aerial oxygen (Gruber, 2008). If this is the case, the chain will integrate peroxide groups (Figure 7).

Unwanted chain termination due to the inhibation of aerial oxygen

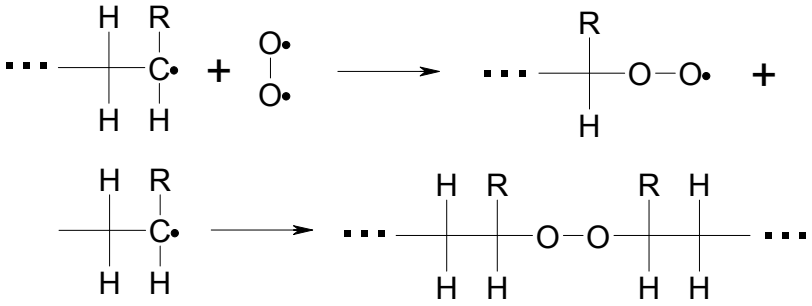

Figure 7: Unwanted chain termination

To store monomers it is sometimes useful to add inhibitors like hydrochinon to the resin in order to prevent untimely polymerisation. To stop the effect it is possible to either increase the concentration of initiator or to clean the resin (hydrochinon can be washed out with an aqueous alkaline solution) (Gruber, 2008).

2.1.4. Chain transfer

The process of chain transfer is very similar to that of chain termination due to *disproportionation*. The unpaired electron is transferred to a reaction partner. The resulting molecule can now start to grow a chain. Chain transfer with polyethylene processes as a radical attaches to a random C-H bond in the middle of the reaction partner's chain rather than with the adjacent C-H group of the reactive end, similar to a chain termination process. This leaves a carbon atom with an unpaired electron, which cannot connect to that of the reactive end. This process can be seen in Figure 8.

Formation of a radical with an unpaired electron in the middle of the molecular chain

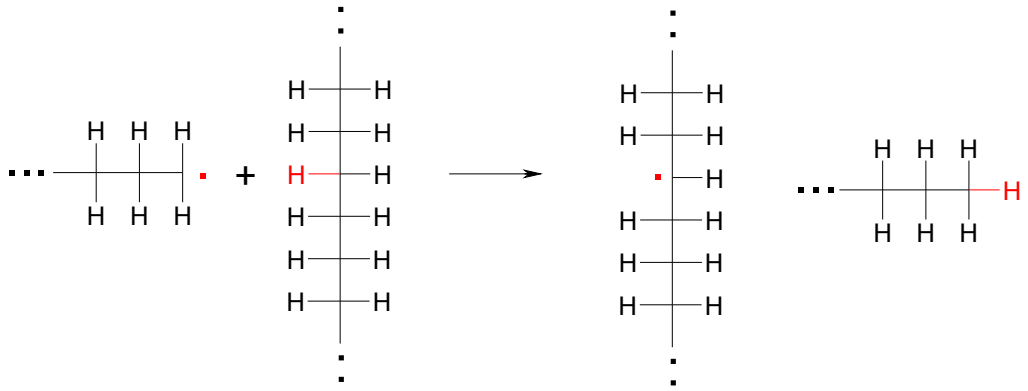

Figure 8: Formation of a radical in the middle of a polyethene-chain

Another molecule can now add onto the new radical end. A new chain starts to grow from the middle of the old one (Figure 9).

Branching the chain

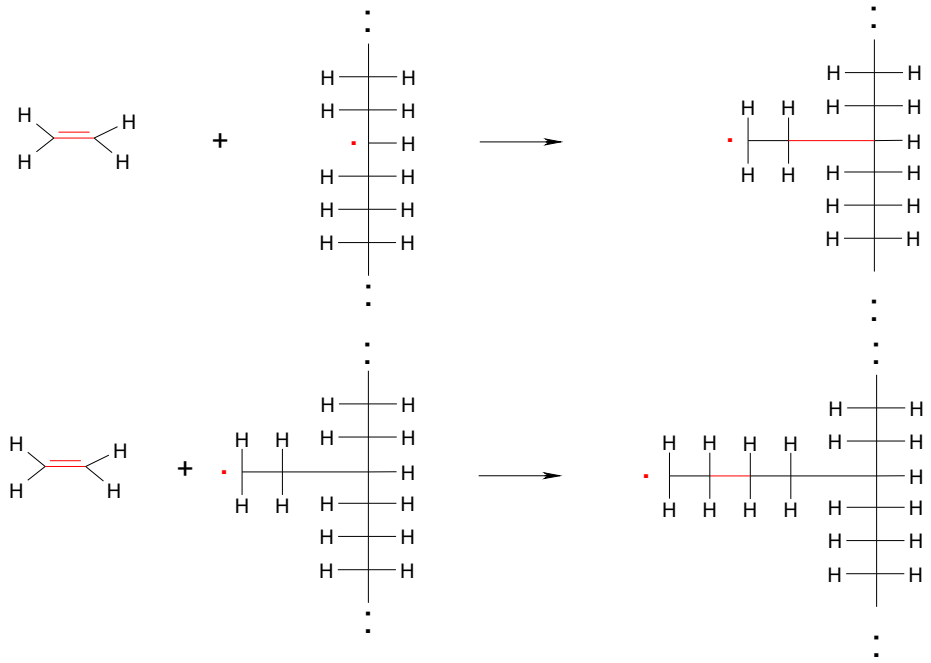

Figure 9: Branching of the polyethene-chain

This transfer reaction renders another polymer molecule. The product is a long-chained branch. The molecule can also react with itself. In this case a short-chained branch results. These two types of polymer transfer reactions can be explained using polyethylene as an example (Figure 10).

Intramolecular transfer to polymer

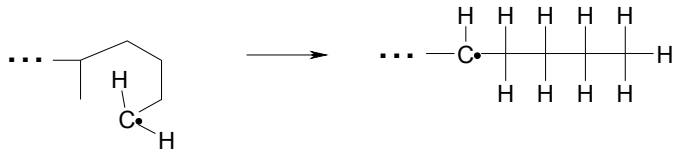

Intermolecular transfer to polymer

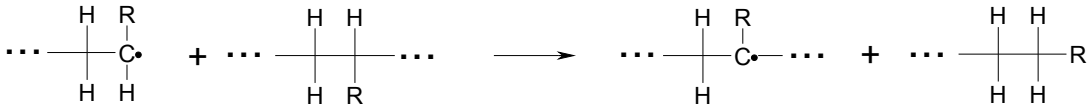

Figure 10: Types of chain transfer to polymer

In addition to these reactions, a transfer to a monomer molecule, to an initiator molecule or to the solvent is possible. The first two reactions do not have any influence on the polymerisation process, whereas a transfer of the reactive group to the solvent or to other potential transfer substances can terminate the chain.

To systematically stop the polymerisation, radical quenchers can be used. Another possibility is to control the molecular mass via a chain-stop induced by a so-called *Transfer Agent*.

3. Stereolithography

In the following chapters the focus will be put on additive manufacturing technologies based on photo-polymerisation. A lot of industrial applications take advantage of the chemical process of one-photon absorption (1PA). In this process, an initiator absorbs one ultra-violet (UV) photon with a short wavelength through linear absorption (Wu, Serbin, & Gu, 2006). This photon is needed to start the polymerisation near the surface of a photosensitive resin. The absorption of such a photon by a specific photo-initiator and its dissociation into two radicals is given as:

$$hv + PI = 2\ R^{\bullet}$$

where *hv* is the symbol for an UV photon, PI the shortcut for the initiator and $R^{\bullet}$ a reactive radical with a minimum of one unpaired electron. Figure 11 shows the polymerisation of a resin by the 1PA process.

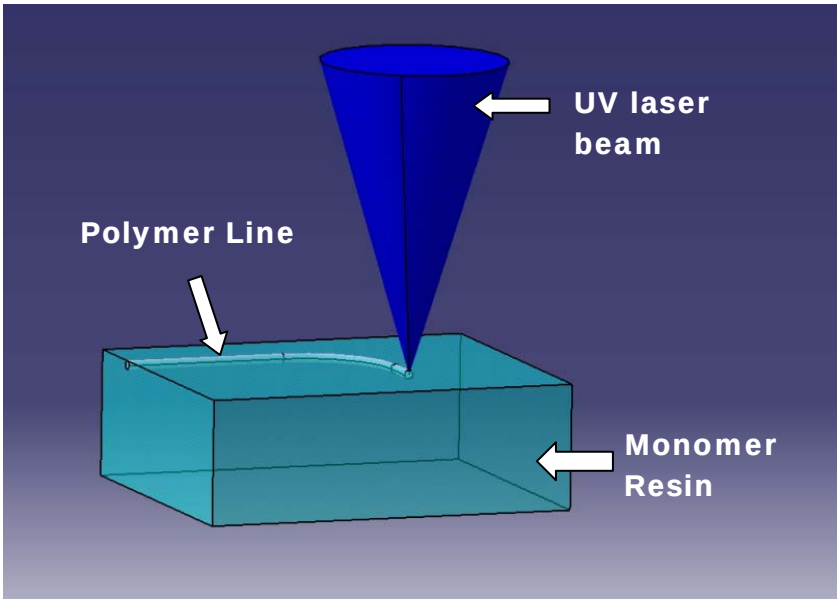

Figure 11: One-photon polymerisation with UV-light

Mainly depending on the concentration of the photo-initiators, the resin absorbs the UV light a few tens of micrometers deep.

In 1986 Charles W. Hull had the vision to use this technique to fabricate polymer parts in short time and with low effort and costs. He pointed out that most polymer parts are injection-moulded, a method that is only economical in high volume production. At that time several other scientists were also thinking of freeform-fabrication processes which require no tooling. In 1977 Wyn Swainson invented a fabrication method for three-dimensional figures by making two radiation beams intersect in a media with two different active components (Swainson, 1977). They each react in the presence of the beams or they produce reactants. The beams' crossover-point moves across the resin's surface and solidifies the intended structure. Inventions following those by Swainson all rely on the same principle. All

improvements of Swainson's process still use the synergetic energisation of selected spots deep in the fluid's volume. A pair of intersecting electromagnetic radiation beams was always needed to perform curing[3] in the desired spots. Later, Hull (1986) claimed that this process is very difficult to control. The radiation intensity and the image forming resolution decrease as the intersecting spot marches deeper into the volume. This creates changes in the radiation absorption of the resin; it leads to different diffraction indices and changes the dispersion. As stereolithography only needs one ultraviolet beam, the drawbacks resulting from an obligatory intersecting spot were nullified (Hull, 1986).

Hull described his invention as a *"system for generating 3-dimensional objects by forming successive, adjacent, cross-sectional laminae of that object at the surface of a fluid medium capable of altering its physical state in response to appropriate synergistic stimulation. The built-up laminae are integrated as they are formed to define the desired three-dimensional object*" (Hull, 1986, p. 6).

As mentioned above, the surface of a resin made of a liquid photo-polymerisable monomer sensitive to UV light gets solidified by a spot beam of movable UV-light, creating a cross-section on the spot it is directed at. After one layer is finished, the part-carrying elevator platform descends by the thickness of another layer. Usually a resin filled blade wipes over the polymerised structure and re-coats the next layer cross-section with fresh, liquid material. After this procedure, the next cross-section can be formed on top of the preceding layer. The process repeats until all layers are fabricated. The part is now ready to be taken out of the excess resin.

The whole process can be compared with the construction of a pyramid in ancient Egypt. Stones were laid side by side until one layer was finished. The next layer of stones was put on top of the previous one as can be seen in Figure 12.

After the structuring process, the part is developed in a chemical bath. Further treatment in an UV-oven is sometimes useful to achieve better hardness.

[33] Curing is the chemical process of solidification.

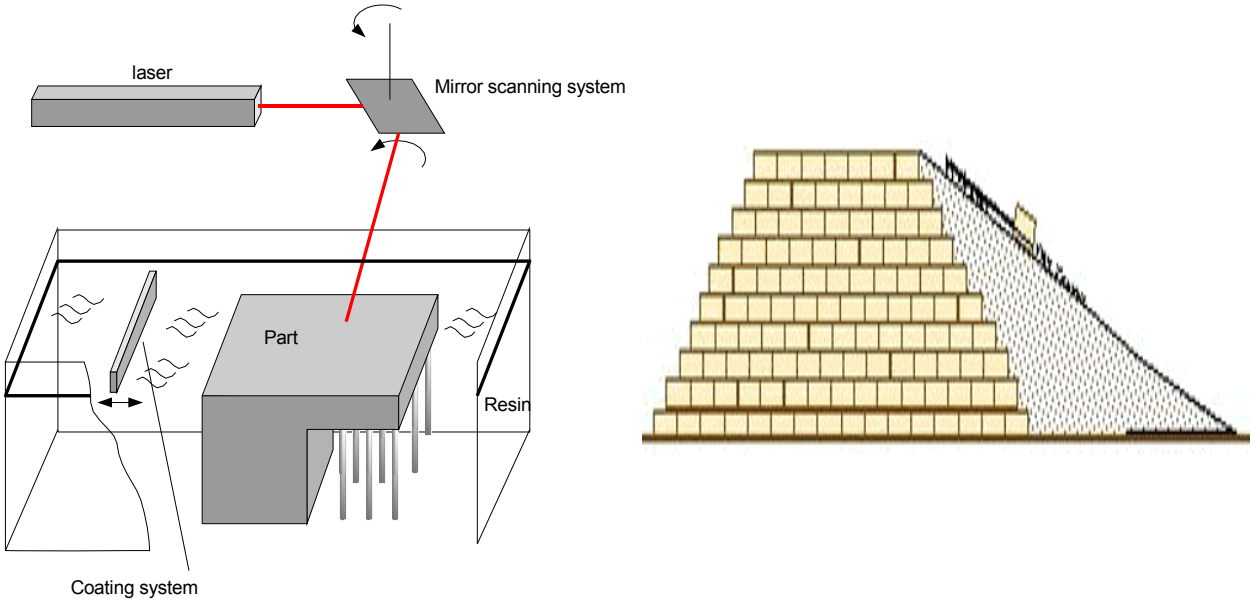

Figure 12: The principle of stereolithography (Stampfl, 2006)

To control the moveable spot beam, on the one hand, and the resin filled blade together with the elevator platform, on the other hand, Hull (1986) proposes a micro-computer. Especially for the fabrication of complex geometries, a complete CAD-CAM system can, accordingly directly translate the information gathered in the design process into information for automatic moulding in a manufacturing system, i.e. the stereolithography machine. A well implemented system can also cope with the main difficulties in stereolithography automatically. Firstly, the fabrication of desired parts requires their attachment to the elevator platform. Secondly, some types of geometry with steep layers require the existence of supporting devices in order to prevent them from sagging, especially when the layer gets stressed by the pressure from the re-coater blade and the additional liquid substance. This can be realized by a supporting material, which can be easily removed from the finished part. A good CAD-CAM system calculates the need for additional material and automatically places supports where they are needed.

The fast growing knowledge in laser systems and CAD-CAM software, together with further research in polymer science and computer technology, has improved the track record of stereolithography. Ever since its first mentioning in 1986, this fabrication method has moved into a variety of fields. Engineering and medical applications are just two important fields this fabrication method is used nowadays.

4. Two-photon-photopolymerisation

Due to the immediate absorption of UV photons as soon as the light hits the resin's surface, one-photon photo-polymerisation is restricted to the surface and thus to the fabrication of planar, two-dimensional layers (Wu, Serbin, & Gu, 2006). The third dimension is realized by adding layers successive on top of each other. The resolution is limited by the minimum achieveable thickness of one layer.

A rather new approach allows to structure real, three-dimensional objects. This process is called two-photon polymerisation (2PP). It is based on two-photon absorption (2PA), a process proposed by Göppert-Mayer (1931) and realized by Kaiser and Garett (1961) together with the development of the laser. Since photosensitive materials are transparent to infrared waves and highly absorptive in the UV range, one can initiate polymerisation within the small volume of material by precisely focused NIR femto-second laser pulses. The material sensitive in the UV range (λ_{UV}) can be polymerized by irradiation with the NIR light of approximately double wavelength ($\lambda_{IR}=2\lambda_{UV}$). Yet this is only possible under the condition that the intensity of the radiation is high enough to initiate two-photon absorption (Chichkov & Osianikov, Two-Photon Polymerization – High Resolution 3D Laser, 2008). This process is therefore involves a double-step. Compared to the one-photon absorption, an additional virtual excited energy interstate is established, which is of very short life-time (several femto-seconds). A second photon needs to be absorbed before the decay of this state. However, the resulting exited energy level of 1PP (S_1) is never the same as that of 2PP (S_2), since the selection rules of the two processes are different (Figure 13).

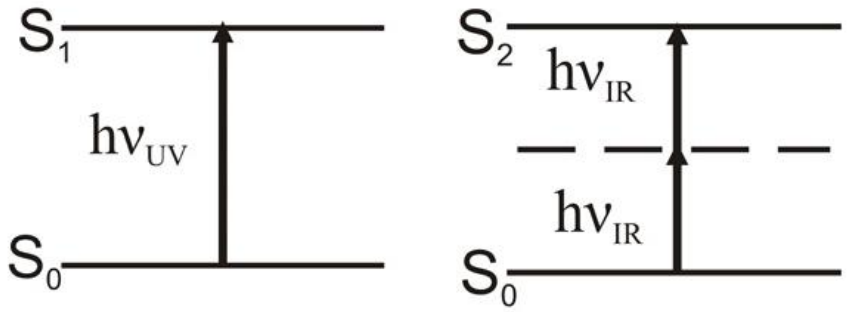

Figure 13: The development of the exited energy state with 1PP (left) and 2PP (right) (Chichkov & Osianikov, Two-Photon Polymerization – High Resolution 3D Laser, 2008)

The material is polymerized along the trace of the moving laser focus. Any kind of three-dimensional structure is thus possible to fabricate by "recording" directly into the volume of the photo-polymerisable resin. The non-polymerized remainder of the monomer is still fluid and soluble in specific solvents, so the built structure can be isolated after "washing away" the remaining fluid part. Figure 14 provides a schematic illustration of the 2PP process.

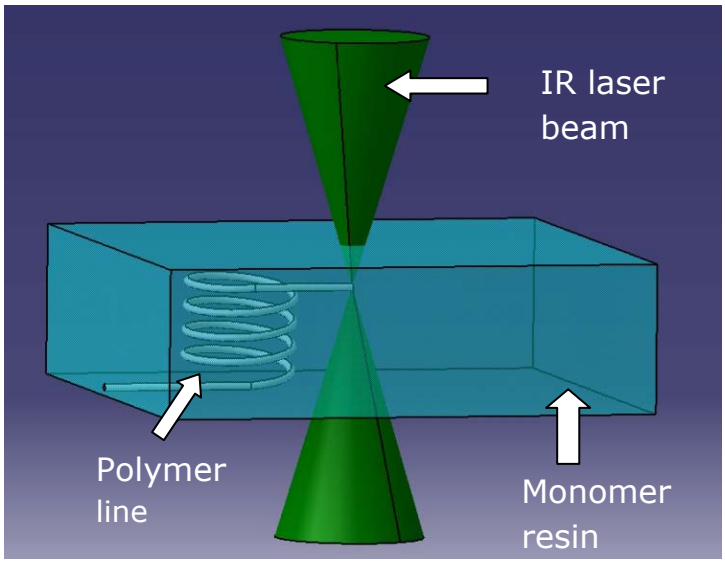

Figure 14: Two-photon polymerisation with a femtosecond NIR laser beam

In 1PP the presence of oxygen on the polymerizing surface can lead to a quenching of the chain propagation and can therefore cause a suppression of chain growth. The structuring of highly resolved models with 1PP claims for an inert gas environment. As 2PP structures are built inside the resin, there is no need for any kind of special resin-enclosing atmospheres (Passinger, 2008).

Apart from the 3-dimensionality and the non-requirement of a special environment, 2PA offers another advantage in terms of resolution. In the 2PP process, laser intensity and photon density raises the probability of two-photon absorption by the power of two. This non-linearity provides the possibility to reduce the size of the polymerised volume below the diffraction limit (Figure 15).

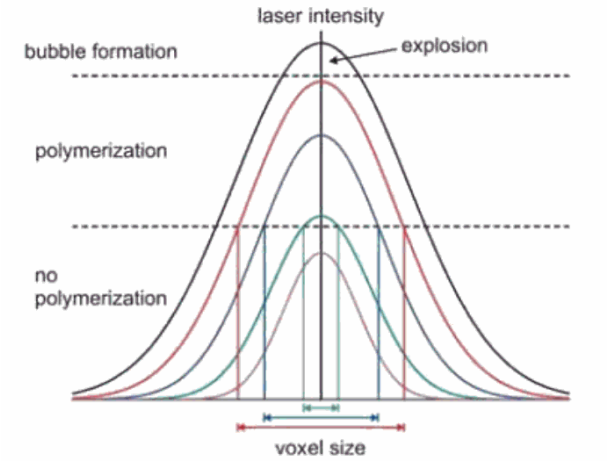

Figure 15: Dependence of the polymerised volume on the laser intensity in 2PP, with the polymerisation threshold and the threshold for polymer destruction as boundaries of the available intensity range (Passinger, 2008).

It is theoretically possible to achieve photo-polymerisation in a very small volume, significantly smaller than predicted by the refraction limit as long as the laser intensity remains within the boundaries of polymerisation (Figure 15). These elements, also called volumetric pixels (voxels) are limited only by the polymer

properties. Yet in reality, laser stability and the machine parameters limit the resolution. At present, resolutions of about 50nm laterally can be achieved (Passinger, 2008).

The disadvantage of 2PP is the slow polymerisation speed. According to Passinger (2008), the achievable writing speeds are less than 1000µm/s currently. Together with a high resolution this leads to long build-up times, even for structures of less than 1mm^3 volume.[4]

Additive manufacturing using 2PP is not a commercial application yet. The slow building process, the small-sized structures and the few resin types available, together with the high costs of the apparatus, make this process rather inefficient and uneconomic. Nevertheless, the possibility to solidify a volumetric pixel inside a resin with only one spot beam combines the advantages of the fabrication method of Swainson (two radiation beams inside a resin) and the stereolithography invented by Hull (layer by layer with one spot beam). According to Bratton et al. (2006), two-photon lithography and the process associated with it is one of the backbones of the nanotechnology revolution. The feature size reduction in the advancing field of microelectronics and lithographically patterned structures for photonic and biotechnological devices are just two implementations of this modern type of lithography. With common lithographic techniques, the resolution of the parts will come to limiting barriers. As the above fields advance, the need for lithographic techniques with higher resolution rises. Thus, two-photon lithography has already been applied to fabricate optical waveguides, microfluidic devices, micro-electro-mechanical systems (MEMS) and data storage devices. In Figure 16, the results of current research in the field of two-photon lithography are shown.

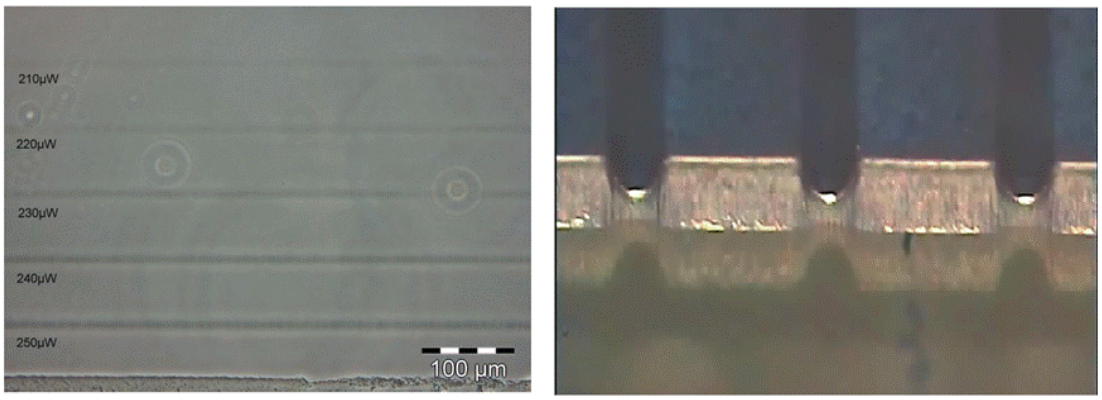

Figure 16: Applications of two-photon lithography

The left picture is a phase contrast microscopy image of optical waveguides written in a poly-dimethyl siloxane matrix at different laser powers (Inführ, et al., 2009). The right picture displays an array of 20µm wide fluidic channels with semi-circular cross-sections fabricated in dry film laminae. Tubular pipes can be formed by

[4] For additional information on the relation between structuring speed and power for the fabrication of reasonably satisfying structures see chapter 10 "Structuring with ORMOCER".

bonding a second, identical but inverted array onto the upper surface of the channels (Burt, Goarter, Hayden, Morris, Rizvi, & Talary, 2006).

The manufacturing of biocompatible structures using 2PP is a further promising field as this method fulfils the demand for parts in high resolution. As biological tissue is very transparent to red and NIR light, the pulsed laser system used for the structuring process in 2PP is not likely to photo-chemically harm a living animal. Therefore, the 2PP process is ideal for the fabrication of parts in a resin containing living organisms. After the description of the experimental realisation of a two-photon lithography machine at the Vienna University of Technology and a short explanation of the model organism Caenorhabditis elegans used for the experiments we will present the results of experimental direct additive manufacturing on the model organisms; a process we will call in-vivo-writing.

5. Anatomical terms of location

In order to describe the animal it is necessary to get a basic understanding of the scientific, non-language specific anatomical terms of description. We will be dealing with an *Vertebrate*, i.e. an animal without a vertebral column (backbone or spine). Like humans, most of these animals are bilateral symmetrical. Thus only one plane divides them into mirror-image halves. The anatomical terms of location are adapted to this symmetry. Figure 17 shows the animal C. elegans together with the location-related terms.

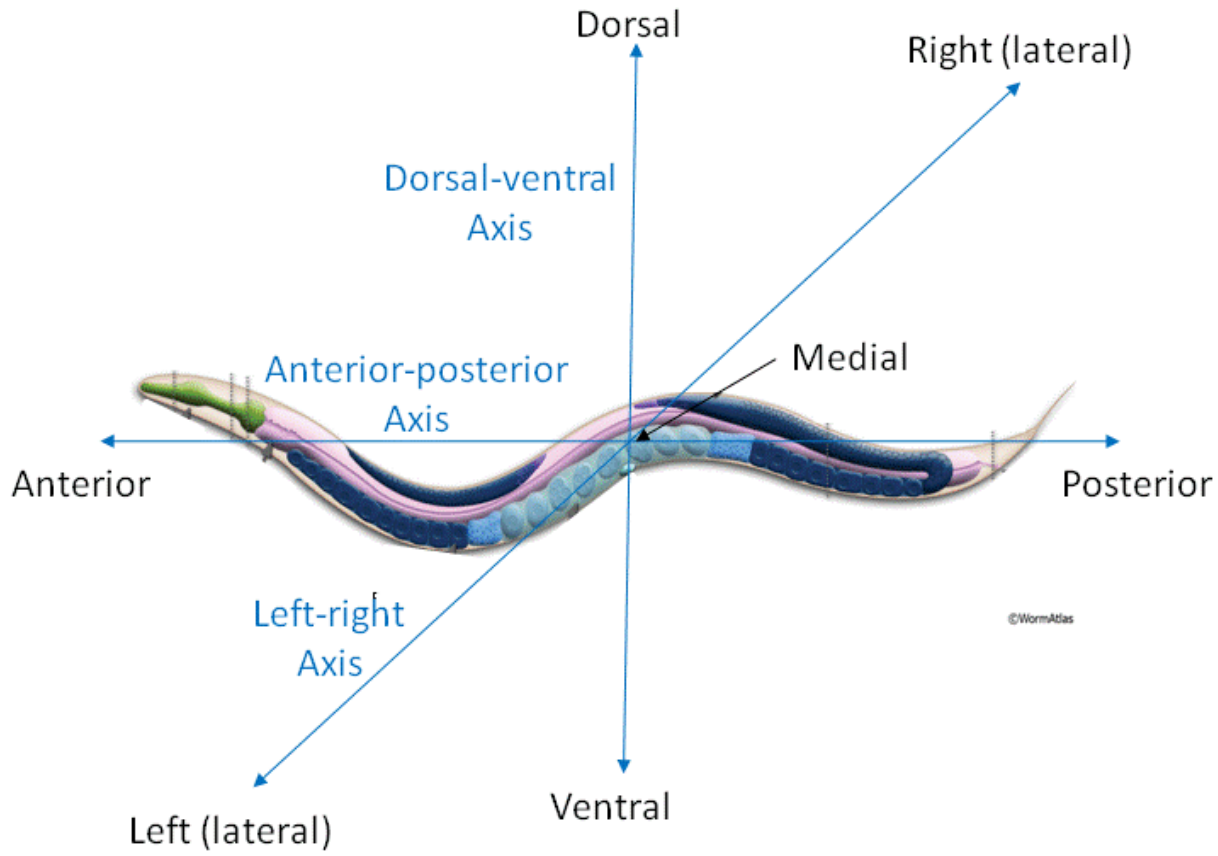

Figure 17: Anatomical terms of location in a picture of C. elegans from wormatlas.org (Albert Einstein College of Medicine, 2009)

In order to describe the organisation of certain body parts in relation to others we must also define some relative terms in addition to the absolute ones mentioned above. Table 1 shows the basic descriptions of directions in relation to the center of an animal's body.

Term of relative location	Descitption
Proximal	Near the center of the body
Distal	Far from the center
Profound	To the center
Superficial	To the surface of the body

Table 1: Anatomical terms of desciption in relation to the center of an animal's body

The planes of the body are of further interest. There are three main reference planes used in zoology. Figure 18 shows these planes for C. elegans. The sagittal plane divides the animal in a right (dexter) and a left (sinister) half. The coronal plane divides the body into front (dorsal) and back (ventral) portions, whereas the transverse plane refers to a schematic cut through the body along the horizontal axis.

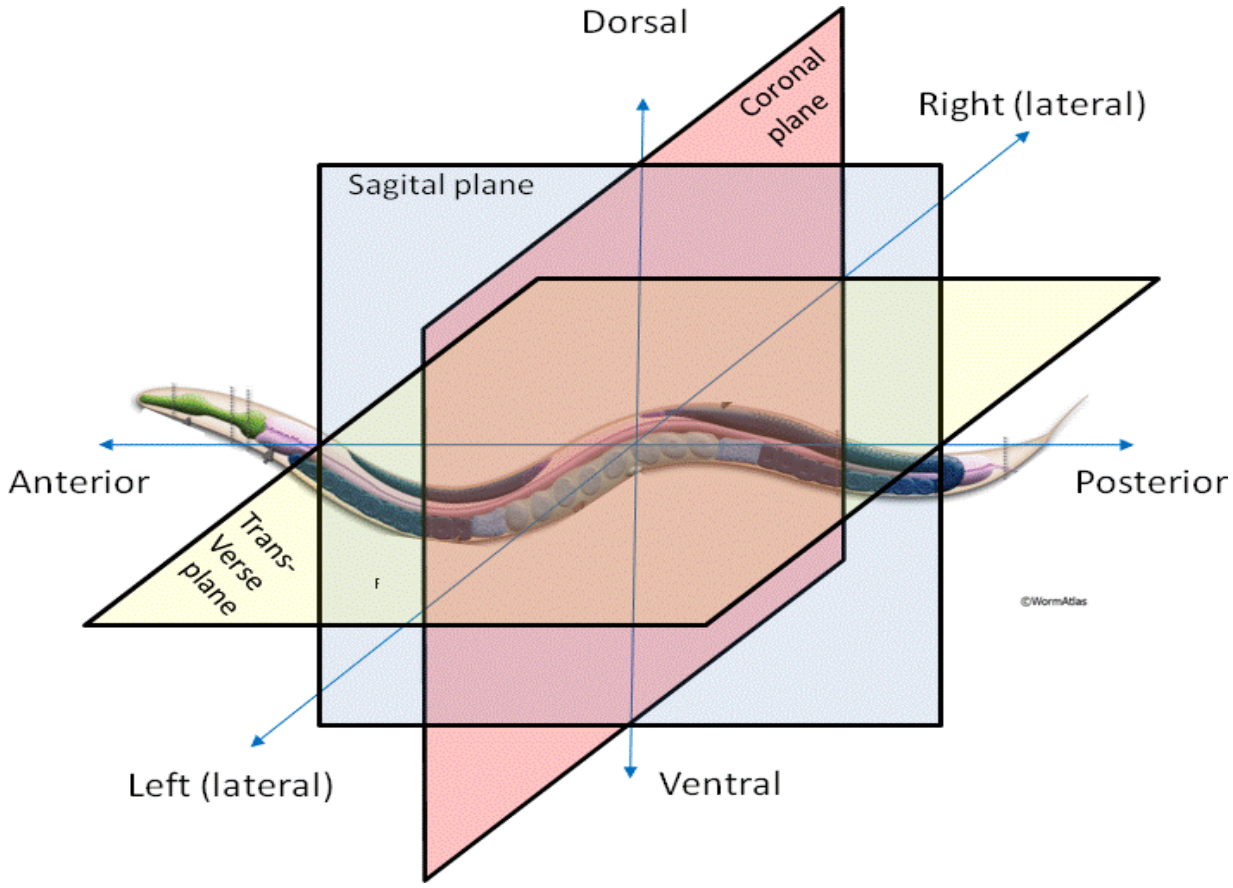

Figure 18: Planes of anatomical reference in a picture of C. elegans from wormatlas.org (Albert Einstein College of Medicine, 2009)

6. The model Organism Caenorhabditis elegans

6.1. Introduction

C. elegans is a soil-living nematode with a total length of about 1mm. It belongs to the family of simple roundworms. In particular, it is a member of the Secernentea, the main class of nematodes. Animals of this class can be identified by their numerous *Caudal Papillae* and their excretory system possessing lateral canals.

> The ugly family of C. elegans
>
> The animal is related to a wide range of parasites, some of them also affecting humans. The threadworm (Strongyloides stercoralis), for example, is a close relative of C. elegans. It belongs to the same subclass, the Rhabditia, and also populates the soil. The worm occurs in subtropical and tropical areas. It infects humans by penetrating the skin. From there on it moves through the lungs to finally reach the intestine, where it grows to an adult. The Ascaridida are very close relatives to the Rhabditidae. They only differ slightly in morphology and in their DNA sequence (University of Arizona, 2005). Worms of this type are world-famous for their robust eggs. This robustness allows them to withstand corrosive chemicals and enables them to persist over many years (Murray, Rosenthal, & Pfaller, 2005). All members of the subclass Ascaridida live parasitically in the intestine of *Vertebrates*[5].

C. elegans is often used as model organism to study animal behavior, genetics and biochemistry as it offers a lot of advantages for laboratory use. Its easy propagation in large numbers using agar plates, rapid life cycle and small body size makes it an ideal organism for researchers (Wood, The Nematode Caenorhabditis elegans). What is unique to this organism is that both number and position of the cells are constant within all wild-types[6] (Wisconsin Outreach Research Modules, 2004). The male adult consists of 959, the hermaphrodite of 1031 somatic cells. In addition, the nervous system always comprises of 302 neurons. Moreover, these cells are easy to track as the worm is transparent through and through. These facts led to the use of this nematode for the research on a wide range of developmental processes. Together with the bacteria *Escherichia coli*, the *Yeast* and the fruit-fly Drosophila, this nematode is one of the most investigated and best understood organisms in the world.

However, it has to be noted that C. elegans is a very special organism, not only due to its cell constancy. In addition to the transparency and the very small body size, these worms have a pretty unique and unusual copulation behavior. Thus the degree to witch the results generated by research on C. elegans can be generalized are limited to a certain extent. This Nematode is indeed a primitive organism but it shares many of its essential characteristics with other animals. On the basis of the broad knowledge on the biology, the genetics and the behaviour of the worm

[5] According to Roberts and Janovy about one quarter of the earth are infected with Ascaris lumbricoides. Infection occurs mainly in region with low education (Roberts & Janovy, 2009).

[6] C. elegans wild-type is the original worm without any genetic modification.

researchers working with C. elegans feel able to draw parallels to higher animals and humans.

C. elegans hase been the model organisms for a variety of different biological investigations. Three Nobel prices over the last few years in very different fields are based on studies on this worm. This shows the popularity and the high quality of research with C. elegans.

In 2002 Sydney Brenner, H. Robert Horvitz and John Sulston got the Nobel price for their work on the genetics of organ development and *Programmed Cell Death* in C. elegans[7]. The Nobel Prize for physiology or medicine 2006 was given to Fire and Mello for the discovery of *RNA interference*[8]. *Green fluorescent protein*, investigated by Martin Chalifie was also based on studies on C. elegans. Last year he got a Nobel price in chemistry for his work[9].

In our eyes, the singularity of C. elegans does not limit the generalisability of the results in this work. We will focus on the resistance to chemicals of this nematode. Hence, only the cuticle, the pores that open to the surrounding of the organism and the worm's excitability to mechanical and chemical influences is important. Investigations will therefore only include body parts of C. elegans, which it shares with a large variety of other animals.

Moreover, the advantages of working with C. elegans including the easy propagation, the transparent body, the robustness and the small size render these animals ideal for the research described in this work. No other popular model organism would have needed less equipment and less skilled treatment. With limited laboratory hardware available at the University of Technology, and the limited biological education on our part, C. elegans was the only proper choice.

Table 2 outlines basic facts on C. elegans.

[7] http://nobelprize.org/nobel_prizes/medicine/laureates/2002/index.html 06.10.2009
[8] http://nobelprize.org/nobel_prizes/medicine/laureates/2006/adv.html 06.10.2009
[9] http://nobelprize.org/nobel_prizes/chemistry/laureates/2008/illpres.html 06.10.2009

Body size		~250-1500µm
Diameter		~65µm (adult)
Body color		Transparent
Food	wild	Bacteria destructing plant material
	laboratory	Mainly *Escherichia coli*
Number of cells	959 (adult)	
Conversion rate of food into body mass	50 %	
Embryogenesis		14 hours*
Postembryonic development		36 hours*
Number of larval stages		4 (3 with Dauer)
Max. number of progeny	Hermaphrodite reproduction	200-300
	Mating with Males	Up to 1000
Life span	Suitable conditions	2 to 3 weeks
	Harsh conditions (including dauer stage)	Up to 3 months
Temperature optimum	12-26 °C	

Table 2: C. elegans facts (at 25 °C)

Anatomy

1,2mm

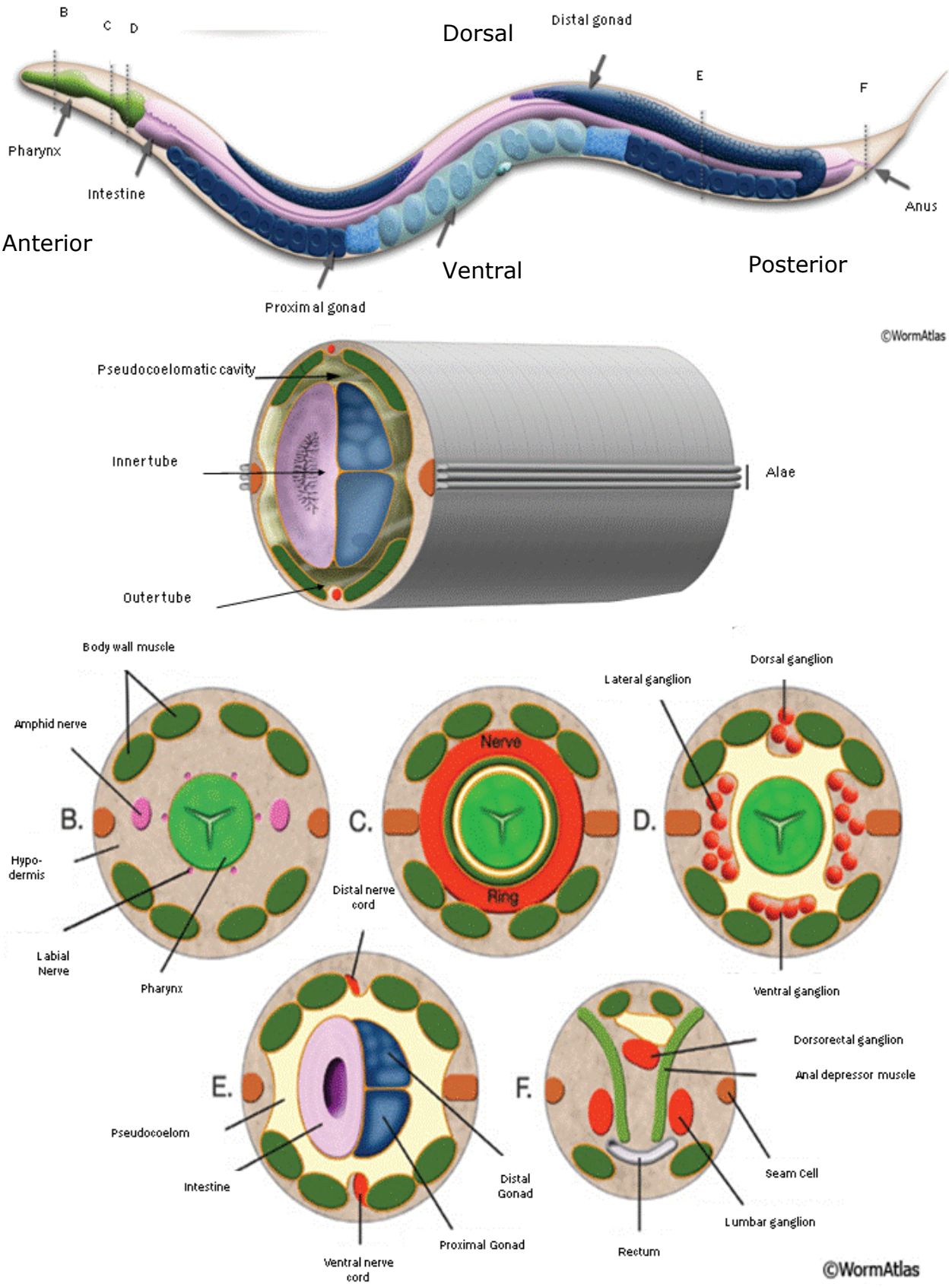

Figure 19: Anatomy of C. elegans (Albert Einstein College of Medicine, 2009)

All nematodes feature the same body plan. They consist mainly of two concentric rings surrounded by the *Pseudocoelom* in between. The shape of the animal is maintained by an inner hydrostatic pressure. The outer loculus comprises of the nervous system, the *Gonad*, the *Coelomocyte* and the excretory/secretory system (White & Sulston, 1988). The inner tube contains the *Pharynx* with its nearly autonomous nervous system and the intestine.

6.2. The cuticle

The cuticle of C. elegans is of fundamental importance for the studies of this thesis. As it is the protective cover of the animal, it determines the animal's resistance to external influences. Thus a closer inspection of this body part is necessary.

The cuticle is the animal's *Exoskeleton*. This protective protein layer is important to maintain the morphology of the worm, to protect him from harmful influences in the external environment and to enable the worm's movement. The cuticle is one of the most complex extracellular structures produced by a living organism (Edgar, Cox, Kusch, & Politz, 1982).

The outer tube is covered by the *Collagen*ous*, Extra-cellular* cuticle, which is secreted by the underlying *Hypodermis* (Kramer, 1997). The cuticle also lines the *Stomodeum* and the *Rectum*. It comprises of a complex structure of *Glycoprotein*s and carbohydrates. Many of the molecules found in the C. elegans cuticle are also part of *Mammalian extra-cellular* matrices.

6.2.1. Structure

The cuticle is connected to the *hypodermis* via hemi-desmosomes. Theses are small stud- or rivet-like cells, situated on the surface of *Keratinocytes* in the *epidermis* of the skin*. Seam Cells* enable the formation of different stage-specific types of the cuticle through the synthesis of various proteins (Thein, McCormack, Winter, Johnston, Shoemacker, & Page, 2003).

Jutting ridges extend over the left and right lateral *seam cells*. These ridges are produced by the *seam cells* themselves and are only existent in the L1, adult and dauer stage[10] (Albert Einstein College of Medicine, 2009). Figure 20 shows an electron micrograph and a schematic picture of the cuticle taken from an adult C. elegans.

Besides the longitudinal alae, there are several circumferential indentations, called the annuli. In between them, a gap of uniformly 1 µm is recognisable. This gap is called furrow. The annuli work like pleats, allowing the worm to fold the cuticle over

[10] A detailed explanation of C. elegans' stages is given in the chapter 6.8 "Survival".

the inner radius and extend over the outer one (Singh & Sulston, 1978). Figure 21 shows an electron micrograph of a bent worm.

As seen in

Figure 22, the cuticle of an adult consists mainly of four layers (epicuticle, cortical, medial and basal layer). It can reach a thickness of about 1µm (Cox, Kusch, & Edgar, Cuticle of Caenorhabditis elegans: Its isolation and partial characterization, 1981).

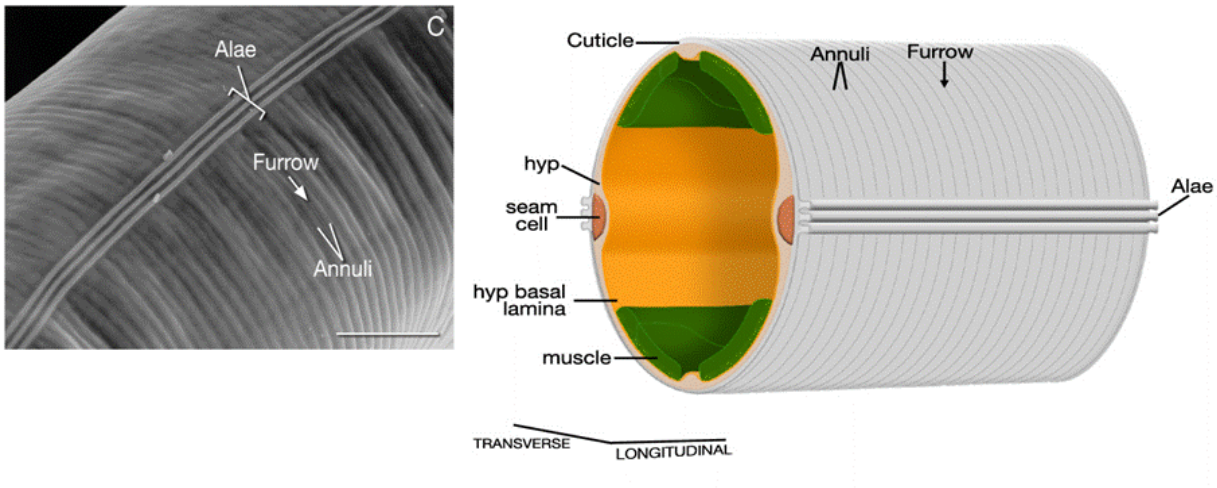

Figure 20: Left picture: electron micrograph of the lateral side, magnification 2200x, Scale bar: 10µm / Right picture: Schematic constitution of C. elegans cuticle (Albert Einstein College of Medicine, 2009)

Figure 21: Adult hermaphrodite lying on its lateral side (Albert Einstein College of Medicine, 2009)

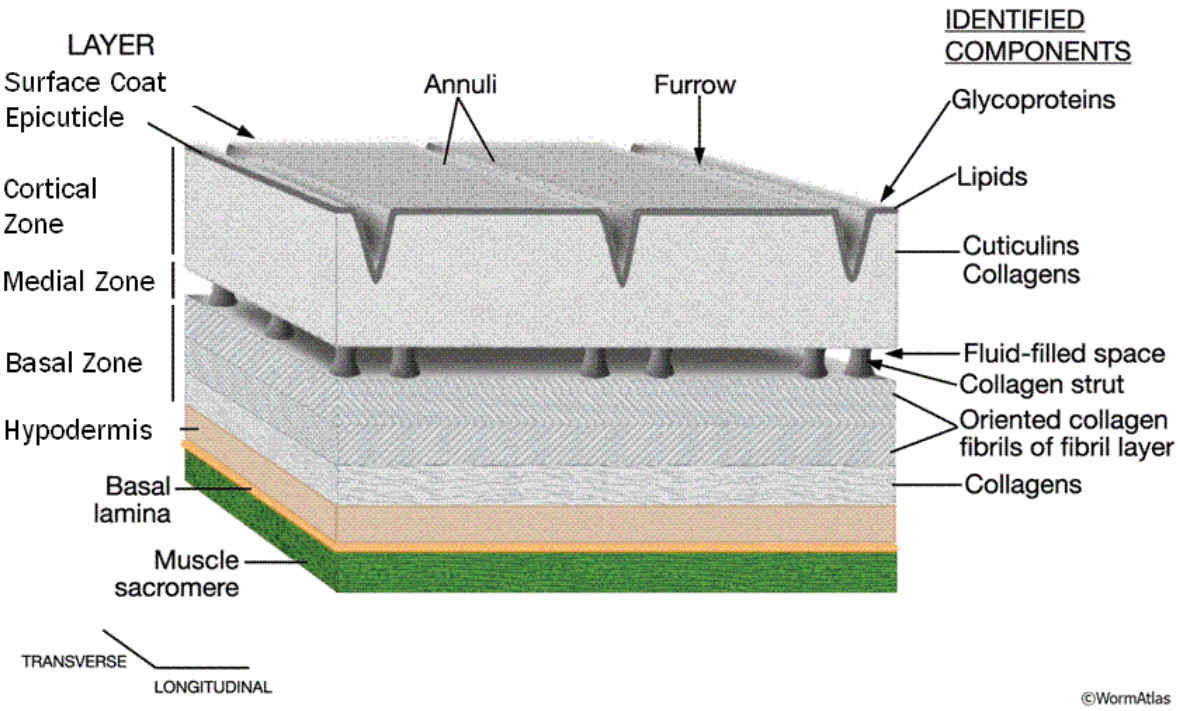

Figure 22: Composition of the cuticle (Albert Einstein College of Medicine, 2009)

The medial zone is only existent in adult stage. It accommodates several blocks of collagenous material called struts. These filaments connect the cortical and fiber layers in the basal zone of the cuticle. Most of the filaments are situated under the indentations (annuli) of the worm's *exoskeleton*. The space between the connections is presumably filled with fluid.

The basal zone of the cuticle accommodates two collagenous fibril layers, which arrange to a 65 degree angle with respect to the long axis of the worm. The outer layer is running clockwise, the inner layer anti-clockwise around the animal (Riddle, Blumenthal, Meyer, & Priess, 1997).

In addition to the six layers, there is a protective coat can on top of the worm's *epicuticle*. Despite extensive research, its composition is presently not very well understood. Yet, it is known that it contains a lot of carbohydrates.

6.2.2. Chemical compounds

The cuticle is highly resistant to solubilisation. The usual procedure to get a sole cuticle is to boil a *Sonicationed* animal in 1% *Sodium lauryl sulfate (SLS).* This treatment dissolves all structures but the cuticle and some insoluble residues (Cox, Kusch, & Edgar, Cuticle of Caenorhabditis elegans: Its isolation and partial characterization, 1981). The *SLS* insoluble cuticle can be further subdivided using a reducing agent.

The most abundant structural components are collagens and non-collagenous *Cuticulin* (Lewis, et al., 1994). The cuticle's proteins are cross-linked with disulfide bonds and non-reducible *Tyrosine*-derived compounds. The estimated molecular weight of the soluble proteins ranges from 53000 to more than 200000, whilst most of the animals exhibit a cuticle with a molecular mass of over 90000. The high *Glycine* and *Imino acid* content indicates the collagenous nature of the soluble part. The insoluble fraction consists of a less collagenous material. Figure 23 shows known compounds in detail (Cox, Kusch, & Edgar, Cuticle of Caenorhabditis elegans: Its isolation and partial characterization, 1981).

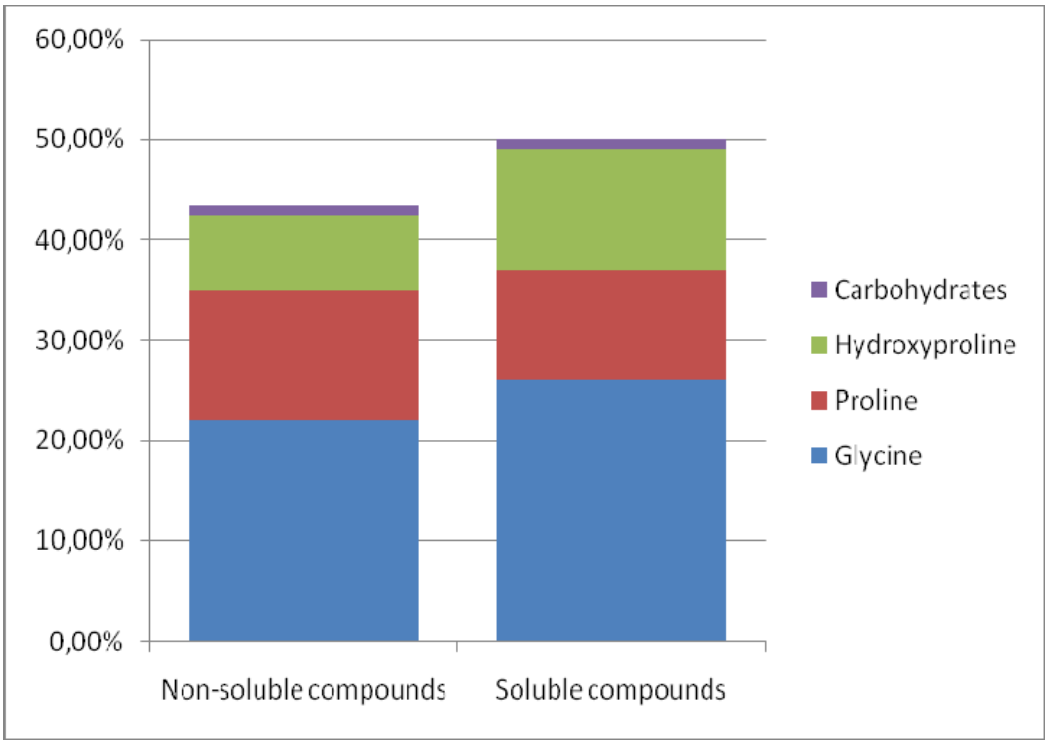

Figure 23: Compounds of Cuticle (Cox, Kusch, & Edgar, Cuticle of Caenorhabditis elegans: Its isolation and partial characterization, 1981)

6.3. Molt

C. elegans grow about one third its body size whilst advancing to the next larval stage. As described in chapter 6.8 (Survival), the worm gets a new cuticle and sheds the old one at the time it reaches a specific age. This process is called molt. During this time the animal enters a two hour lasting period of *Lethargous*. The pumping of the *Pharynx* and the movement is suppressed. The connections between the *hypodermis* and the cuticle are broken and a new cover begins to form. After a while, the animal starts to spin around its long axis. The *pharynx* begins to contract spasmodically and finally breaks up the old cuticle. The animal then moves backwards and crawls out of its old cyst (Singh & Sulston, 1978). This has to be taken into consideration in further studies as every change in the non-adult cuticle's structure resulting from external influences is only temporary.

The period of *lethargous* must be taken into account for the life-death analysis. Since pharynx pumping is considered to be an indicator for a living organism and pumping is suppressed during *lethargous*, death numbers maybe miscalculated.

6.4. Movement, muscles

During movement, muscle forcesare transferred from the *hypodermis* to the cuticle via small filament connections. Nematodes do not have opposing muscles. The high inner hydrostatic pressure and the elasticity of the protective cover provide the reset force for the animal to go back into its idle state (Francis & Watersen, 1985).

The body musculature consists of four longitudinal strips, attached to the cuticle through a thin layer of *hypodermis*. The movement is enabled by the subventral and subdorsal muscle fibers. Contraction and relaxation of these muscles in different areas of the body allows the animal to move forwards and backwards in the dorsal-ventral plane (Riddle, Blumenthal, Meyer, & Priess, 1997). Thus the movement is limited to the stiffness of the surface the worm is moving on.

6.5. Nervous system

Most of the neurons are located around the *pharynx*, along the ventral midline and in the tail. As shown in the B section of Figure 19, most of the cells form a ring around the basement membrane that surrounds the *pharynx*. Some are connected to the ventral and distal nerve cord as shown in the E section (Rand & Nonet, 1997). Most mechanical and chemical receptor neurons transfer the information received to the nerve ring. There the information is integrated and sent to the motor neurons in the head or along the nerve cords. Some receptor neurons have extensions into the tail or along the body. The nerve ring is shown in sector C in Figure 19.

6.6. Digestion

The *pharynx* pumps the ingested food into the intestine. There it is grinded and pumped through the worm. The central *Lumen*, surrounded by the intestinal cells, connects directly to the anus located near the tail (Figure 19). The single excretory cell is the largest cell in C. elegans. It contains excretory canals running through the animal's sides, which are connected to the excretory pore on the ventral side of the head. The excretory/secretory system is also in charge of the *Osmoregulation* and the maintenance of the cuticle by secreting *glycoproteins* (Riddle, Blumenthal, Meyer, & Priess, 1997).

6.7. Reproduction

C. elegans has two sexes: males and hermaphrodites. Thus, the animal is able to reproduce itself sexually and asexually. The number of progeny a hermaphrodite can have with sexual reproduction exceeds the possible number of asexual and therefore clonal offspring. According to Hodgkin and Barnes (1991) , a hermaphrodite nematode has the potential to get up to 1000 progeny when mating with males, whereas only 300 offspring are possible without. Inside the hermaphrodites' body there is space for about 10 eggs. The old ones are laid as fast as new ones are developed (Waksman, 2001/2002). Figure 24 shows a hermaphrodite carrying eggs.

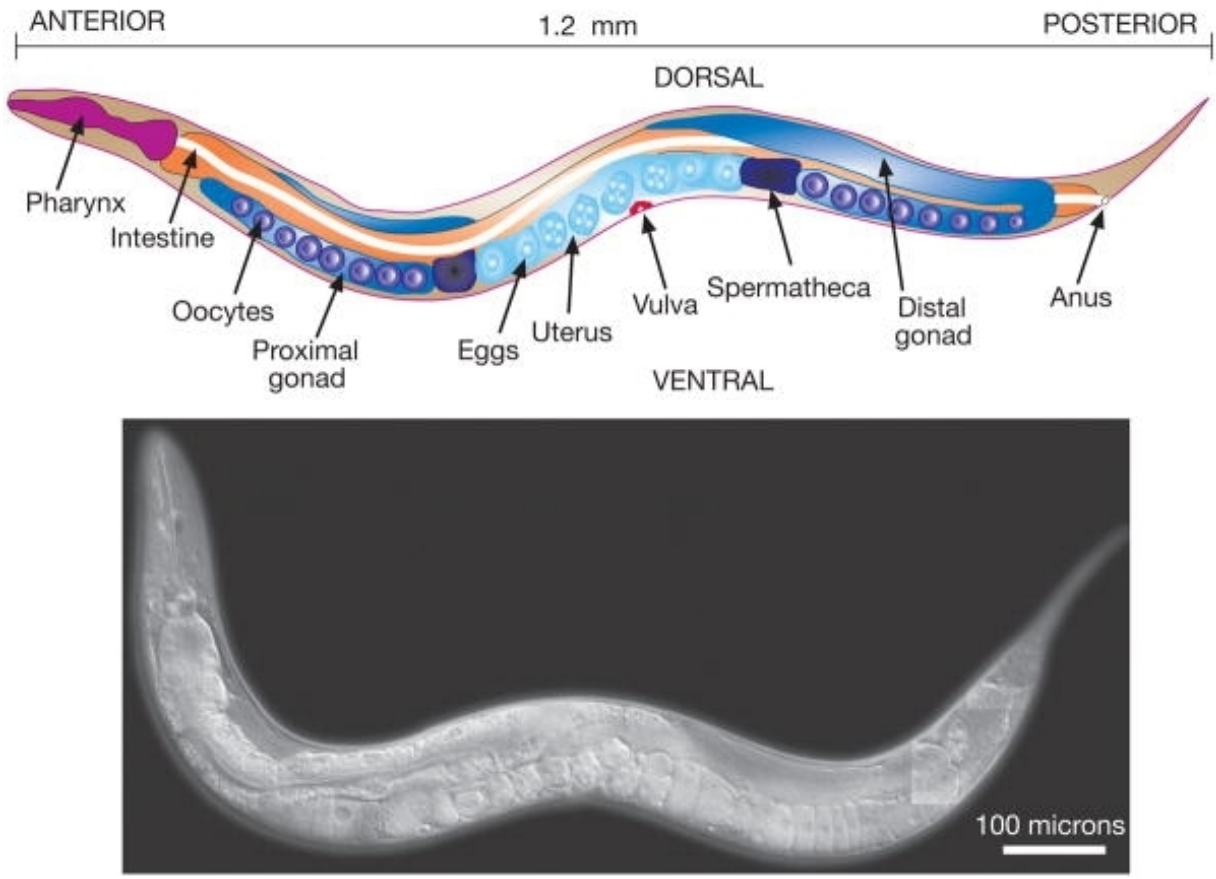

Figure 24: Composite diagram and photograph of a hermaphrodite C. elegans (Cummings & Esko, 2009)

The possibility to reproduce in the described two modes has made C. elegans an important laboratory animal for genetic research. Especially the availability of mutants with an increased life-span motivates scientists to research on aging with these model organisms (Johnson & Wood, 1982).

6.8. Survival

The animals are predators eating anything that fits into their mouths. In the wild the animals inhabit nutrient and bacteria rich environments. Their food sources are bacteria that develop on decaying vegetable matter. In the laboratory they are grown on agar plates seeded with the bacteria *Escherichia coli*. The animals convert the bacteria *Escherichia coli* with an efficiency of nearly 50 percent into their body mass (Wood, Basic culture methods, 1995).

As the soil is an unstable environment, the Nematodes have to withstand an uneven distribution of microbial food, temperature and moisture variations and a lot of encounters like fungi in the wild (Gray, 1988). In addition to that, C. elegans do not form self-sustaining populations in the soil. The animals have the tendency to overgrow their competitors. Following this strategy they will eat up the resources in the soil as fast as possible. The rapid life-cycle and the large brood size are both indicators for C. elegans being an r-selected animal[11] (Hodgkin & Barnes, 1991).

If there is no more food available for growing on one spot, the nematodes will move to another, richer area. With their short life-cycle and their immense need for food it is quite difficult to travel long distances. Therefore C. elegans developed a strategy, which enables them to withstand harsh conditions and to survive until another, more suitable habitat is found. The facultative dauer stage allows C. elegans to survive many months up to 10 times its life span (Riddle & Albert, 1997). Whenever it finds suitable environmental conditions it can continue its life-cycle from stage L4 on, that means it "jumps over" L2 and L3 stage (Figure 25). By hermaphrodite reproduction, the worm escapes the dauer stage since it enables one single animal to have offspring. So whenever a population of C. elegans finds a suitable spot for living, they get out of dauer stage and begin to propagate asexually. Thus a population that has to deal with harsh environmental conditions often is more likely to consist of clonal worms.

[11] Survival strategies are classified into r- and K-selection. r-selected animals have a lot of progeny with a little probability of survival. They usually inhabit little populated areas. K-selection is the opposite survival strategy. These animals put more effort in their offspring so they are more likely to survive. K-selected animals exploit crowded areas (Chapman & Reiss, 1999).

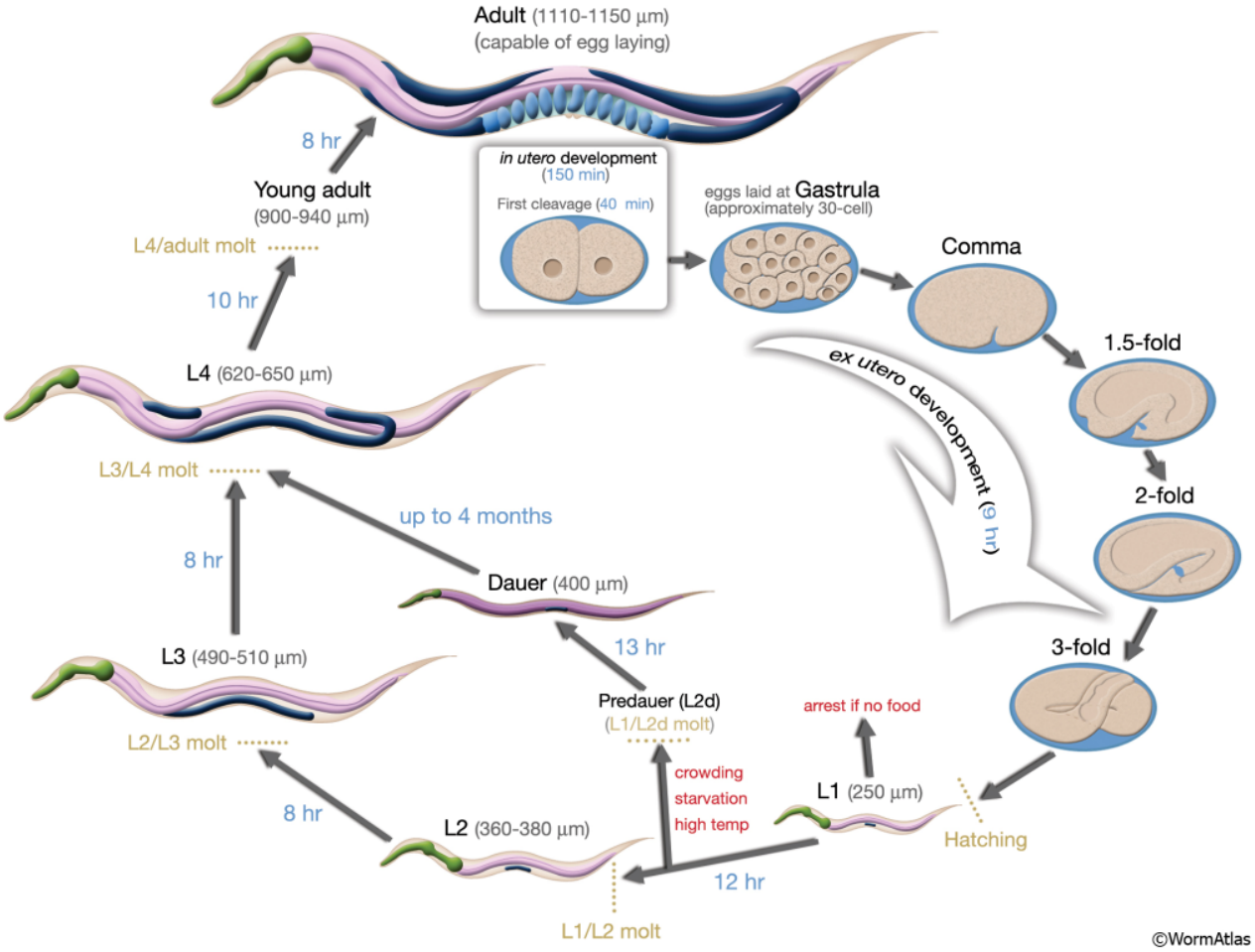

Figure 25: The life-cycle of C. elegans (Albert Einstein College of Medicine, 2009)

7. Experimental 2PP Setup “M3DL”

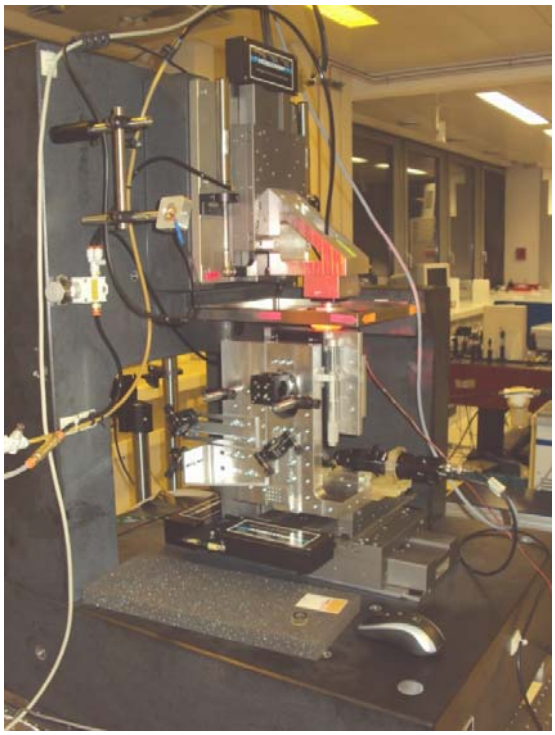

Figure 26: Experimental 2PP Setup M3DL

The basic setup of the 2PP system used for this work can be seen in Figure 26 and in Figure 27. The femto-second laser beam passed through an acousto-optic-modulator. This shutter diffracted the laser beam so that first order waves could be used for polymerizing. The intensity was adjusted by a λ/2 waveplate and a polarizing depending beam-splitter. Before the beam exposed the resin it got focused through a microscope objective. The X- and Y-movements of the laser beam were realized by high precision air bearing axes. The Z-movement was done by a similar axis which carried the resin container. The mirror system ensured that the X- and Y-movement was only parallel to the direction of the laser beam, so that the guidance of the beam was stable throughout the whole structuring process. For the online process observation a camera viewed along the laser beam and got focused on the polymerisation spot through the same objective. The axes were mounted on a hard stone frame, which was designed to damp vibrations. The whole setup’s base was an optical table with an air friction damping, again to suppress vibrations. For the control of the machine, the axes and the laser intensity power meter were plugged to an electronic device, which processed the commands given by the control computer. The sample was illuminated using a red LED lamp to prevent premature polymerisation.

To get a better overview of the experimental setup and to understand the functions of the compounds, the next few chapters will deal with the devices’ basic functionalities and their technical details.

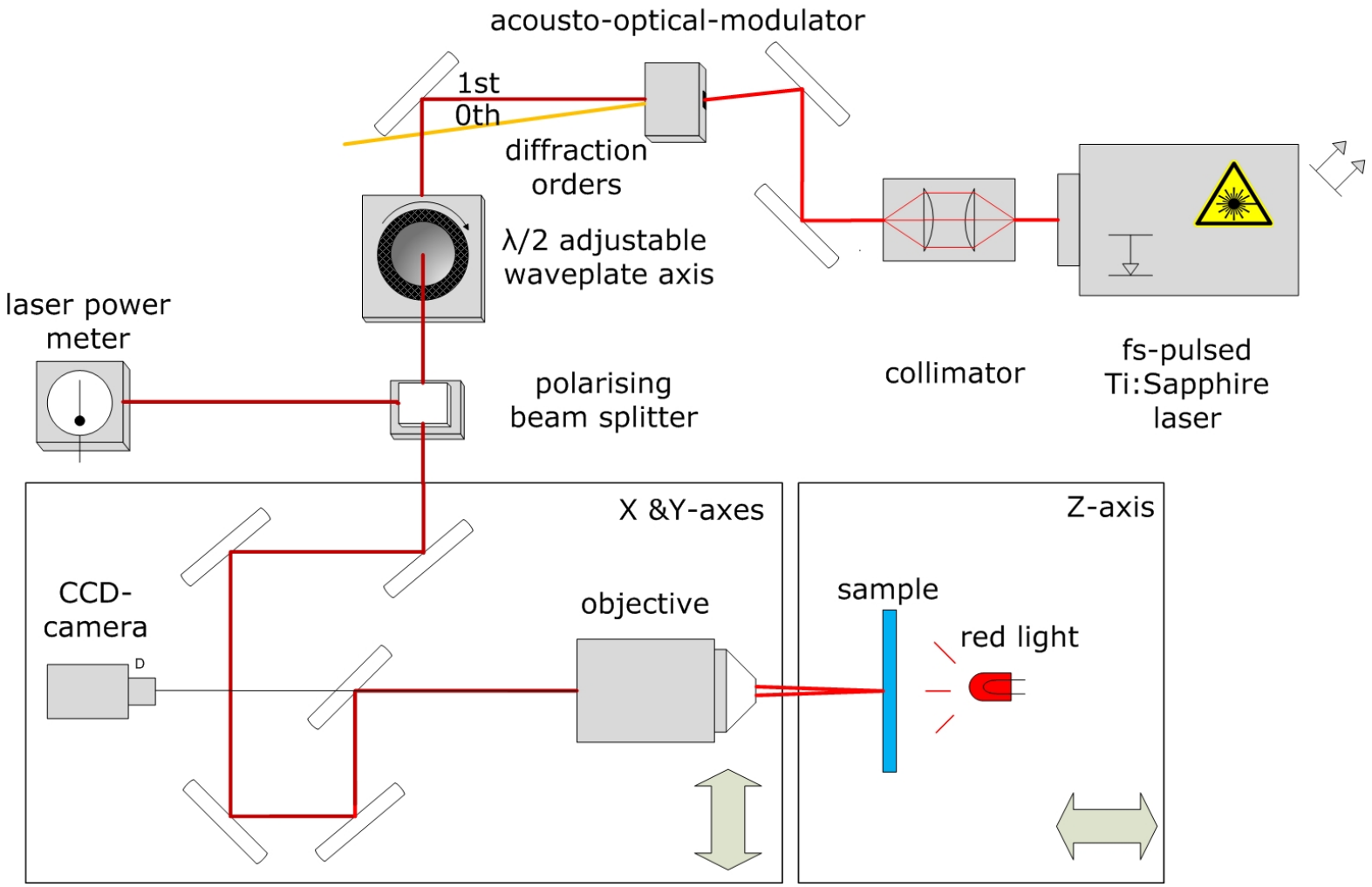

Figure 27: Schematic picture of the 2PP experimental setup M3DL

7.1. The Laser

The laser used for this experimental setup was an all-diode-pumped Ti:Sapphire Laser from HIGH-Q LASER (Model Number IC-800-200fs) with a pulse length of 160fs and a wavelength of 810nm. The pulse repetition rate was 73Mhz. The near-gaussian beam profile allowed a line width of 14nm. The constant output power was 200mW, the operation temperature was kept to 18°C by an external cooler. Figure 28 is a photograph of the laser and its additional devices.

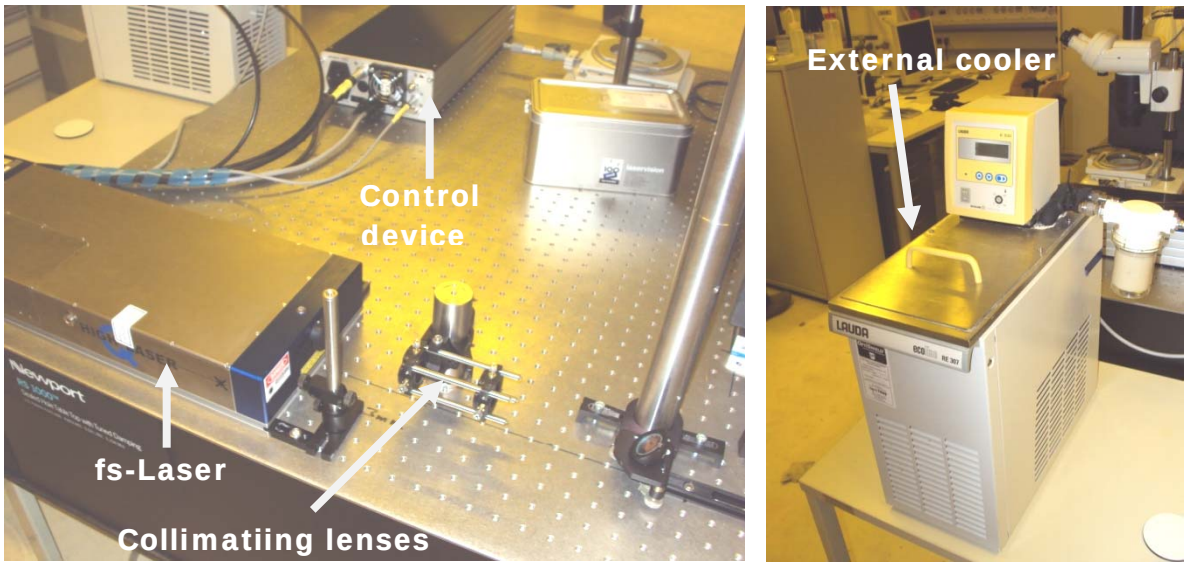

Figure 28: Left Picture: High-Q femto-second Laser Source with control device; Right Picture: Laser cooler

7.2. The Collimator

The output laser beam had a particular divergence. In order to be able to structure with the maximum output of 200mW, it was necessary to align the beam along the optical axis. This was done by a collimator which consisted of a concave and a convex lens. The devices were mounted directly after the fs laser. These lenses ensured a small diameter of the beam cross section. Thus the laser beam passes the distracting mirrors centrally.

7.3. The Acousto-Optical Modulator

Acousto-optical modulators (AOM) are generally applied to 2PP setups for two reasons: Inside the lasers' resonators, a modulator of this type can act as a Q-Switch so that laser pulses with high intensities are generated. Acousto-optic Q-switching provides switching capabilities at very high repetition rates and can handle high average beam powers up to several kWs (Hodgson & Weber, 2005). That makes them the most common devices for generating short pulses with high intensities.

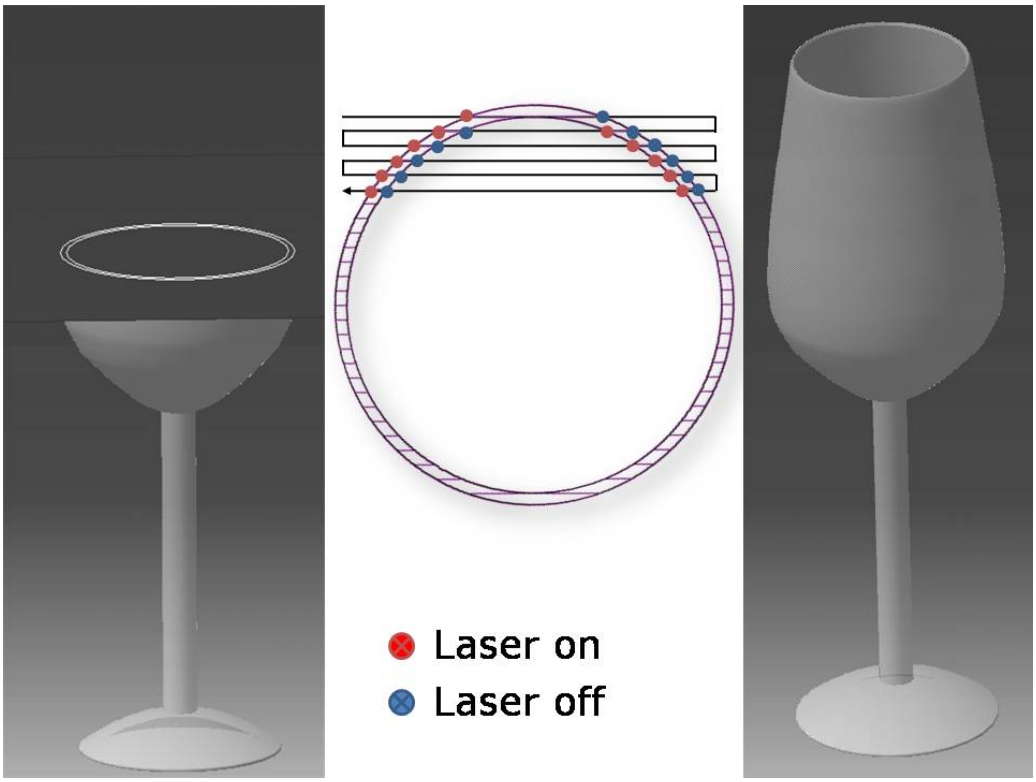

Figure 29: Building a model of a wine glass with 2PP

Our AOM, which was mounted after the collimator, however, had a different function. It acted as a switch for the laser beam. Light waves of the first order of diffraction were used to realise a fast beam-switching device. An electric signal feeding the AOM was used to shut the laser. This allowed determining the area to be polymerised and can be illustrated by a fictional fabrication process of a wine glass shaped object in Figure 29. One cross-sectional layer of the object under construction is shown in the middle of the picture. The X- and Y-axes move constantly over the structure and the AOM turns off and on to polymerise only the spots needed for this specific form.

AOMs are the fastest shutters available. They fulfil the needs of 2PP perfectly. The modulator we used is shown in Figure 30.

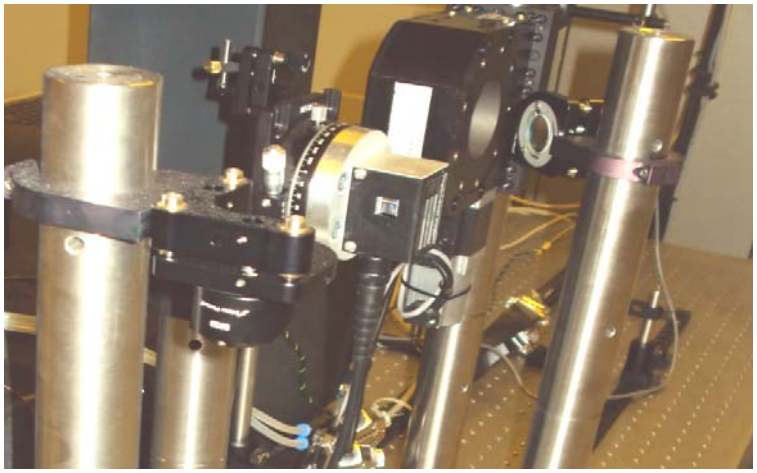

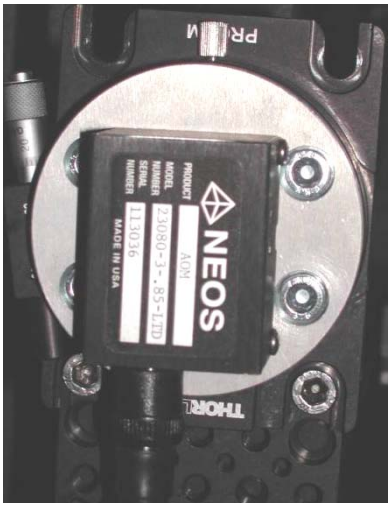

Figure 30:The AOM

7.4. The Power Control

The constant output power of the laser was 200mW. The accessible first diffraction order waves provided 80% of the resonator's intensity. We could therefore fabricate structures using a maximum power of 160mW. For the current purposes, this intensity was far too high for the fabrication of optically satisfying parts. Therefore a power control device was necessary. The Laser Zentrum Hannover (LZH) provided us a λ/2 polarizing waveplate, a polarization dependent beam splitter together with a laser power meter as seen in Figure 31 and Figure 32.

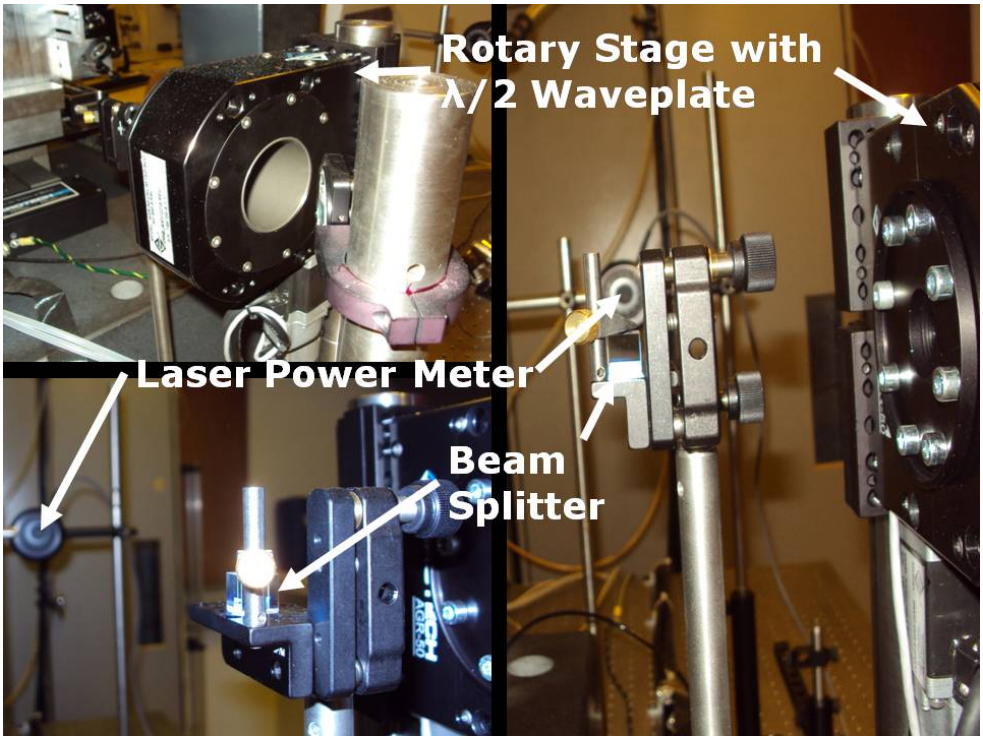

Figure 31: Photograph of the power control devices

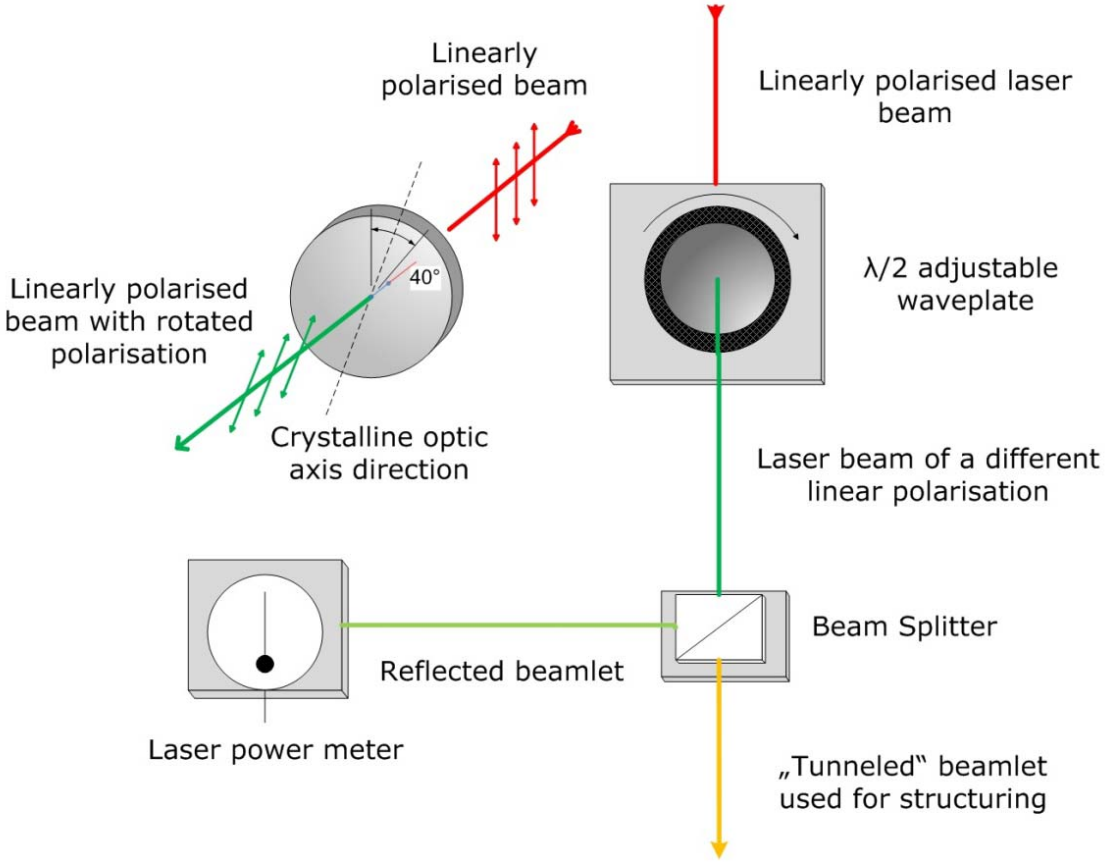

Figure 32: Schematic picture of the power control setup

7.4.1. The adjustable optical waveplate

An optical waveplate is a transparent birefringent crystal plate, which is carefully adjusted in its thickness and shape. It alters the polarisation of a beam by shifting the phase of its two perpendicular polarised components. Following the shape of the crystal, light polarised along the "optical axis"[12] travels through the crystal at a different speed compared to the perpendicularly polarised light. This creates a certain defined phase shift of the emitted beam with respect to its two polarisation planes (Paschotta, 2009). To regulate the intensity we used a beam splitter to deflect a certain beamlet so that only the desired intensity would reach the specimen. To do so, we needed the beam to be linearly polarised. Thus we used a λ/2 waveplate. The component of the polarization oriented along the "optical axis" was advanced relatively by 180° compared to the component of the perpendicular axis. This led to the rotation of an emerging incident beam by an angle to the optical axis twice the angle of the incident beam. Thus if the polarisation of the incident light fell together with the optical axis of the plate, there was no shift in the resulting polarisation. A separation angle of 45° to the

[12] The "optical axis" is a fictious axis parallel to the surface of the waveplate.

incident polarisation resulted in a polarisation was shifted by 90°. The output remained linearly polarized with the same amplitude. The orientation of the exiting polarisation changed depending on the angle of the "optical axis". Any amount of rotation was possible depending on this angle (Peatross & Ware, 2009). A schematic explanation is provided in Figure 32.

Figure 33: Left picture: Aerotech Rotary Stages type ART 300 (Aerotech, 2009); Right picture: beam splitter

The waveplate with a diameter of 50mm was rotated by an Aerotech AGR-50 rotary stage (right picture in Figure 33). It could rotate 360° and had no designated home (zero) position. It was driven by a precision worm gear with a 51.1:1 motor-to-table ratio and could move to designated angles with an accuracy of 120arc-sec. Repeatability[13] was, according to the manufacturers, 10arc-sec for a bidirectional movement and 30arc-sec for an unidirectional movement. It could move to positions with a resolution of 2arc-sec and a rated speed of 30rpm. Motion errors due to fabrication imprecision were specified with 5µm in the axial and 10µm in the radial direction. Tilt error was specified with 10arc-sec (Aerotech, 2009). It was energized by the control device and could be adjusted by control computer software.

7.4.2. The Beam Splitter

In general terms, a beam splitter divides a light beam into two separate beamlets. It consists of two prisms putted together on their basis. The device works on the principle of "frustrated total internal reflection". After the light beam has gone through a thin optical material it meets a dense optical material. Dependent on the distance to this partly reflecting surface, parts of the decaying wave get transmitted ("tunnelled")to a third material positioned adjacent to the reflecting surface (Figure 32). The actual totally reflected wave deflected by 90° declines in its intensity. The division ratio of the deflected and the "tunneled"

[13] Repeatability is defined as the range of positions attained when the system is repeatedly commanded to one location under identical conditions (Aerotech, 2009).

beamlet is dependent on the wavelength of the laser beam. In our setup, the impinging beam could be modified in its wavelength by the λ/2 waveplate as described above.

Using devices of this type we were able to adjust the beam ratio being "tunneled" through the beam splitter. The beam could then be further deflected and transferred to the structuring devices. The reflected beamlet could be measured by a Laser Power Meter. The subtraction of the measured reflected beamlet power from the maximum power of the laser beam after the AOM (160mW) gave us information about the power used in the structuring process. A picture of the beam splitter used for the experiments can be seen in Figure 33.

7.4.3. The Laser Power Meter

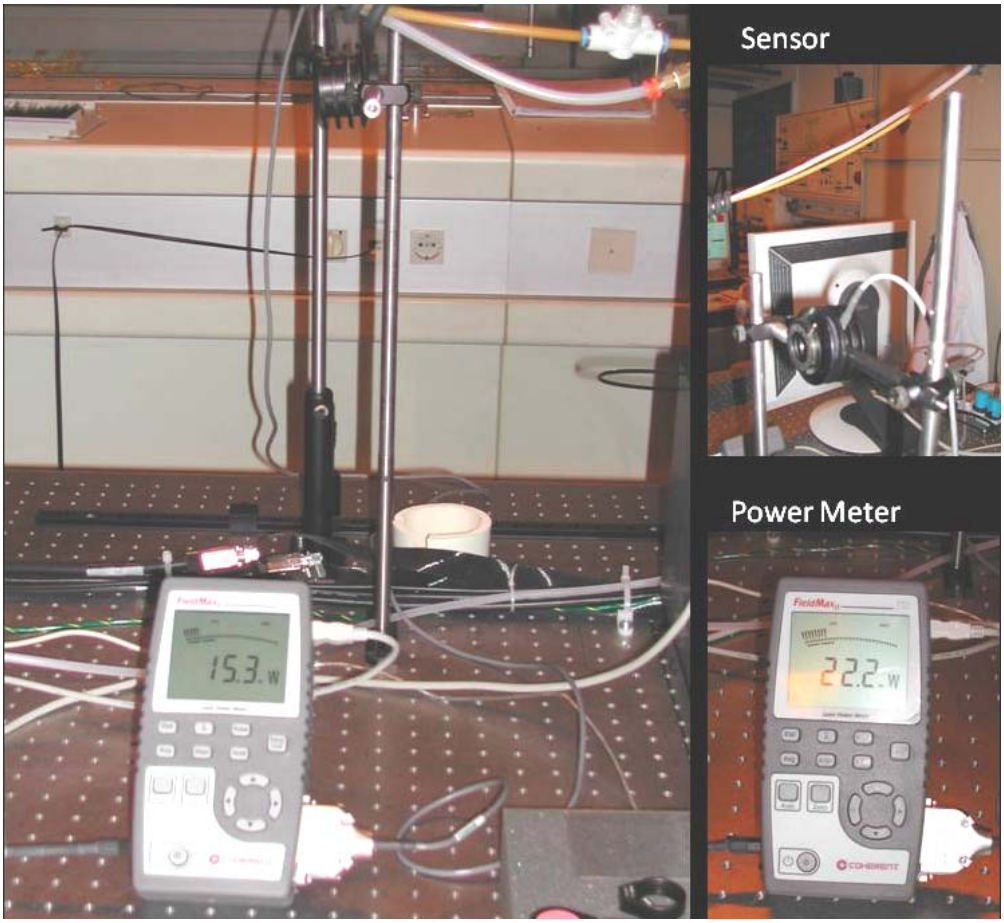

Figure 34: The power meter with a pyroelectric sensor

The power meter used was a Coherent Field Max II-P Laser Energy Meter. It used a sensor exploiting the pyroelectric effect. In general, these sensors create a temporary electrical potential as they are heated up by the laser beam. Pyroelectric crystals are ionic crystals with permanent polarisation. A temperature change causes the opposite faces of the crystal to charge oppositional, leading to a potential difference. Subsequently, the surface charge

gets compensated by charge carriers absorbed from the environment. Thus only abrupt changes in temperature - such as a temperature increase caused by modulated radiation - also cause a change in the electric potential. Using this sensor it was thus possible to filter out non-modulated disturbing background radiation.

The small changes in the electrical field caused by the sensor got amplified by the Laser Energy Meter. The measureable energy ranged from 1nJ up to 300J (Coherent, 2010). The device was connected to the computer via USB. Its control was integrated in the M3DL Software. A function describing the relation between the angle of the waveplate axis and the intensity of the reflected beamlet was created. As mentioned above, the power used for structuring was calculated from the difference of the intensity of the deflected beamlet to the maximum power, indicating the power of the "tunneled" beamlet.

7.5. The Axes

Figure 35: X- and Y-axissystem, type Aerotech ABL10150 (Arotech, 2009)

The X- and Y-movement was carried out by two Aerotech high precision air bearing axes (type ABL10150). The Y-axis was mounted on top of the X-axis as seen in Figure 35. The Z-movement was achieved by an independent Aerotech air bearing axis of similar type (type ABL10100), which carried the resin container. Each axis was driven by a linear brushless servo-motor. The maximum velocity was 3.78m/s, the acceleration limit was $10m/s^2$. The maximum load of the X-Y configuration was 10kg; the Z-axis was able to work under load of 15kg (Aerotech, 2009). This values where measured under normal loading conditions[14]. With Aerotech controls, a high accuracy linear encoder (type LN) and a special Hal calibration, the X- and Y-axis had maximum accuracy of 0.5µm; the Z-axis could access designated positions with an accuracy of 0.2µm.

[14] The normal loading condition is results as the load is attached to the stage with the center of gravity force positioned directly above the bearings. This leads to a moment arm of zero (Aerotech, 2009).

Rrepeatability[15] was 50µm for each axis. The resolution of fabricated parts was also limited due to standard fabrication errors of the axes, which caused a deflection of the incoming fs-laser beam. The deviation of straightness[16] and flatness[17] of one part of the axis system caused a positioning error in the other. According to the manufacturers, these errors were kept as low as possible. The difference in height between the two ends of a stage was 0.25µm with a maximum deviation of 0.4µm. The pitch[18] and yaw[19] of the X- and Y-axis was ±1.5arc-sec, respectively; the maximum error in the Z-axis was ±1arc-sec. A displacement error caused by two-dimensional angular errors would emerge for any position other than the centres of rotation (Aerotech, 2009).

7.6. Preparation of the microscope slide

The structuring was done upside down. The beam focus was positioned on the resin, which was carried by a microscope slide. This slide was moved along the Z-axis. To prevent the resin from flowing away, a coverslip was put onto the slide at a specific distance, specified by a piece of Tesa chemical resistant adhesive tape with a thickness of 120 µm. A piece of 48 mm wide tape was cut laterally, leaving two stripes. These stripes were bonded onto the slide such that they covered the top and the bottom (Figure 36 top right). The space in between constituted the building area, which was then filled up with a photo-sensitive resin. An injection needle was used to apply the resin onto the slide. As the coverslip was placed on top, it had to be ensured that there were no air inclusions in the resin. Figure 36 shows a photograph and a schematic drawing of the prepared slide. The adhesion force of the resin ensured that the coverslip did not fall down. The whole setup was adhered to the specimen holder of the Z-axis by a vacuum pump.

[15] Repeatability is defined as the range of positions attained when the system is repeatedly commanded to one location under identical conditions (Aerotech, 2009).
[16] Straightness is the deviation from the true line of travel perpendicular to the direction of travel in the horizontal plane (Aerotech, 2009).
[17] Flatness is deviation from the true line of travel perpendicular to the direction of travel in the vertical plane (Aerotech, 2009).
[18] Pitch is a rotation around an axis in the horizontal plane perpendicular to the direction of travel (Aerotech, 2009).
[19] Yaw is a rotation around an axis in the vertical plane perpendicular to the direction of travel (Aerotech, 2009).

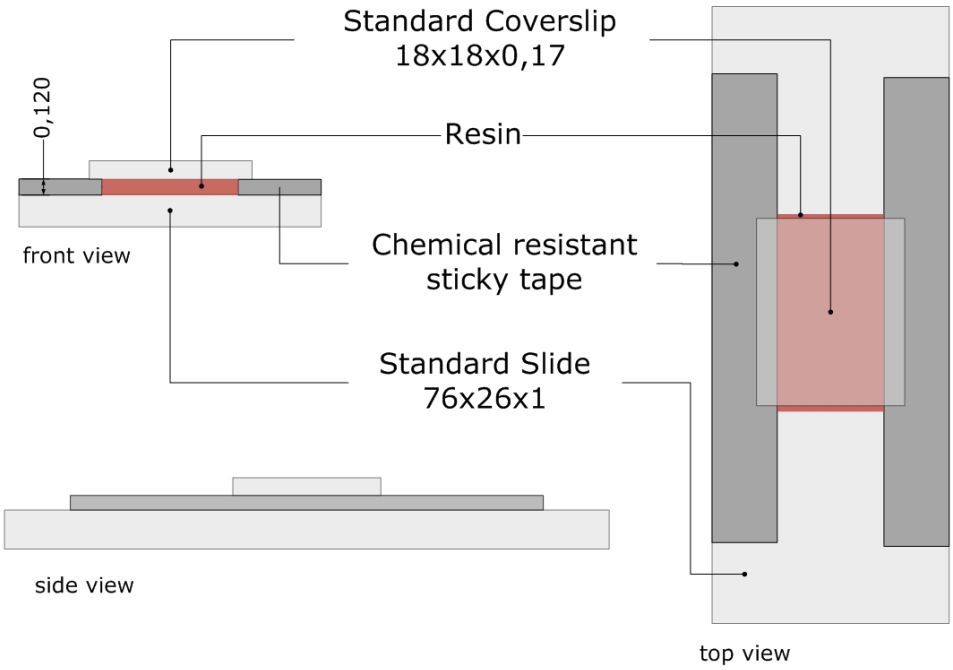

Figure 36: Preparation of the resin carrying slide for the structuring

7.7. The Mirror System

The mirror system had to ensure that in all positions of the X- and Y-axis, the beam met the object perpendicular to the slide. Therefore all mirrors behind the power control devices were mounted linked to the X-axis. Figure 37 is a schematic drawing and a photograph of the mirror system starting from the "tunneled" beamlet and ending in the objective is shown. It can be seen that the movement of the X- and Y-axis altered the distance between the mirrors responsible for the focus point movements. As long as the adjustment of the mirrors was correct and the beamlets between the mirrors were perfectly straight, no deviation of the voxel position emerged.

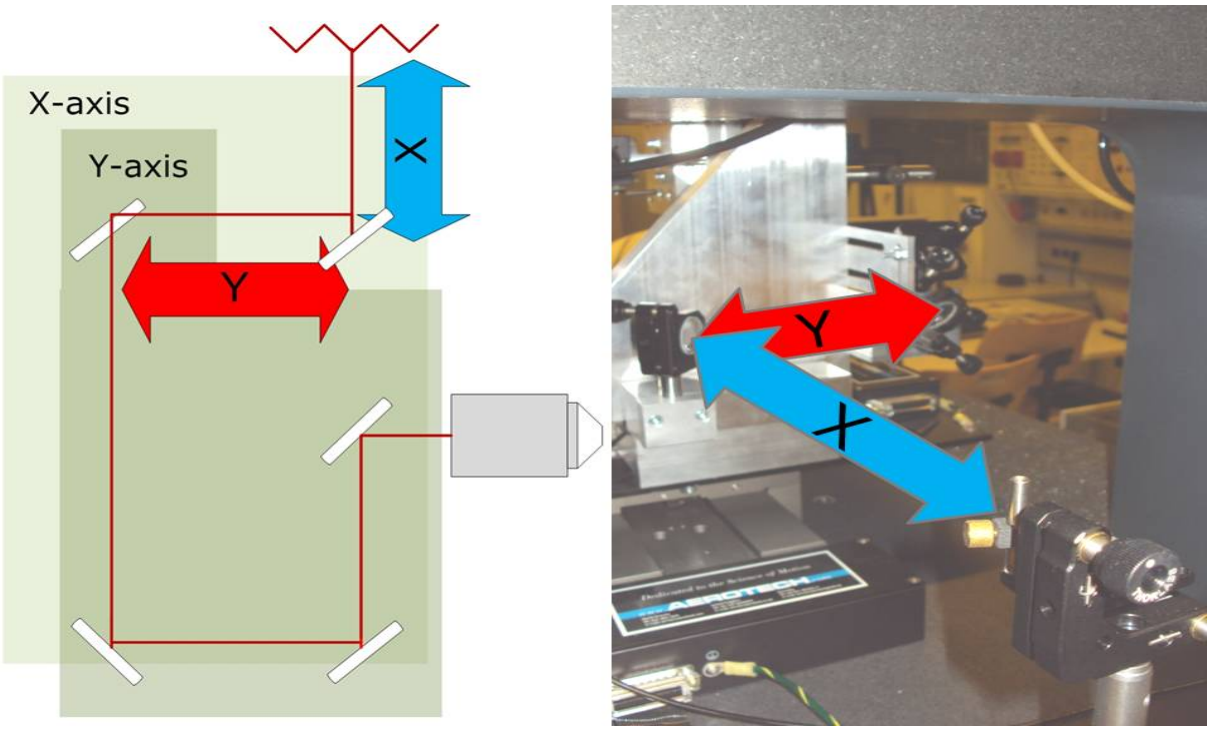

Figure 37: Distance changes due to the movement of the X- and Y-axis system

7.8. The Camera

Monitoring the fabrication process was necessary for two main reasons. The specimen had to stick on the slide, so it would not get washed away during the development. Therefore a part of the focal point had to be positioned so that half of it was positioned in the glass body of the slide during the fabrication of the first layer. This can be seen in Figure 38. The position of the focal point could be altered using the Z-axis or by turning a micrometer screw. Observing the structuring process live allowed us to assign the approximate process window[20]. The camera picture also gave us information on inadequate settings: too little power and/or too high speed resulted in little chance for two-photon-absorption taking place. Explosions of the resin were due to exceeding power and/or low speed.

[20] The process window is the range of feasible writing speeds and laser powers for the structuring process.

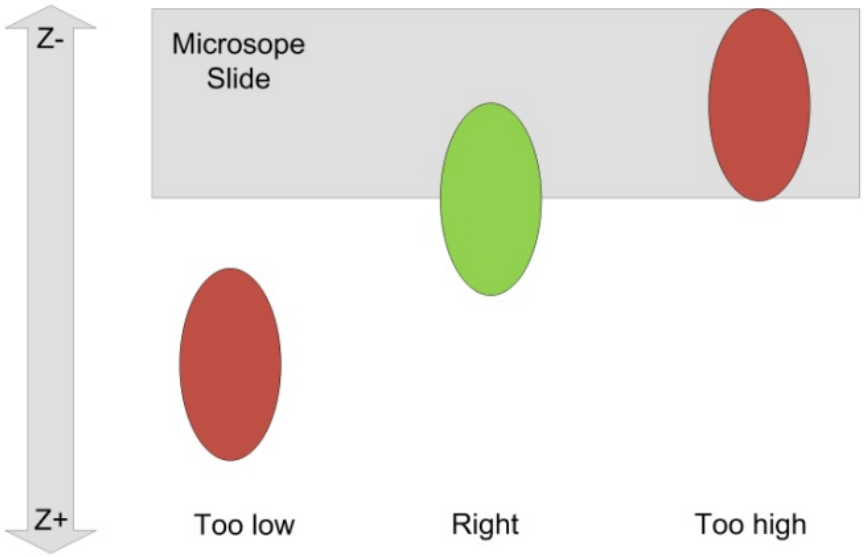

Figure 38: Positioning of the focal point for the fabrication of the first layer of a part

For observing the 2PP process, a high resolution CCD camera was mounted prior to the laser focusing microscope objective. To focus the beam and the camera picture in a desired position in the resin, it was necessary to mount a half-transparent mirror so that the laser beam got deflected and the camera could operate through the device (Figure 39).

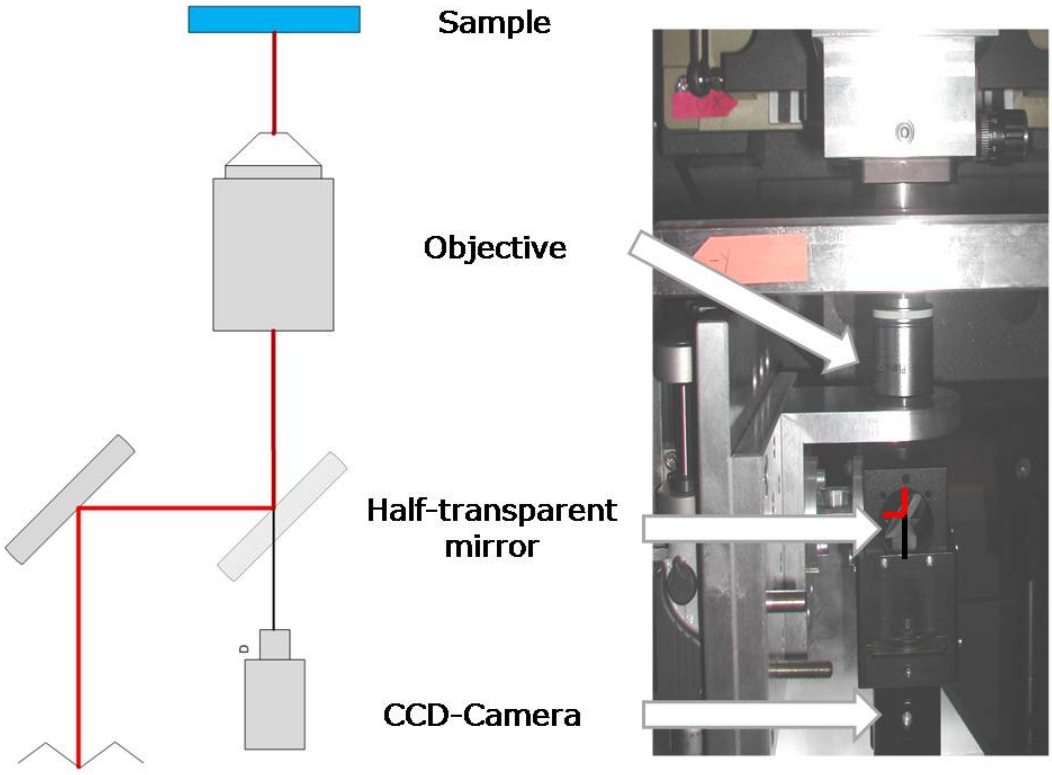

Figure 39: The half-transparent mirror

Figure 40: The CCD-Camera

The camera we used was a Watec WAT-902B monochrome camera with a ½-inch interline transfer CCD image sensor (Figure 40). The number of effective pixels was 768x494[21]. It had an internal synchronizing system and an unbalanced composite video output with 1V and 75Ω. The resolution was 570TVL[22], the minimum illumination was 0.003lux. The camera had an electronic shutter with controllable speed, an electronic iris, backlight compensation, AGC[23], gamma correction and a flickerless mode (Watec, 2010).

7.9. The microscope objectives

A microscope objective is generally comprised of lenses, and sometimes mirrors, mounted in a cone. The inside of this cone is black or corrugated to prevent scattered light disturbing the image formation. The key parameters of an objective are its focal distance and its magnification. A variety of applications use microscope objectives to produce an image of a specific object. Despite this common task, there exist a lot of different types with particular, very specific characteristics. The ideal objective is described as a collective optical system that *"produces a symmetrical diffraction limited image of an airy pattern from an infinitely small object point"* (Abramowitz, et al., 2003). The image plane is generally located at a fixed distance from the microscope objective front lens. Between this image and the lens, there is a medium of defined refractive index.

Depending on their intended use, objectives are fabricated to have specific characteristics. Thus they function well in the designed-for applications while

[21] The first value applies to the horizontal amount; the second value stands for the vertical number of pixels.
[22] When referring to fixed pixel displays or the resolutions of digital-television formats, the term "pixel" is correct. When referring to an analog television's horizontal resolution, the term "TV Line" (TVL) is more appropriate. This specification is the number of vertical lines the television can resolve per picture height (Harley, 2002).
[23] Automatic gain control is used to feed back an electronic output signal in order to adjust it to a appropriate level for a variety of input signals.

creating insufficient images in other. They come with various optical corrections for monochromatic[24] and polychromatic (due to light colour influences) aberrations. Selecting the right objective for the desired application, other characteristics like the field size and flatness, the transmission wavelength, the freedom from fluorescence as well as the birefringence and many other factors contributing to background noise have to be considered. The various types of microscope objectives are generally classified into achromates[25], fluorites[26] and apochromates[27]. In addition, some special types are named "plan", standing for low curvate and distortion (Abramowitz, et al., 2003).[28]

We will focus on three important specifications provided by the manufacturers; the magnification (M), the working distance (WD) and the numerical aperture (NA). M describes the ratio between the appearances of an object, observable through the objective compared to its real dimensions. WD describes the actual focal distance. The manufacturers specify two different WDs, one corrected for a particular coverslip designed for the objective; the other relating to the distance to an open specimen. NA is a dimensionless number. It describes the range of angles over which an optical system can accept or emit light. In microscopy, this value is calculated as the product of the refractive index *n* and the sinus of the half-angle of the maximum cone of light that can enter or exit a specific lens. The size of the finest detail to be resolved is proportional to the wavelength of light λ used in a specific application, divided by NA. Figure 41 provides a schematic illustration.

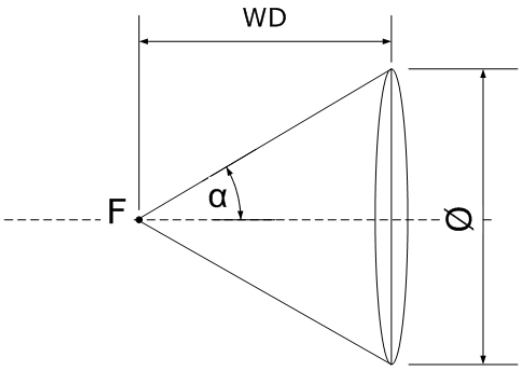

$$NA = n * \sin(\alpha)$$

$$Rsol = \frac{\lambda}{NA}$$

Figure 41: Schematic explanation of the numerical aperture (F…focal point; Rsol…resolution power)

[24] Monochromatic aberrations can be divided into spherical aberration, astigmatism, coma and distortion (Abramowitz, et al., 2003).
[25] Chromatic aberration corrected objectives (Global Spec, 2010).
[26] The hexagonal structure of the fluorite crystals allows objectives of this type to emit evenly refracted light. The crystal also allows correcting spherical aberrations (Schüngel, 2005).
[27] Objectives of this type expand the chromatic aberration correction to the IR and UV range (Schüngel, 2005).
[28] Rather than explaining all optical aberrations in detail, we refer to the informative website of Abramowitz et al. (2003), where all aberrations of microscope objectives are listed, explained and animated with small Java applications.

These variables, among others, profoundly influence the shape of the focal point, i.e. the voxel. For a sufficient structuring process, we are particularly interested in round shaped voxels. At this point we can draw parallels from a more developed scientific field. Kuba & Nakayama (1998) tested various microscope objectives for their applicability for the imaging of Ca^{2+}-sensitive probes with a two-photon laser-scanning microscope. In their work they used a Ti-sapphire laser with a pulse rate of 85Mhz and a wavelength of 700nm. Their findings prove that the brightness of the images of the examined beads greatly varied mostly depending on the NA of the objectives used. The lateral dx and axial dz resolutions were defined as the half-decay length of the fluorescence intensity. The authors took a reference image of a spherical bead using a microscope objective with a 40x magnification and a NA of 0.75. The sizes of the fluorescing spots were 0.12 and 0.42μm in 0.3μm and 5μm beads, respectively. Their findings show that dx linearly increased with 1/NA, whereas dz linearly increased with $n/(NA)^2$ except for an objective with large NA (1.3). The respective graphs are shown in Figure 42.

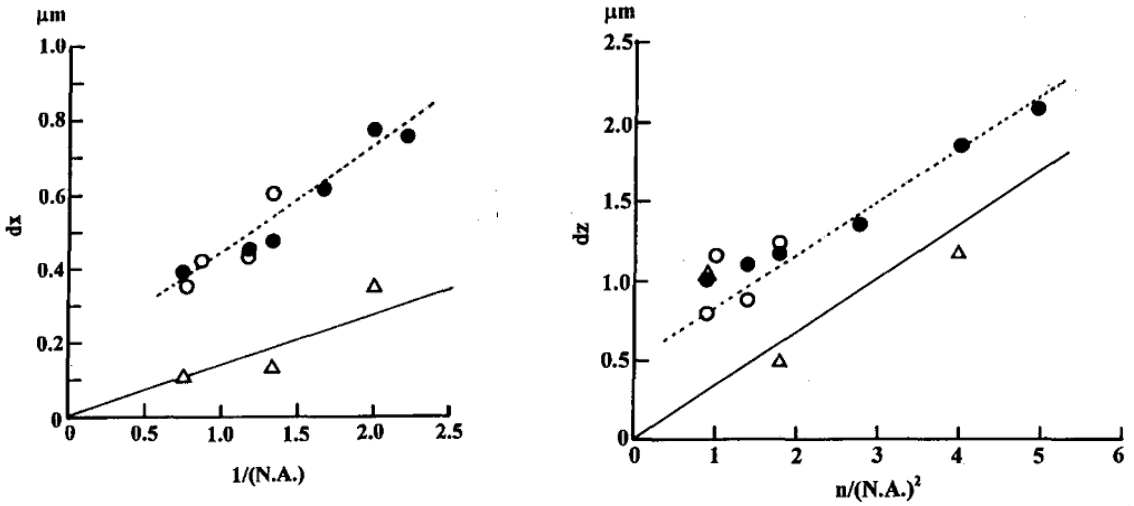

Figure 42: Left picture: Relation between dx and the inverse of NA. 5μm beads; infinite focal length (closed circles);finite focal length (open circles); 0.3μm beads (triangles). Straight line calculated; interrupted line estimated, Right picture: Relation between dz and $n/(NA)^2$, same symbols (Kuba & Nakayama, 1998).

The transmission efficiency[29] and the group delay[30] dispersion (chirping) effects were also heavily dependent on NA values (Kuba & Nakayama, 1998). The laser power caused an expected linear increase of the fluorescence with a rise of the square of the average laser power using any objective (Figure 43) while the fluorescence measured largely varied with different objectives. However, the

[29] The transmission efficiency was measured by recording the intensities of the laser beam with and without objective and collimating planconvex lenses in the laser path (Kuba & Nakayama, 1998).

[30] Group delay is the retardation of a signal caused by the transit through a specific device under test. It is measured versus frequency. The group delay dispersion is the frequency dependency of the group delay, or (quantitative) the corresponding derivative with respect to angular frequency. It is specified in fs^2 or ps^2 (RP Photonics Consulting GmbH, 2008)

authors found a rough proportionality to the product of the fraction of light (1-cos(α))/2 collected by an objective, and to the third of the transmission efficiency of the objective (T). As shown in the right picture of Figure 43, the 100x magnification, high NA, oil immersion microscope objective did not review any such dependence. According to the authors, this is due to a strong group delay dispersion[31] affected by the oil.

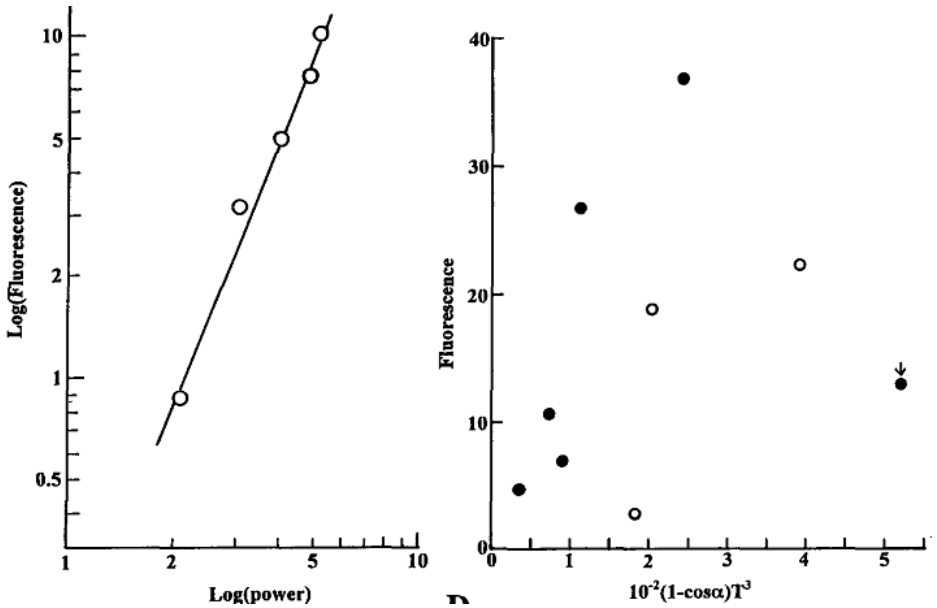

Figure 43: Left picture: relation between fluorescence intensity and the square of laser power; Right picture: relation between fluorescence intensity and the product of aperture angle and the third of transmission efficiency of objectives. 5µm bead; infinite focal length (closed circles); finite focal length (open circles); Point with arrow: oil-immersion objective type CF fluor/oil M 100 NA 1.3 (Kuba & Nakayama, 1998).

Obviously, the extent of the coverslip thickness compensation drastically affected the X-Z scanned image formation of the 5µm bead. At constant laser power (1.5W) the extents of compensation for the best circular shape of the fluorescing spot differed among all objectives. Generally, the purpose of such compensation is to preserve the focal plane of non-paraxial rays by reducing or eliminating the additional path length produced by a coverslip that has a different refractive index than the medium between the objective and the examined specimen. Kuba and Nakayama (1998) claim that this correction has to be made at each Z-level to completely eliminate the spherical aberration caused by this effect.

For the applications of Kuba and Nakayama (1998), objectives with a large NA of high magnification appear to be suitable to create a focal spot of circular shape. Yet a serious spherical aberration emerges as the refractive index of the immersed objects under study strongly differs from that of the coverslip.

However, two-photon laser-scanning is a different application than 2PP. The laser power used is much higher and the specimens have different refractive indexes

[31] The group delay dispersion is the derivative of the group delay with respect to the angular frequency. The group delay is a measure of the time delay experiences by narrow-band light pulses in an optical device (RP Photonics Consulting GmbH, 2008).

and are not homogenous in their optical properties. In addition, the wavelength of the laser beam used in the above studies is different from the wavelength used in this work (700nm and 800nm, respectively). Nevertheless, we can roughly classify and benchmark the objectives available for the structuring with M3DL. The findings allow us selecting approximate writing parameters. Of special interest is the influence of the NA on the shape of the fluorescent spot. For a rough approximation we can assume that the spot size dependencies outlined by Kuba and Nakayama (1998) correspond to the voxel shape. This may help estimating the impacts of an objective change, a power increase and/or a change in exposure time, and can help to decide the installation of appropriate optical correcting devices.

Figure 44: Available objectives for the structuring with M3DL

Two objectives were available for structuring with M3DL; one with a 20x magnification and one with 100x with NA 0.4 and 1.35, respectively. The 20x "LD Plan Neofluar"[32] objective was manufactured by Carl Zeiss. According to product specifications, this objectives had an extra long working distance (8.4-7.4mm). Using an installed correction collar, the objective could be adapted to various optical conditions like coverslip compensations in the range from 0 to 1.5mm. The field of view was 25mm and its parfocal length[33] was 45.06mm. The transmittance for light of 800nm was approximately 85% (Carl Zeiss, 2005-2006). A photograph of the objective can be seen in the left image of Figure 44.

The 100x objective was also fabricated by Carl Zeiss and was of the "Plan-Appochromat" type. It provided high resolving power, colour purity, contrast and image flatness. According to the manufacturers, it was designed for the use in fluorescence applications. The working distance was 0.17mm, corrected by a coverglass thickness of another 0.17mm. Immersion oil had to be applied between the objective lens and the coverslip. The image diameter (field of view) was 25mm. The parfocal length was 45.06mm and approximately 72% of the NIR light of 800nm was transmitted through the device. A photograph of the objective can be seen in the right image of Figure 44.

[32] In this context, "plan" refers to an installed correction of the field of curvature aberration.
[33] In the specified range, the focus remains constant as the focal distance is changed.

7.10. The Control

The X-, Y-, Z- and the rotary waveplate axis were plugged to an Aerotech A3200 digital automation platform (Aerotech, 2010). This platform featured a software-only controller (Nmotion SMC) in charge of the axis motion control. Position, velocity and current loop closure were handled by the network drive, trajectory generation was done in the PC using a real-time operating system running with a higher priority than Windows. The PC executed the tasks and sent the results to the network drive via FireWire. The Nmotion SMC offered a programming interface that could be accessed with a variety of programming languages (C, C++, Visual Basic, AeroBasic). It converted information fed in from other PC programs into movement parameters. Doing that, the Nmotion synchronized the axes with the data input from the PC. Data such as process parameters, loading conditions of the axes and acceleration were collected and taken into account as the movement was calculated.[34]

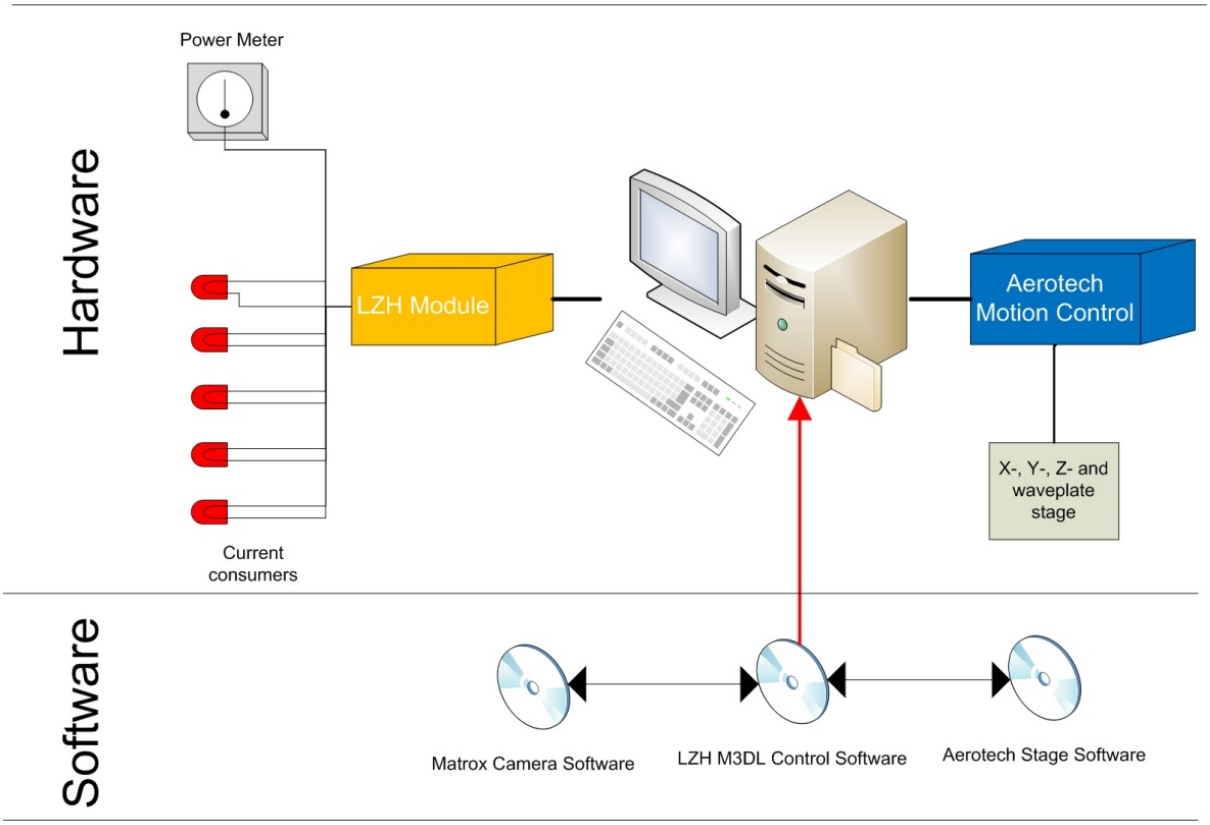

Figure 45: Hardware and Software of M3DL

The movements could be controlled with the Nview human-machine interface installed on the control PC. It combined a system analysis tool with plotting utilities, an axis parameter editor, an input/output controller and a diagnostics tool. This software could be used to control the axes manually and to alter their processing parameters. Under normal conditions the Aerotech control device was

[34] For more detailed information about the Ndrive see (Aerotech, 2010).

actuated by a Visual Basic program provided by LZH. In addition to axes control, this software tool also provided control of the AOM, collected the data from the laser power meter and accessed the software of the CCD-camera[35]. Five regulators (1-5V) for current output could also be adjusted using this tool. Figure 45 provides a schematic view of the software and hardware modules of M3DL and their inter-connections.

7.10.1. M3DL control software

In addition to the manual control of the axes, the control software provided a program for the structuring of standard scaffolds, STL files, dotted lines, voxel tests and parameter search. Moreover, external programs written in G-code[36] could be integrated and processed by the M3DL software. We will focus on the fabrication of standard scaffolds and the structuring of STL files as well as on conducting voxel tests.

Figure 46 is a screenshot of the main window of the software. The standard programs could be accessed via pushing the "Standard Programs" button in the menu bar. External programs were also accessible via the menu bar. Under the menu bar, the camera picture is displayed. At the time the screenshot was taken, a couple of scaffolds were fabricated, to be seen at the bottom of the live view window. With the commands on the right side, the camera image could be adjusted. It could be turned on and off with the "Start Grabbing" button and also be zoomed and panned using the scroll bars. Videos and pictures could be captured and stored in a created folder via the "Capture Video" menu.

[35] The camera image was digitized by Matrox Imaging library, separate software written in C++ (Matrox, 2010).
[36] G-code is a modification of CNC-Code developed by Aerotech.

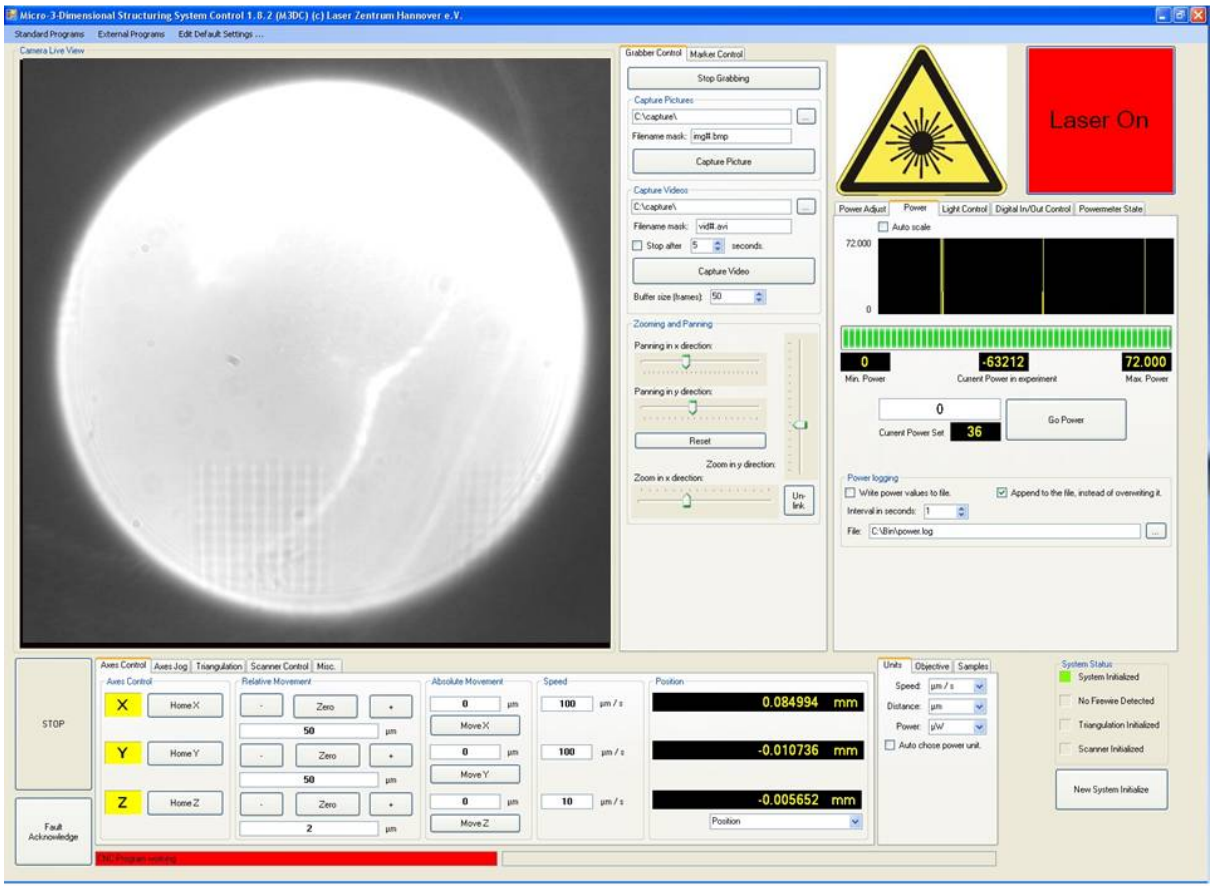

Figure 46: Main window of the M3DL control software

On the right hand side of the camera control, the laser control is displayed. With the button "Laser on" the AOM was accessed. Using this command, the resin-impinging laser beam could be switched on and off. Right below this command, the laser power could be adjusted. At the time Figure 46 was taken, the "Power" tab was open. The desired intensity could be typed in the white field below the recorded graph of laser powers (at the time 0 was displayed in this field). As soon as the "Go Power button" was pushed, the axis would move to a specific angle, polarizing the laser beam in a way that only needed intensities arrived at the objective. As the waveplate had no particular home position, it needed to be calibrated every time the software was started. For this adjustment, the tab "Power Adjust" could be used. In general, there were two different possibilities to calibrate the power device; the manual and the automatic way. The first step of the manual approach was to find out the maximum power measured after the AOM. This could be found out turning the waveplate axis so that the beam was polarized and completely deflected to the power sensor. Subsequently, the axis was rotated until only half of the maximum was displayed on the power meter. This power value was then typed into the software. As a final step, the "Accept" button was pushed (Figure 47). However, the resulting function was not very accurate as it was only based on three measurement points (maximum, half and zero intensity).

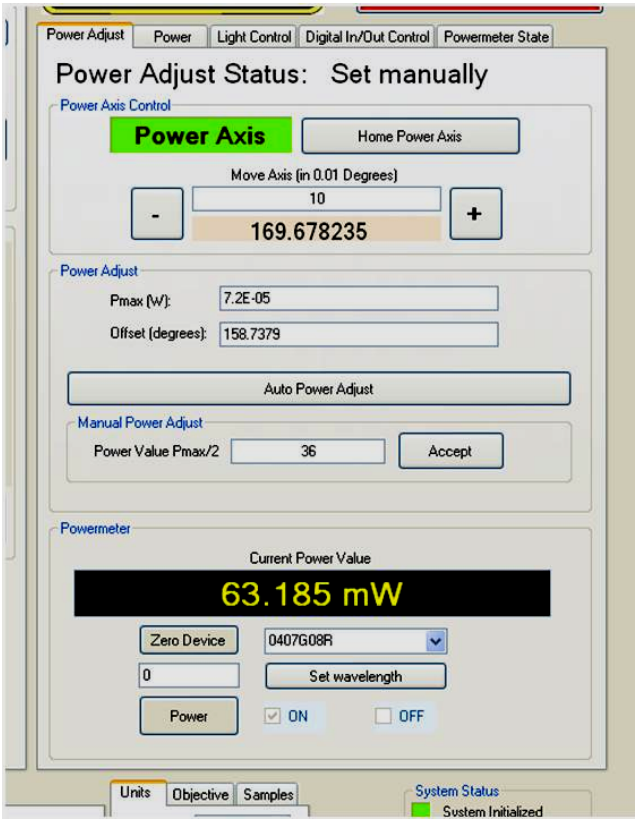

Figure 47: Power adjustment

The automatic calibration created a function based on 60 values. For more accuracy, the waveplate was rotated 720° to calculate an entire sinus function with associated intensity values. The function is displayed in Figure 48. The "Auto Power Adjust" process took approximately a quarter of an hour.

In Figure 47 an additional tab can be seen: "Light Control" was designed to control five additional current users, for example LED light sources needed for an illumination of the specimen (Figure 27) necessary for a proper camera picture.

Using the commands in the lower area of the main window in Figure 46, the X-, Y-, and Z-axis could be manually moved. Speed and distance could be controlled in different units. The "Stop" and "Fault Acknowledge" button ensured that the operation could be terminated manually in case the parameters did not result in a satisfying structuring process. Using, the tab "Triangulation" the position of slides not oriented perfectly orthogonal to the laser beam could be corrected. The axis was moved in three different positions. In each, the position of the focal point was determined so that half of it stayed in the slide.[37] After the positions were determined, the software calculated a correcting function in order to guarantee orthogonality of the slide in relation to the surface of the clamp. As the structures in this work were of small size, we did not use this compensation. For the fabrication of structures with larger size it is definitely recommended.

[37] For more detail see chapter 7.8 "The Camera".

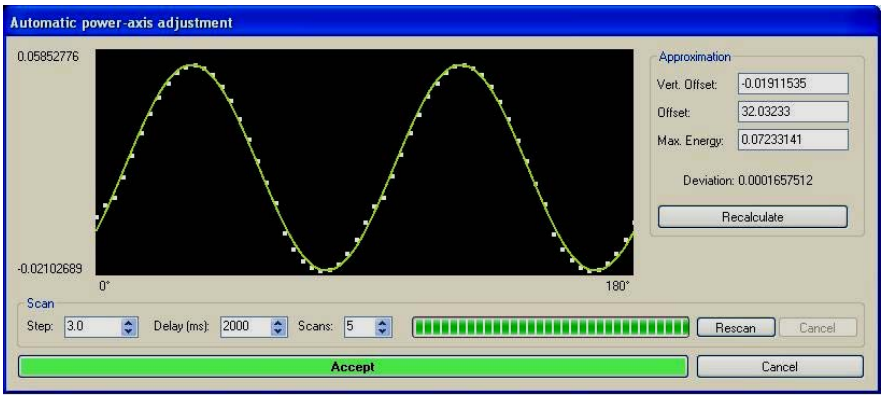

Figure 48: Automatic power adjustment

The standard programs used were "Photonic Crystals", "STL files" and "Voxel". With the help of "Photonic Crystals", an array of standard scaffolds with different sizes, hatch distances, layers, speeds and power settings could be fabricated. These factors could be altered within the array as well. Figure 49 shows that the number and extent of the changes, as well as number of scaffolds and the distance in between them, could be adjusted.

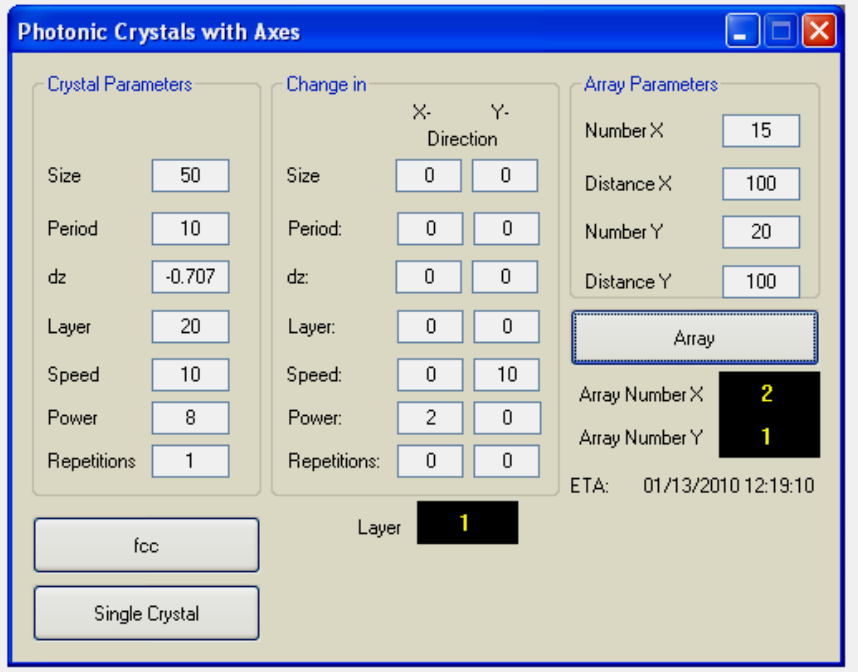

Figure 49: Standard program "Photonic Crystals"

STL files were built using the standard program "STL files". This software tool sliced an STL file into layers according to the value typed into the field "Step" (Figure 50). This value indicated the distance between the layers fabricated. The computer automatically calculated the number of slices with respect to the "Step" value. Adjusting the "Slice direction" determined the beginning and the direction of the slicing process. Thus the CAD file could either be sliced upside-down or bottom-up. After pressing the button "Slice STL file" the process speed could be adjusted. In addition, the distance between the X- and Y-hatches could be adjusted separately. The function "Separately Write Contour first" allowed

structuring a surrounding layer around the part under fabrication. During this process, the outline of the CAD file was retraced in order to form a nicely shaped, solid part.[38] The "Writing direction" buttons determined whether X- and Y-hatches were built up in the same layer ("X and Y") or in different layers ("X or Y"). Setting the tick to "only X" or "only Y" led to the fabrication of solely X- or Y-hatches in every layer. We only used the setting "X or Y".

The "Hatch direction" determined whether the next slice was built above or below the previous one. Using this function, the parts could either be fabricated sticking to the top cover of the resin, i.e. the microscope slide, or adherent to the bottom, i.e. the coverslip.

Prior to the fabrication process, a choice has to be taken between two modes of reconciling differences between the travelling speed by which the object is approached (laser off) and the writing speed during the polymerisation process (laser on). Under the function "Woodpile Hatch", acceleration or deceleration from travelling speed to writing speed took place with the laser turned on. In other words, the objective moved to an assigned point, where polymerisation was intended to start, the beam was turned on and only then the objective accelerated or decelerated to writing speed, i.e. under the polymerisation process. Under the function "Fast Hatch", acceleration/deceleration took place before the objective arrived at the assigned point of polymerisation start, i.e. during the travelling process with the laser beam off. This caused an effect which we will discuss later. After choosing one of the modes, the 2PP process parameters were calculated according to the specifications. Unfortunately, "Fast Hatch" was not available for this work but will be available soon, according to the programmers of the M3DL software.

As a last step, the power at which a part should be fabricated could be adjusted. Using the tab "Array(dPower)" several objects of the same type but with different laser intensities could be structured. It was again possible to adjust the space between the structures to be fabricated. Unfortunately, a change of speed, hatch distance and step within one array was not possible since. The whole 2PP process was dependent on these parameters. If several structures were fabricated in one array it would have been necessary for the software to calculate process parameters for each structure separately. This would probably be a useful modification for a new version of the software.

[38] See chapter 10.1 "Structuring Parameters with the 100x microscope objective".

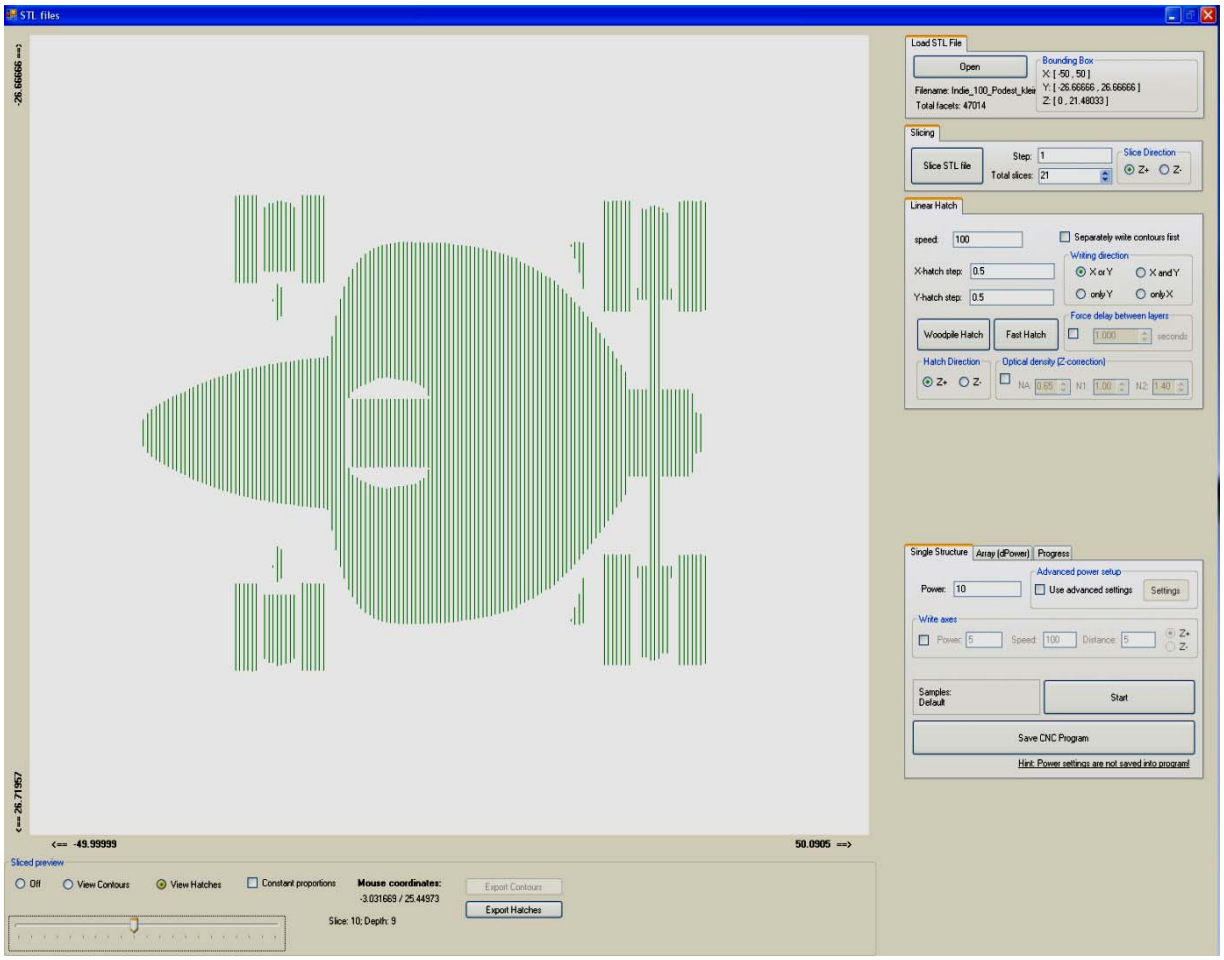

Figure 50: Standard program "STL files"

The last tool we used during the experiments was the standard program "Voxel" (Figure 51). Similar to the tool "Photonic Crystals", this program allowed changing the number of structures, the space between them, the power at which they were fabricated, the travelling speed as well as the number and extent of the changes in the X- and Y-direction. An additional parameter was necessary for building a field of voxels. "Shot time" indicated the time the resin was exposed to the specified power. For an analysis of the voxel length, the "z-Start Position" as well as the extent of the Z-position change (dz) could be defined.[39]

In addition to creating a voxel field with parameters changing, other voxel fields could be specified with the same changes in their parameters but starting from different base values.

[39] A detailed explanation of the experiment "voxel test" is provided in chapter 10.2 "Structuring Parameters with the 20x microscope objective".

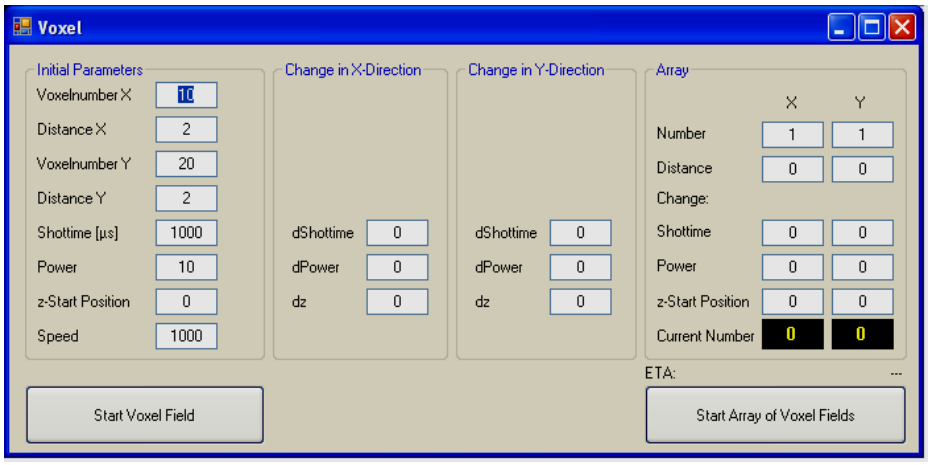

Figure 51: Standard program "Voxel"

8. Modifications of the setup

For our experiments it was necessary to adapt the setup slightly. As the worms were embedded in the resin, they moved a lot and it was hard to set the focal point so that the worm would be captured in the structure. At lower temperatures, worms of the species C. elegans get slower until they stop moving at temperatures below 0°C. For the fabrication process, only little movement of the animal was acceptable. For this reason the target was to construct a clamp for the microscope slide allowing to lower the temperature of the resin below 5°C. This clamp should also be able to illuminate the resin to get a better camera picture. Initially, the quality of the live picture was not satisfying. The difficulty was to make sure that the vacuum pump clamping the slide to the Z-axis functioned properly. Thus, a hole had to be drilled through the clamp. A constructive problem arouse as the position of the light source had to be kept in the centre of the clamp. This was necessary for a proper camera picture[40]. A solution was found that could be fabricated on an additive manufacturing machine available at the Institute of Material Science and Technology at the Vienna University of Technology. The layer-by-layer fabrication method of Objet EDEN 250[41] allowed the build-up of a small frame for a 3mm LED inside the hole drilled for the vacuum exhaust. The current cables were plugged to the LED through a small access hole fabricated orthogonally to the hole for the vacuum exhaust (Figure 52).

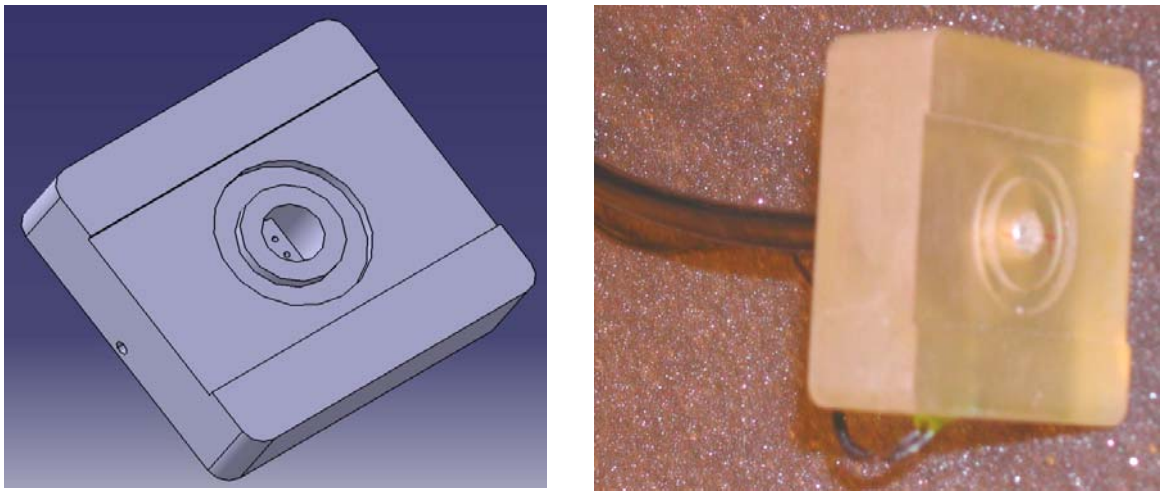

Figure 52:Slide clamp prototype

[40] In the beginning, we used a considerable number of mirrors for focusing both, camera picture and laser beam to the resin. Unfortunately the mirrors did not only reflect the camera picture and the laser beam to a 90° angle. A small share of the beam and the surrounding light was reflected backwards, towards the camera. This created a disturbing incidence of light inside the camera, to the effect that we could hardly adjust contrast and brightness.

[41] More information about Objet EDEN 250 can be read at http://www.objet.com/3D-Printer/Eden250/

The vacuum pump and the clamp were connected through a tube attached to the underneath of the part using two-component adhesive. After the current cables were attached to the 3mm LED, the additional space between the walls of the access hole and the current cables were sealed with silicone.

After a position change of the camera accomplished by Dipl.-Ing. Klaus Stadlmann, the live picture could be improved considerably, suppressing the disturbing incidences of light in the camera picture almost totally. In Figure 53, the camera pictures before and after the modification are shown.

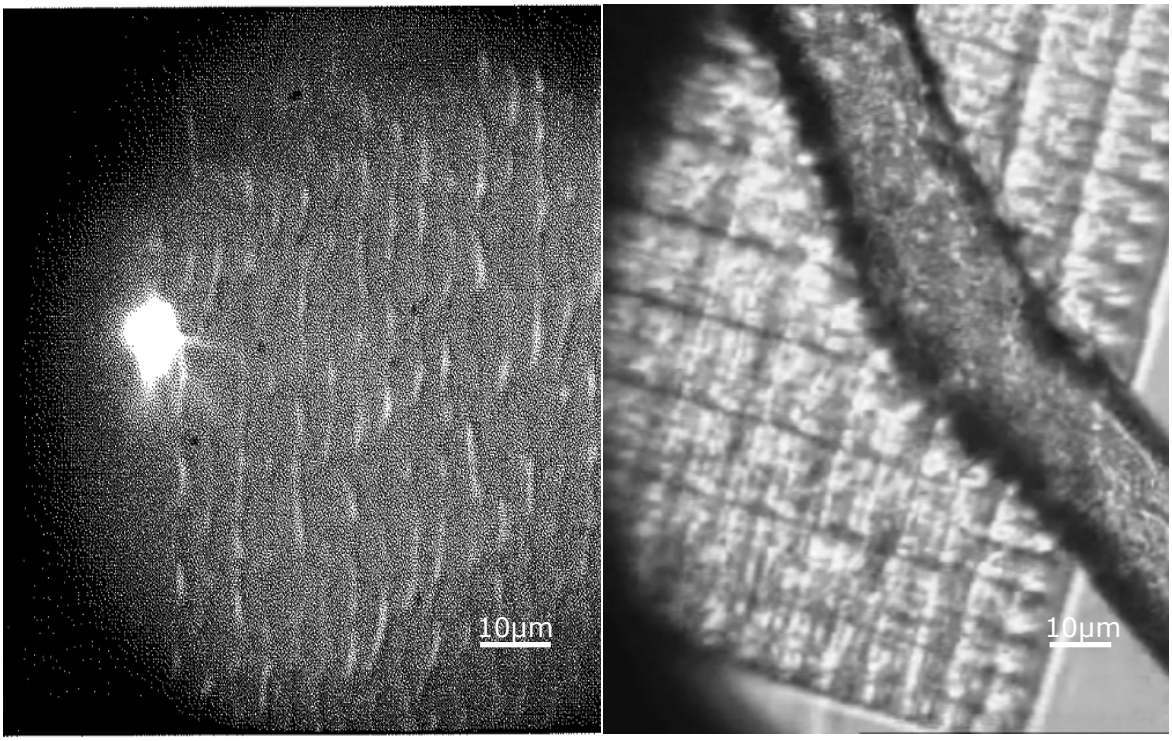

Figure 53: Camera pictures before (left) and after (right) the modifications on the camera setup

The prototype clamp fulfilled the expectations. It served quite a long time as a standard for all structuring processes. However, cooling could not be accomplished using the prototype as the available polymeric material for the additive manufacturing machine, FullCure 720, did not conduct heat and would deform if exposed to higher temperatures. Therefore the heat produced by the cooling device would not be diverted away from the specimen. An aluminium clamp had to be designed. In order to manufacture the clamp as a swivel, it was designed being round (Figure 54).

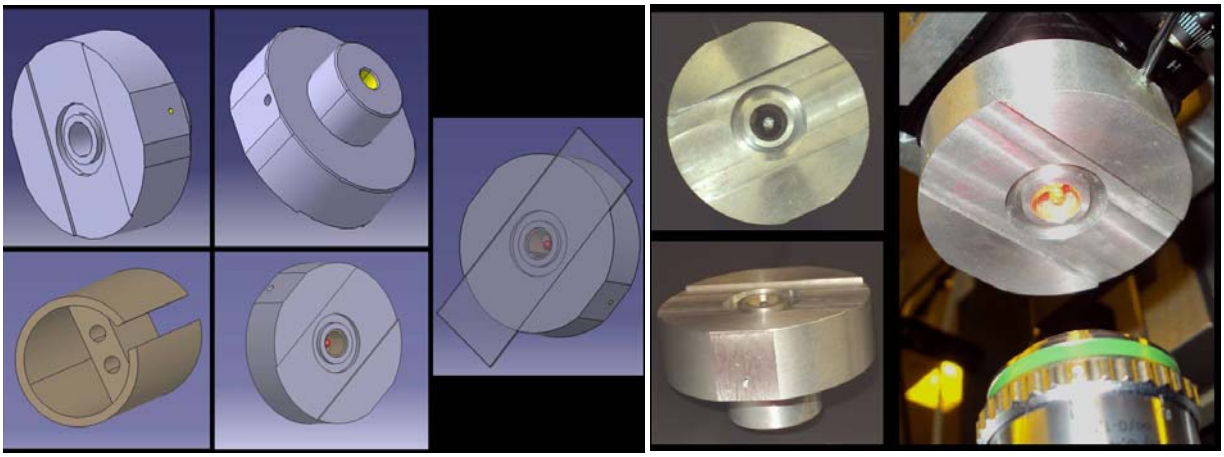

Figure 54: CAD file and photos of the aluminium clamp without cooling device

The specimen illumination apparatus was based on the prototype. Yet a separate LED holder was designed and manufactured using the Objet EDEN 250. A 3mm LED was plugged into the holder. The current cables were soldered to the wires and plugged through a hole drilled orthogonally to that of the vacuum exhaust. The hole was again sealed with silicone. In this state of assembly the part replaced the prototype as the standard clamp for all structuring processes.

To cool down the sample, an additional sheet crawl was used. It attached the hot side of a Peltier-Element type RH 1.4-32-06L from Melcor to the aluminium clamp[42]. The heat was dissipated as the clamp, its socket and the Z-axis conducted heat. A synthetic connector provided access to the vacuum-exhaust needed for the attachment of the slide. This ring-shaped part was manufactured using the Objet EDEN 250 and could be plugged into a specially designed slot on the clamp (Figure 55).

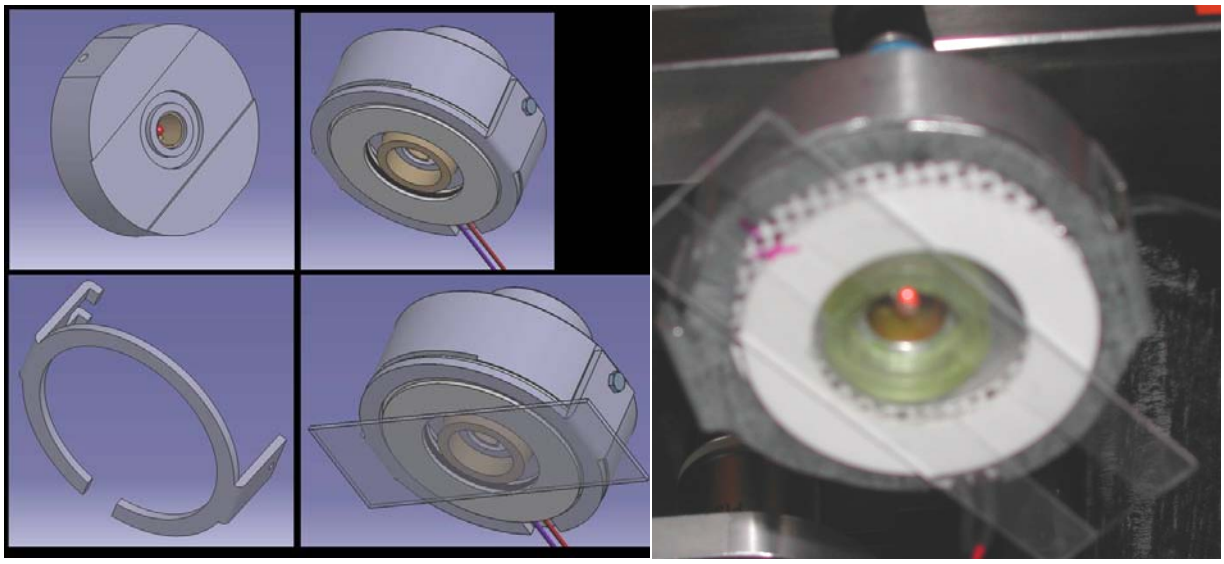

Figure 55: CAD file and photo of aluminium clamp with cooling device

[42] For more details see http://www.knap.at/datenblaetter/pel/pel_mel_ctrhole.pdf

The change in temperature was checked using a slide carrying a drop of water and a temperature sensor. The device cooled down the water to 15°C within 5 minutes. Unfortunately, the heat on the hot side of the Peltier-Module was not sufficiently dissipated by the body of the Z-axis. After 10 minutes, the water was actually heated up instead of cooled down. For future experiments it is therefore necessary to integrate an adequate heat removing device. A water cooler could ensure that the temperature on the hot side of the Peltier-Module was kept on a constant level.

9. Stress response in C. elegans caused by infrared laser

Biological tissue is very transparent to red and IR light as everyone knows who has been shining with a flash-lamp through his hands. A relatively new technique, optical tweezering, takes advantage of this fact. In particular living cells inside a biological tissue can be manipulated without mechanical contact and independent from their position. In this application, a focused near-infrared laser beam gives rise to forces that make possible the optical trapping and the manipulation of a variety of micron-sized objects, including cells and organelles (Ashkin, 1997). These microscopic dielectric objects are moved by attractive or repulsive forces caused by a strong electric field gradient in the narrowest region of the focused laser beam (beam waist) (Moffitt, Chemla, Izhaky, & Bustamante, 2006).

However, IR light exerts a powerful influence on the temperature of the spot it is shining on. This is due to the fact that this light, emitted across the visible spectrum, is a part of heat radiation. Depending on the refractive index of particular substances, larger or smaller parts of the light get absorbed and transferred into heat. The soothing warmth coming from within the body during a visit in an infrared cabin derives from the IR light that is penetrating the skin and warming up the whole body.

Nevertheless, too high intensities can cause damage at the cellular level. Laser irradiation can damage proteins directly by heat (denaturation[43]) or indirectly by generating free radicals, which can give rise to oxidative damage. In general, cw-lasers (continuous-wave-lasers), as well as pulsed lasers in the IR range, can generate light intensities in the tens of megawatts per square centimetre range due to diffraction-limited focusing. These intensities can cause significant temperature increase and can give rise to harmful photo-chemically induced processes (Vorobjev, Liang, Wright, & Berns, 2993). This results in the disruption of cell activity and can lead to cell death.

Optical trapping, done intercellular or in the interior of living organisms requires considerably high laser powers in the range of many hundreds of milliwatts (Leitz, Fällman, Tuck, & Axner, 2002). This is due to the high viscous resistance of the cytoplasm or the extra-cellular matrix. Similarly high laser intensities are necessary if forces inside biological systems are to be measured by optical tweezers. Therefore the authors investigated the potential damage high laser powers can cause to the object under study. A transgenic strain of C. elegans

[43] Denaturation is a process in which proteins or nucleic acids lose their secondary (three dimensional form of biopolymers) and tertiary (3-diemensional structure defined by the atomic coordinates) structure (Ophart, 2003). This is caused by an external stressor or a compound such as acid, base, inorganic salt, organic solvent or heat.

(PC72) was used as a sensor device to respond to the external stress caused by the NIR cw-laser beam implemented in their setup. This strain of the model organism carried a reporter gene (E. coli lacZ) that is under the transcriptional control[44] of a specific heat shock protein. Under the influence of external stressors this gene promoter activates the transcription of lacZ, which leads to the production of β-galactosidase protein. This protein, in turn, could be detected in situ by histochemical staining.[45]

In order to immobilise the worm, the authors used levamisole (L[-]-2,3,5,6-tetrahydro-6-phenylimidazo{2,1-b}thiazole from Sigma-Aldrich) as anaesthetic. A liquid drop consistent of 4µl of 0.5mM levamilsole in M9 buffer[46] was placed onto a 0.5mm layer of 3.0% agar noble flattened out on a microscope slide. Single worms were selected and put into the drop. The sample was covered with a thin coverslip and transferred to the optical tweezers setup. The beam emitted by an argon ion laser-pumped titanium-sapphire laser with a tuning range from 675 to 980 nm and a maximum power of 2.3W was directed through an inverted microscope and focused by a high numerical aperture microscope objective (Magnification 100x/ NA 1.35) (Leitz, Fällman, Tuck, & Axner, 2002).

For wavelengths in the range of 700-850nm, the objective transmission varied between 48% and 67%. The laser power was adapted so that the exposed intensities were constant throughout the examined range.

The laser radiation was focused on the large excretory cell near the pharynx. Its nucleus was drawn into the centre of the focal point. The depth of the focal region depended on the animal's position and the position of the excretory cell within the animal and amounted to approximately 10 µm. After the exposure the animals were put on a NGM[47] petri-dish with separate, thin and spread out areas of E. coli OP50[48]. The animals were allowed to recover 1-4 h and were then transferred into a small droplet of M9 buffer on a diagnostic microscope slide. Control animals were mounted in the same way and were then either heat-shocked at 37°C for 1-2 h or not exposed to stress at all. For staining the animals were cryofixated by bringing them rapidly in contact with a -76°C cold aluminium block. Then they were dried and made permeable with cold acetone and assayed overnight for β-gal activity in a humidified chamber in the dark (Leitz, Fällman, Tuck, & Axner, 2002).

---

[44] This means that hsp16 turns on and off the expression of the gene.

[45] Histochemical staining is used to give contrast to biological tissue as well as to highlight particular features of interest (Cobweb, 2009)

[46] M9 buffer consists of 3ml KH_2PO_4, 6ml Na_2HPO_4, 5ml NaCl per 1l H_20. After filling the liquid in an autoclaved basin, 1ml $MgSO_4$ is added.

[47] Nematode Growth Medium; A medium consistent of 12g NaCl, 64g Agar, 10g Bacto-peptone and 4l distilled water is prepared. This medium is then flattened out on an autoclaved petri-dish together with 4ml cholesterol, 4ml 1M $MgSO_4$, 4ml 1M $CaCl_2$ and 100ml 1M KPO_4 (ph 6.0) (Wood, Basic culture methods, 1995).

[48] OP50 is a uracil auxotroph of *Echerichia coli* bacteria (Pyrmidin Base) whose growth is limited on NGM plates. It is used as a limited bacterial lawn and is desirable because it allows easier observation and better mating of the worms (Stiernagle T. , 2005)

The temperature sensitive hsp16-lacZ transgene's activation temperature is between 29°C and 31°C (Stringham, Dixon, Jones, & Candido, 1992). A stable expression is achieved at 33°C. The background temperature in the experiments of Leitz et al. (2002) was 25°C. For the activation of the hsp16 promoter a temperature increase of 4-6°C was required. Figure 56 shows that the illumination by 360mW of light in the 700-850nm region caused temperature increases ranging between 0.7°C and 4.1°C, with the highest temperature increase for the longest wavelengths and the lowest for the shortest. In addition to gene expression, calculated temperature increases in the closest proximity to the focal region are shown on the right vertical axis of Figure 56. The amount of laser light impinging the animals' cells was calculated as the product of the laser power before the objective, the proportion of laser power that passed the entrance pupil of the objective and the objective transmission. As the first component of the calculation could be measured easily using a laser power meter, the latter were determined using a technique recently described (Leitz, Fällman, Tuck, & Axner, 2002). On the basis of these considerations, the values of Figure 56 could be calculated using the heat equation and assuming that the thermal conductivity and the absorption coefficient of cells were close to those of water. Furthermore, it was assumed that all absorbed light was transferred to heat in the excretory cell of the animals' pharynx.

Regarding Figure 56, it is to be noted that to activate the hsp16 promoter at wavelengths below 800nm increases in temperature far below the values calculated in the simulations were required. Above this threshold of 800nm the temperature increases required are lower than calculated. Hence, the gene expression triggered by a laser beam with a wavelength below 800nm is likely to be due to photo-chemical processes.

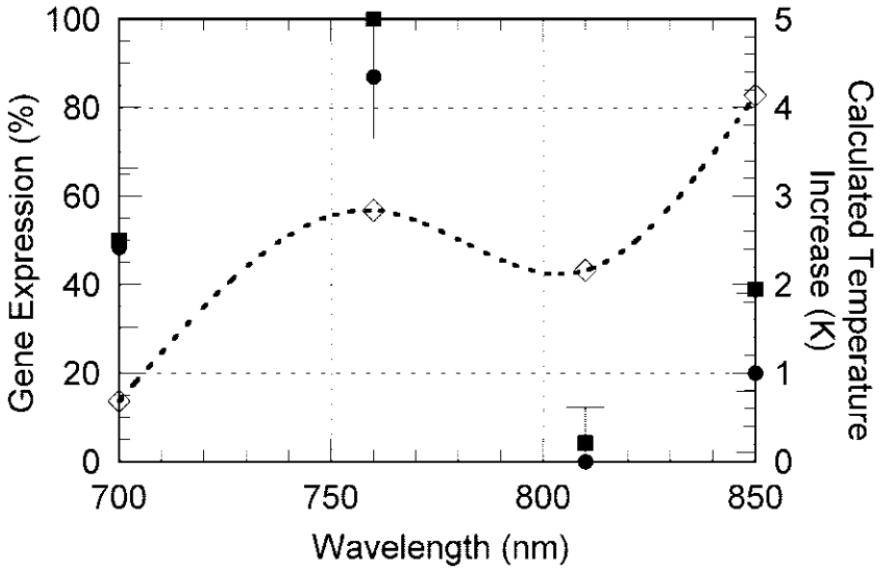

Figure 56: A comparison between gene expression and calculated temperature increase as function of wavelength, laser power 360 mW, two irradiation times (● 120 s, ■ 240 s, ◇ calculated temperature increase). The error bars represent a 95 % confidence interval (Leitz, Fällman, Tuck, & Axner, 2002).

It is questionable whether the amount of photo-chemical damage at a given wavelength increases with intensity of the beam and remains constant at a given laser power irrespective of the exposure time. If gene expression was due to photo-chemical stress only, its amount would increase with increasing exposure time. If stress was of photo-thermal origin, higher laser intensities over the same exposure time would lead to higher levels of gene expression. However, Figure 57 shows that this is the case for an irradiation by light of 810nm. The agreement between the data and the best linear fit is poor. Only data measured using the highest intensities seem to correlate. Furthermore, it should be regarded that increasing laser powers and decreasing exposure time resulting in an exposure of 58J, respectively, cause a significant rise in the level of gene expression. Exposing the animal to 480mW for 120s caused expression in 40% of the cases, whereas no animals showed any response to the exposure of a 240mW laser beam for 240s. Therefore the gene expression caused by light of this wavelength can be assumed to be mainly caused by photo-thermal stress.

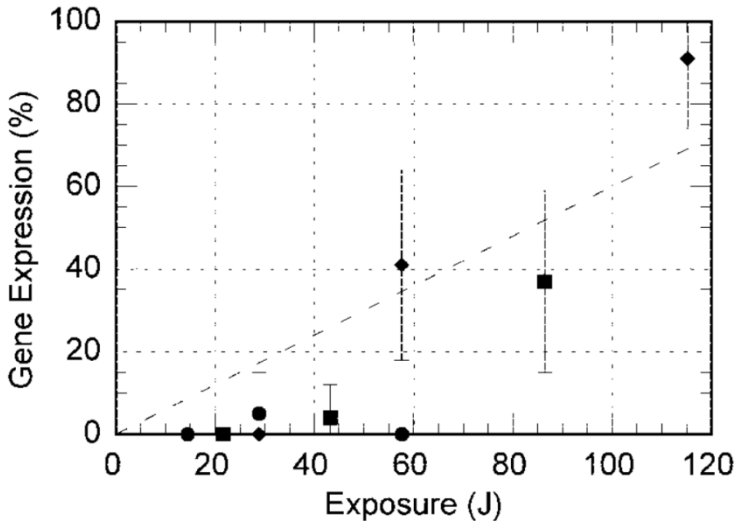

Figure 57: Gene expression as a function of exposure (laser power times irradiation time), irradiation by 810 nm light, three different laser powers (● 240, ■ 360 and ◆ 480mW). The straight line represents the best linear fit to the data that passes the origin. The error bars represent a 95 % confidence interval (Leitz, Fällman, Tuck, & Axner, 2002).

These findings confirm that in general situations in which the stress is caused by photo-thermal effects -like it is the case here- no stress will occur for low laser powers irrespective of the illumination time. Above a certain threshold the frequency of expression is expected to increase with both laser power and illumination time (Figure 58).

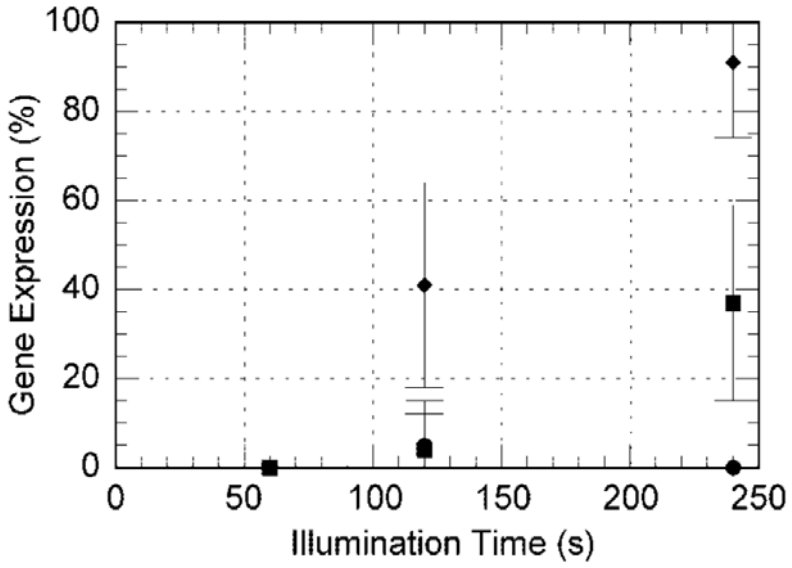

Figure 58: Gene expression as a function of exposure time, irradiation by 810 nm light, three different laser powers (● 240, ■ 360 and 480mW). The error bars represent a 95% confidence interval.

Leitz et al. (2002) have made further investigations to proof the photo-thermal origin of the stress caused by a beam of 810 nm wavelength. Based on a simple temperature-shift experiment they found that gene expressions at such levels only occur after significantly longer periods of time or at significant higher temperatures compared to the ΔT values calculated in the simulation. This leads us to suppose that there either is a photo-chemical stimulus that lowers the threshold for heat-induced gene expression, or that the temperature increase caused by a beam of 810nm wavelength is actually greater than 2°C because substances other than water absorb light of this wavelength. The latter possibility is substantiated by the fact that gene expression increases significantly with small temperature increases. In our experiments we used a pulsed, near-infrared laser beam with intensity up to 160mW together with two different microscope objectives (magnification 100x, NA 1.40 and magnification 20x, NA 0.4). The light emitted by the laser had a wavelength of 810nm. Though the laser system differed from that used in the experiments of Leitz et al. (2002) we could draw parallels to a certain extent. Initially, we assumed that all stress at the cellular level caused by light of 810nm was mainly photo-thermal. The fact that only the exposure of one cell (excretory cell) to the focal point of a 240mW beam for a period of 120s showed an expression in 5% of the animals led us to the assumption that no animal experienced any cellular damage at all. One might claim that the laser powers of a pulsed laser cause a significantly higher impact than a cw-laser, because the power of pulsed lasers in general is calculated as the average over all pulses. Therefore peaks of twice the power indicated can impinge the cell. However, the cell is not exposed to this power constantly. Between the pulses, heat can be transferred that leads to short recovery phases. Even at really quick pulses, the laser power and therefore the emerging heat will not be as strong as it would be with a continuous wave laser with a power value of twice that of the pulsed laser. The maximum power we were able to adjust

was 160mW. Twice this value (320mW) would indeed cause stress in about 5 to 10% of the animals, but only if irradiation time would exceed 120s. Most animals have cells that have a diameter of approximately 30-40µm (University of Bern, 2002). That would lead us to writing speeds of 0.25-0.33µm/s. So far, none of our resins required such high laser powers and such small writing speeds.

Furthermore, a higher proportion of the laser power emitted through the 20x magnification microscope objective impinges on a larger focal point, leaving a more spread distribution of heat and leading to an even lower intensity per unit area compared to the 100x magnification microscope. This was verified as the same laser powers caused a thermal explosion of an ORMOCER resin with the 100xobjective, whereas it led to a sufficient structuring process with the 20xobjective.

The assumptions were tested in an experiment. Several animals were exposed to the maximum power available for a couple of minutes. After that, the animals were put on NGM petri dishes. There was no significant change in their behaviour as they reproduced similar to the reference animals. Therefore we can say that the cellular stress afflicted to the model organisms would only be caused by the chemical toxicity and the polymerisation temperature of the resin.

10. Structuring with ORMOCER

No water soluble photo-initiator suitable for 2PP resins was available. Therefore, the first experiments were made with an acrylate-based substance group called ORMOCER, an anorganic-organic hybrid polymer. It is produced by sol-gel synthesis[49] with a molecular-level mixing of different components (Chichkov, Femtosecond pulses generate microstructures, 2002). Micro resist technology GmbH provided us a slightly modified substance called ORMOCORE with the material number R41B59D. It is liquid, transparent and has a characteristic smell. Melting point, boil and flashpoint are not determined but assumed to be below 0°C, above 100°C and above 100°C, respectively. The density ranges from 1.172 up until 1.18 g/cm^3 at 25°C. It is insoluble in water and has a viscosity range of 3100 to 3900mPas at 25°C. The ignition point is not determined and no assumptions are given by the manufacturers. Only toxic ingredients are listed (Micro resist technology GmbH, 2008). The photo-initiator 2-benzyl-2-dimethylamino-4-morpholinobutyrophenon is admixed at a percentage range of 0.25 to 2%. Because of this ingredient the material is classified R and S, meaning that it is toxic for water organisms and that a disposal into the environment should be avoided. In the long term it can cause damage to aqueous environments as it is hardly bio-degradable. The recommended storage temperature is stated to be in the range of 10 to 15°C. The material should be kept away from ignition sources and prevented from electrostatic charge. Heat and UV light such as sun light cause early polymerisation. During storage the material should therefore be kept away from any light sources except red light.

The acute LD_{50}[50] toxicity tested on rats was above 2000mg/kg as it was administered orally and dermally. As the substance was administered to a population of fish, a dose of 0.46mg/l for 96h was enough to kill 50% of the laboratory Zebra Danio fish. EC_{50}[51] values were also measured. For a population of crustacea (Daphnia magna) a dose of 0.8mg/l within 24h and for a population of algae (Scenedesmus subspicatus) a dose of 4mg/l within 72h caused effects in 50% of the cases examined. The initiator 2-Benzyl-2-dimethylamino-4-morpholinobutyrophenon is specified to be the main source of this toxicity.

The reason for our choice of this resin was its high viscosity. It provided two main advantages. Initially, the movement of the test animal was restricted as it was difficult for the worm to find its way through the viscous substance. This led to a reasonably constant position of the animal in the resin necessary for the structuring process. Secondly, the viscosity prevented the oral intake of the

[49] A procedure to produce nonmetallic inorganic or hybrid-polymeric materials out of a colloidal dispersion also referred to as sol (Ionescu, Mera, & Toma, 2002).
[50] This toxicity value applies to a dose of the specific substance administered, which caused death in 50% of all organisms.
[51] This toxicity value applies to a dose of the specified substance administered, which caused a defined effect other than death in 50% of all organisms.

substance. Although the pharynx of the worm kept pumping, the toxic substance could not make its way to the inner organs of the animal. The water-insolubility of the resin led to the build-up of a protective aqueous coat around the animal (see Figure 59). Hence, ORMOCER was chosen for the pre-experiments despite its rather high toxicity.

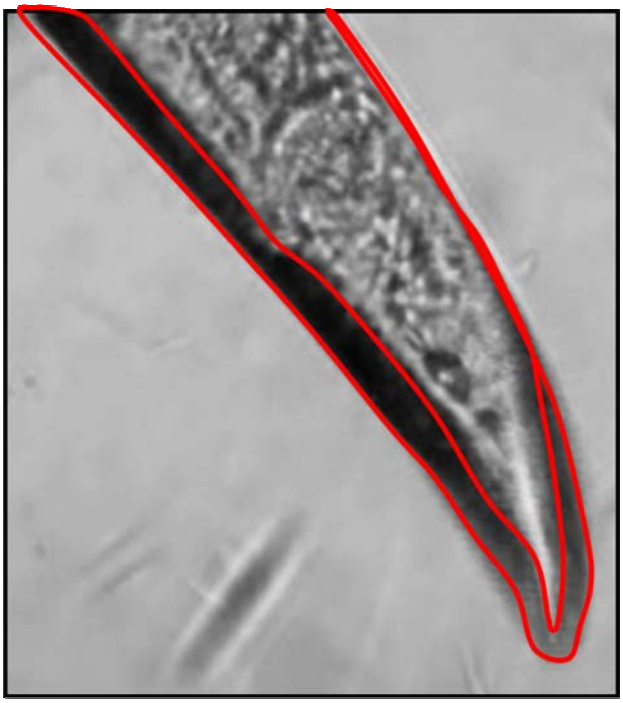

Figure 59: Protective aqueous coat around the animal's tail (red line)

The high reactivity of these substances and the extensive experience regarding their use in 2PP structuring were also major benefits of these resins. The materials can be polymerized in high resolution and have high optical transparency[52] with adjustable refractive indices (in the 1.47 to 1.56 range), exceptional thermal and mechanical properties and a high chemical resistance (Chichkov, Femtosecond pulses generate microstructures, 2002). These advantages made them the standard materials for most 2PP research, even for 3-D parts sub-µ scale (Houbertz, et al.). Moreover, ORMOCER structures with a resolution below 200 nm were generated using 2PP (Chichkov, 2007), such as microneedles for transdermal drug delivery and ossicular (ear bone) replacement prosthesis as well as 3-D functional biological tissue scaffolds (Doraiswarny, et al.). The studies show good adherence of different cells to resins of this type. A growth rate comparable to common bio-active materials was achieved, which, together with the high resolution achievable, constitutes a major step towards the development of bio-active and bio-resorbable heterogeneous 3-D scaffolds.

[52]Low losses at data and telecommunications wavelength with less than 0.06 dB/cm at 1300 nm

10.1. Structuring Parameters with the 100x microscope objective

Although the above references show just a small number of the applications ORMOCERs have been used for, one might notice its high potential. The broad experience gave us a rough idea of the appropriate 2PP structuring parameters. Figure 60 is a SEM picture of an array containing default scaffolds produced using different writing speed and power settings (dv/dP). These structures were built with our experimental 2PP setup using the 100x objective and the software tool "Photonic Crystals"[53].

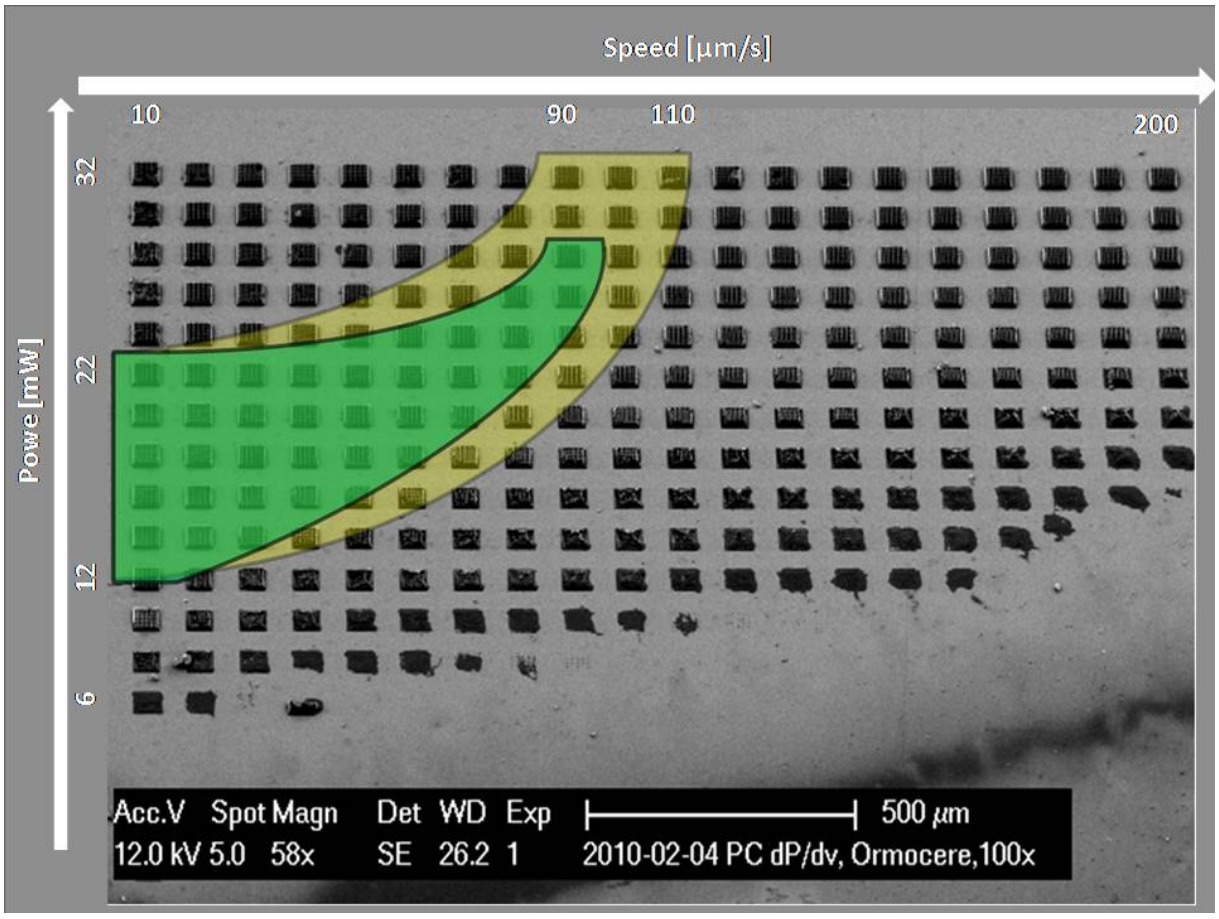

Figure 60: Scaffold Array dP/dv, Ormocer, 100x

On the bottom left side, the first scaffold was fabricated. It was written with a speed of 10µm/s at a power of 6mW. This marks the polymerisation threshold. The horizontal row, containing 20 scaffolds, was fabricated with no power changes and the writing speed changing from 10 to 200µm/s by steps of 10µm/s. Results of changes in power are shown in the vertical columns. Beginning at 6mW, the power was increased by steps of 2mW until the last scaffold was fabricated at 32mW. All specimens' dimensions were equal. The

[53] The functionality of the software can be read in chapter 7.10.1 "M3DL control software".

base area was 50x50µm and the distances between the single layers were 0.71µm.

The structures were classified according to the arrangement, the regularity and the thickness of their hatches. The scaffolds were then assigned to three categories. The red category was to be discarded. Structures in this category were either written with too little power or too high speeds and too high power or too little speed, respectively. This category is not emphasised in Figure 60. The yellow category contains satisfying structures. The hatches are recognisably more regular. Yet the lines are sufficiently wide, they don't stick together (Figure 61). The scaffold at the top-right was fabricated with a laser power of 32mW at a structuring speed of 90µm/s, while the bottom-left one was manufactured at 28mW and110µm/s.

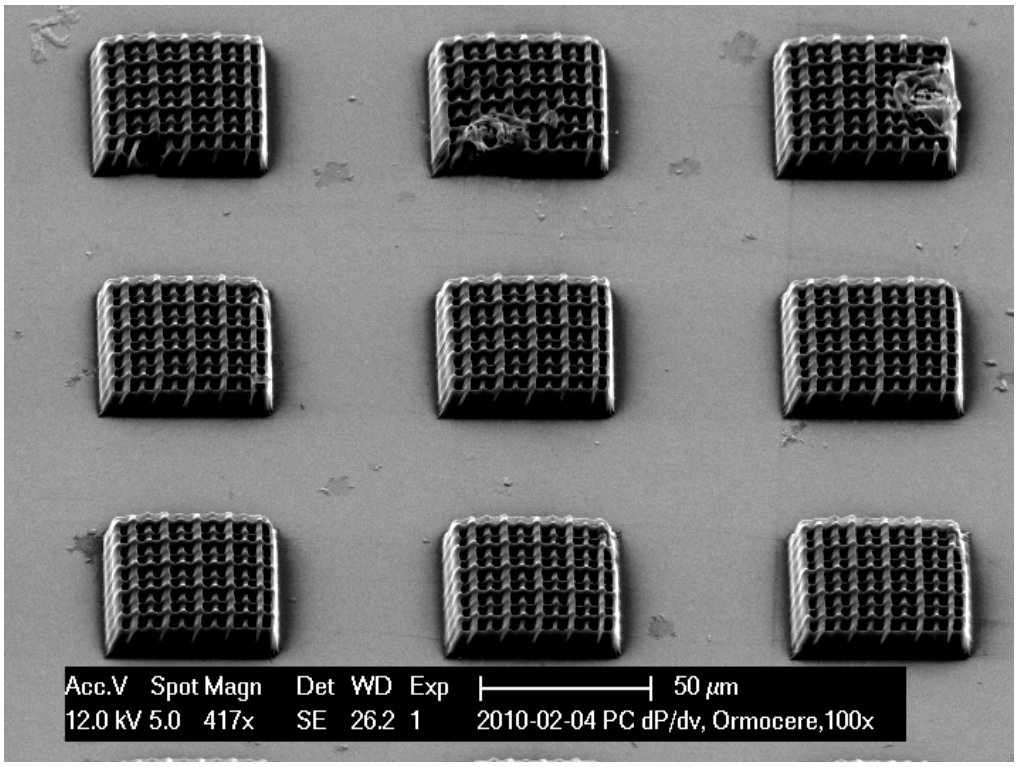

Figure 61: Scaffolds classified yellow (power change 28-32 mW, vertical; speed change 90-110 µm/s, horizontal)

Finally, the green category contains the most satisfying structures. The hatches are perfectly round and stick to the covering layer on the intended places. Figure 62 shows a couple of green scaffolds together with a close-up of the top-left one and a detailed picture of its hatches. This structure was fabricated at 10µm/s writing speed and 20mW power. The structures are perfectly flat and no monomer residue can be seen.

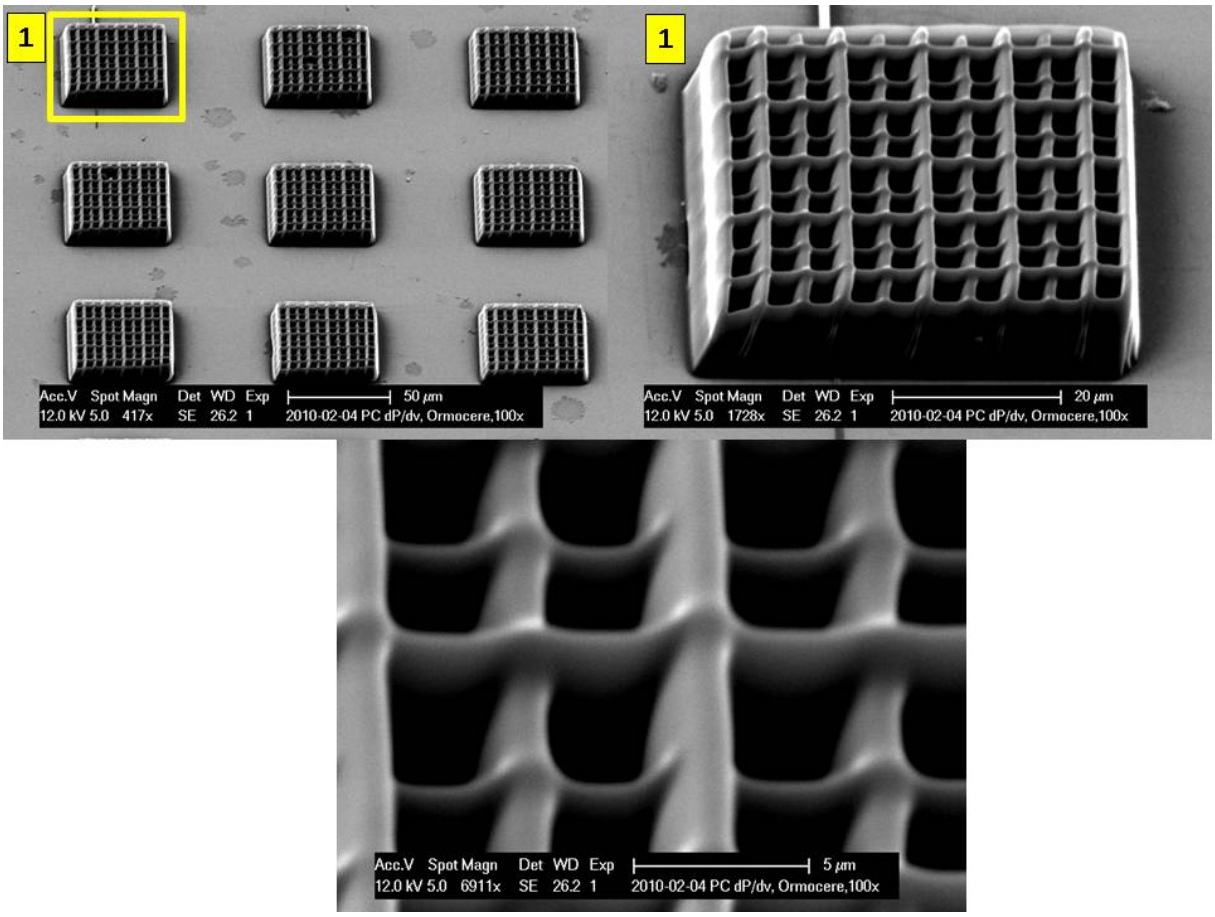

Figure 62: Scaffolds classified green (power change, 16-20mW, vertical; speed change 10-30 µm/s, horizontal)

The findings show that writing powers between 12 and 28mW, as well as writing speeds between 10 and 100µm/s give rise to optically reasonably satisfying structures. The 2PP writing power and speed values are the basis for the parameter function shown in Figure 63. The best fit (R^2= 0.9904) is a polygonal equation of third order. In the described range this function can be used to calculate suitable writing speeds in dependence of power values.

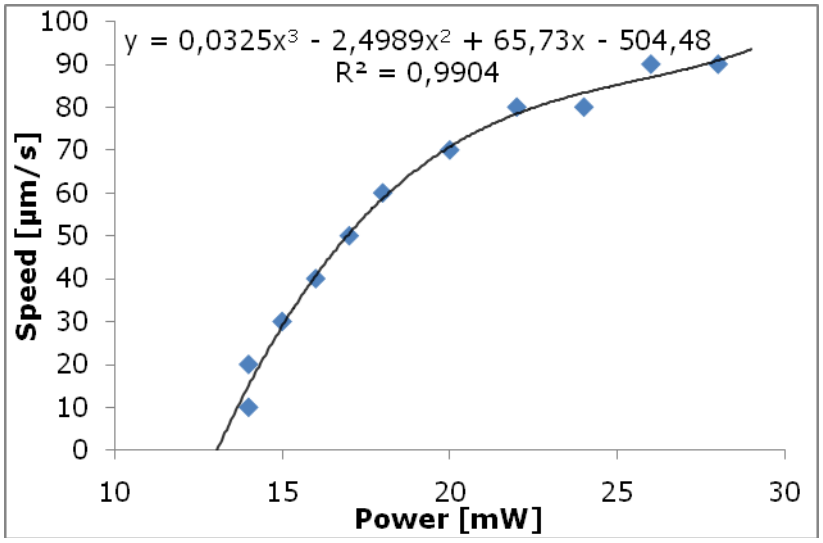

Figure 63: Writing powers and speeds for optically satisfying structures, Ormocer, 100x

Within the green category, structures fabricated at low process speeds have significantly more distinct walls. A direct comparison between a scaffold fabricated at 22mW and 10µm/s and a specimen manufactured at 26mW and 110µm/s can be seen in Figure 64. The left structure looks reasonably more regular. In contrast, the single hatches as well as the side walls of the right structure appear bent. Hence, the green category of Figure 60 only includes structures fabricated at manufacturing speeds up to 110µm/s. Structures fabricated at higher speeds get thoroughly polymerized but the single hatches are insufficiently straight.

The comparison between the structures of Figure 64 brings us to another important issue. Despite the only slight power difference (4mW) between the two, the speed difference is of remarkable 100µm/s. Thus we can say that a change in speed is generally of far less influence than a change in power, all part dimensions being equal.

Throughout all structures, the single lines of the layers are indistinguishable as all side walls appear to be solid. Owing to this fact, this dP/dv array should be repeated in a further experiment, leaving all parameters but the distance between the layers equal. The same parameters as in the described experiment were used by Dipl.-Ing. Klaus Stadlmann at our institute. He structured scaffolds using another monomer (ETA-TTA)[54]. All lines, no matter whether situated in the horizontal or vertical plane, were fully developed and perfectly round. The presumption is that the different refractive index of this monomer leads to a different elliptical shape of the voxel. This is also in agreement with other findings (Kuba & Nakayama, 1998). Apparently the length-to-width ratio is higher than it is using ETA-TTA. A voxel test with ORMOCERE could substantiate this claim.

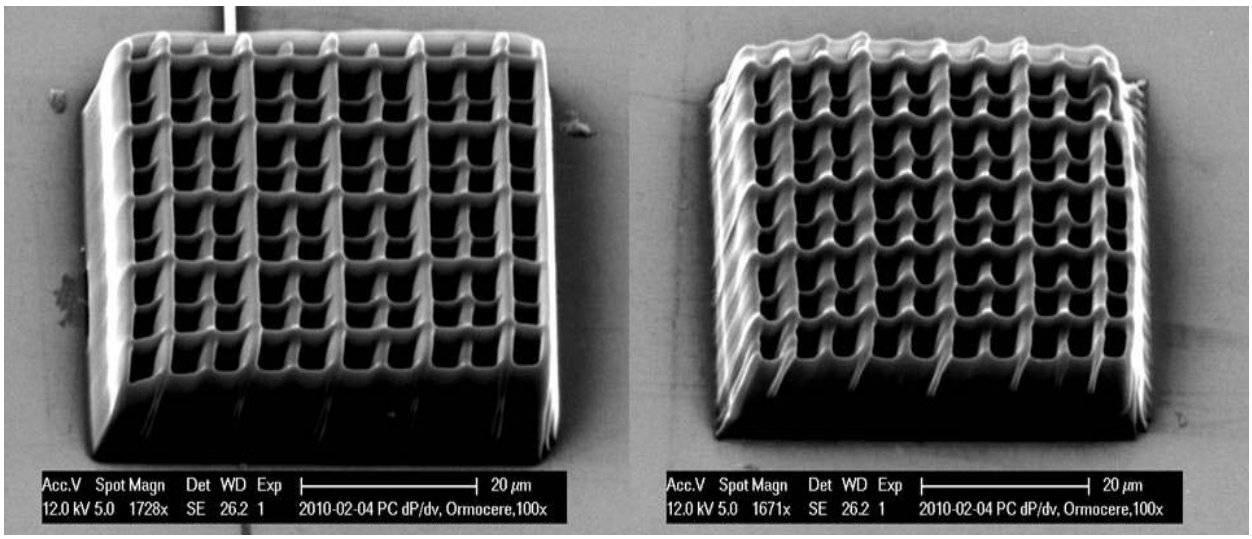

Figure 64: Speed influence; left scaffold 22mW,10µm/s; right scaffold 26mW, 110µm/s

[54] Highly reactive acrylate based monomer.

The reasonably good results of the scaffold array gave rise to the intention of structuring a 3-D STL file using ORMOCER. We designed a micro-scale model of the monument "Wormser Tor", located in the German city Frankenthal in the state Rheinland-Pfalz. Pictures from each side of the triumphal arch monument were taken as basis for the construction of a 3-D object in Catia V5 Release 16. It has to be noted that this model has no claim to be an accurate replica as it is designated for illustrative purpose only.

Based upon the knowledge of the "Photonic Crystal" array, the writing parameters were chosen. The software tool "STL files"[55] only allowed us to fabricate an array with structures of different laser powers. The distance between the hatches in X-, Y- and Z-direction as well as the writing speed could not be altered. Therefore a couple of optimisation steps were necessary including various changes in the size of the object, hatch distance and development methods. In addition, a base plate was attached to the structure in order to guarantee the adherence of the replica to the microscope slide. We decided to use the option "Separately write contour first" in order to achieve a smooth surface. Figure 65 is a SEM picture of the 6 models fabricated. Each replica had an approximate 80x80 µm wide base area and a height of 80 µm. The writing speed was constantly 80µm/s with power ranging from 9 till 19mW, changing by 2mW steps with every model. The hatch distance was 0.8µm. Between the structures there was a space of uniformly 150µm.

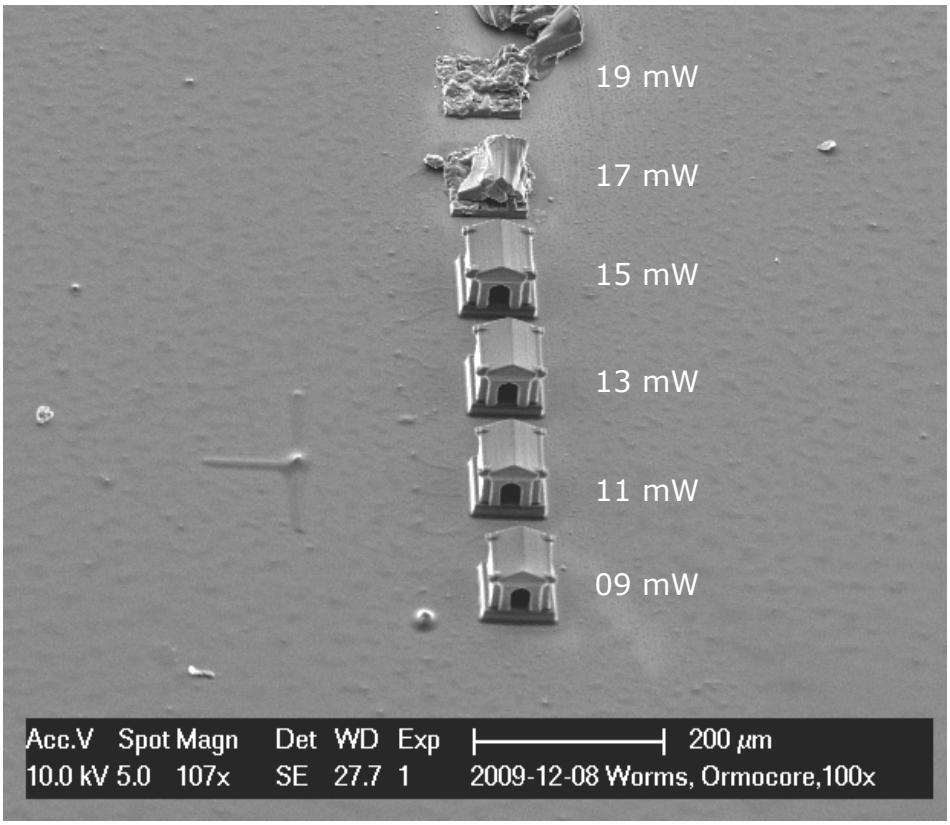

Figure 65: Array of miniature replicas of the "Wormser Tor", Ormocer, 100x

[55] For more information about the functionality of the software tool "STL files" see chapter 7.10.1 "M3DL control software".

A first look at the picture suggests that writing powers above 15mW cause an exceeding absorption of laser light. Because of the high thermal stress the resin "explodes", which means that it polymerises thermally leaving a completely unusable structure. This leads to the conclusion that the processing window for this special model with its hatch distance, writing speed and separate contour reaches from 9 till 15mW. While structuring at powers below 9mW is possible, replicas fabricated at 13 and 15mW are of far better quality. A direct comparison between the replicas fabricated at 13mW and 9mW can be seen in the close-ups in Figure 66.

This comparison provides us an insight of the size changes depending on the writing powers. The right replica appears to be much closer, though the magnification is the same (black information bars below the images). The walls appear to be much straighter in the right picture, especially as the observer takes a closer look at the platform. The corners of the left replica look crumbled away, whereas the corners of the right model seem to be fully developed. This is simply due to an insufficient polymerisation at 9mW. We can therefore draw the conclusion that structures fabricated at powers below 9mW are not of satisfying quality, a further extension of the processing window is, at least to our opinion, not necessary.

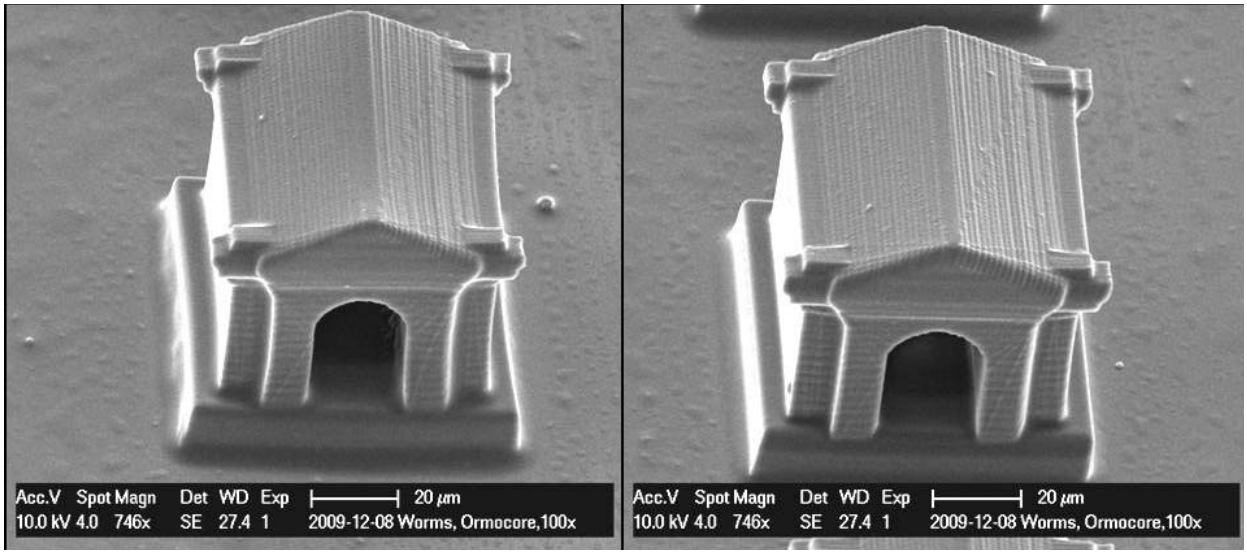

Figure 66: Comparison between replicas fabricated; left miniature 9mW; right miniature 13mW

The impression of Figure 66 can be confirmed with an investigation of the longitudinal view of the models. Figure 67 shows a comparison of the two objects rotated by 90 degrees. Again, the difference in the size of the two replicas as well as the quality of the hatches is conspicuous. In both pictures the corners of the models are not to a perfect 90° angle. This could attribute to the difference between writing and traveling speed . Thus the speed of the movement with the laser turned on differed from the movement with the laser turned off. Depending on the adjustment of the operator, the axis had to accelerate or decelerate the

whole moveable body of the M3DL. With the "Woodpile hatch" setting[56] the changes in speed occurred with the laser turned on. Under the fabrication of the corners the laser was switched on and off very rapidly. Several speed changes during the writing process were therefore necessary and could have caused the observed deviations from the desired dimensions of the CAD file. The fact that bevel structures appear throughout all replicas (white arrows in Figure 67) indicates that the deviation can not be due to power or writing speed influences.

However, this effect does not appear on the front side. This might have two reasons. Initially, the hatches were less frequent on this side, so the laser was not switched on and off constantly. A change in speed was less often necessary. Furthermore, the hatches forming the front side (orthogonally to the front of the replica) were fabricated as the Y-axis moved over the structure. This axis was mounted on top of the X-axis.[57] As a result, the load of the X-axis was substantially higher. Due to safety reasons, its acceleration parameters were manually lowered.

The assumption should be confirmed by repeating the experiment with the STL file shifted by 90°. Then the Y-axis would fabricate the lateral layers and the X-axis would form the front side. If the same result was achieved, the bevel of the corner would be a result of the software setting "Woodpile Hatch", which implies that the acceleration is done during the writing process. Setting the travel speed equal to the writing speed should then solve this problem.

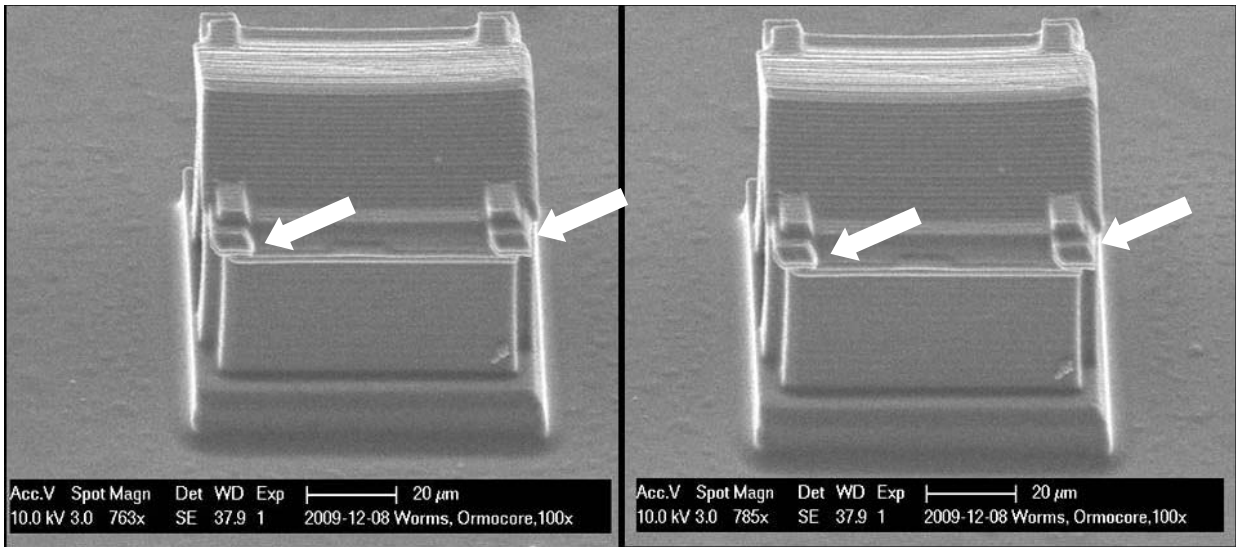

Figure 67: Comparison between replicas structured with 9 and 13 mW, lateral view (white arrows: bevel structure)

[56] See chapter 7.10.1 "M3DL control software"
[57] See chapter 7.5 "The Axes"

10.2. Structuring Parameters with the 20x microscope objective

Due to the high toxicity of the resin, polymerisation time had to be kept short. Therefore, a high writing speed was paramount for a successful in-vivo-writing process. Furthermore, the adult N2 wild type worms[58] had a length of approximately 1mm and a body diameter of around 50µm. Upon closer inspection, the animal could even be seen without the help of a microscope. For the live picture, a microscope objective with only small magnification (5-20x) was sufficient, such as the 20x magnification objective from Carl Zeiss. However, a problem occurred as we tried to find out appropriate structuring parameters. None of the fabricated parts, no matter whether they were "STL files" or simple "Photonic Crystal" arrays, had any similarities to the CAD files.

In the beginning we wanted to create a picture of a nematode in an apple, just for illustration purposes. Therefore we designed the motive of half an apple in Catia V5R19. The base area had a diameter of approximately 80µm, the height was 35µm. Using the software "STL files" this part was fabricated in ORMOCER at a step value of 2.5, a writing speed of 250µm/s and a writing power of 40mW, with results not satisfying (Figure 68). Although the base area roughly corresponded to the part's dimensions, the structure was far too high. Furthermore, the structure did not represent half an apple in any way. This disappointing result prompted us to assume that the voxel was of such an elliptical shape that the configured distance between the layers was too close. To substantiate our claim, this distance was varied within a dv/dP "Photonic Crystal" array (Figure 69).

The power ranged from 20 to 70mW, with steps of 5mW between each scaffold in the columns. The first scaffold was built at the bottom left. The distance between the layers was initially 0.5µm and increased by 0.25µm for each scaffold in the horizontal rows. Therefore the layers of the scaffolds on the right side had a space of 4.75µm between the layers. The writing speed was set to a constant value of 100µm/s and the distance between the scaffolds to 200µm.

[58] For more information see chapter 6 "The model Organism Caenorhabditis elegans".

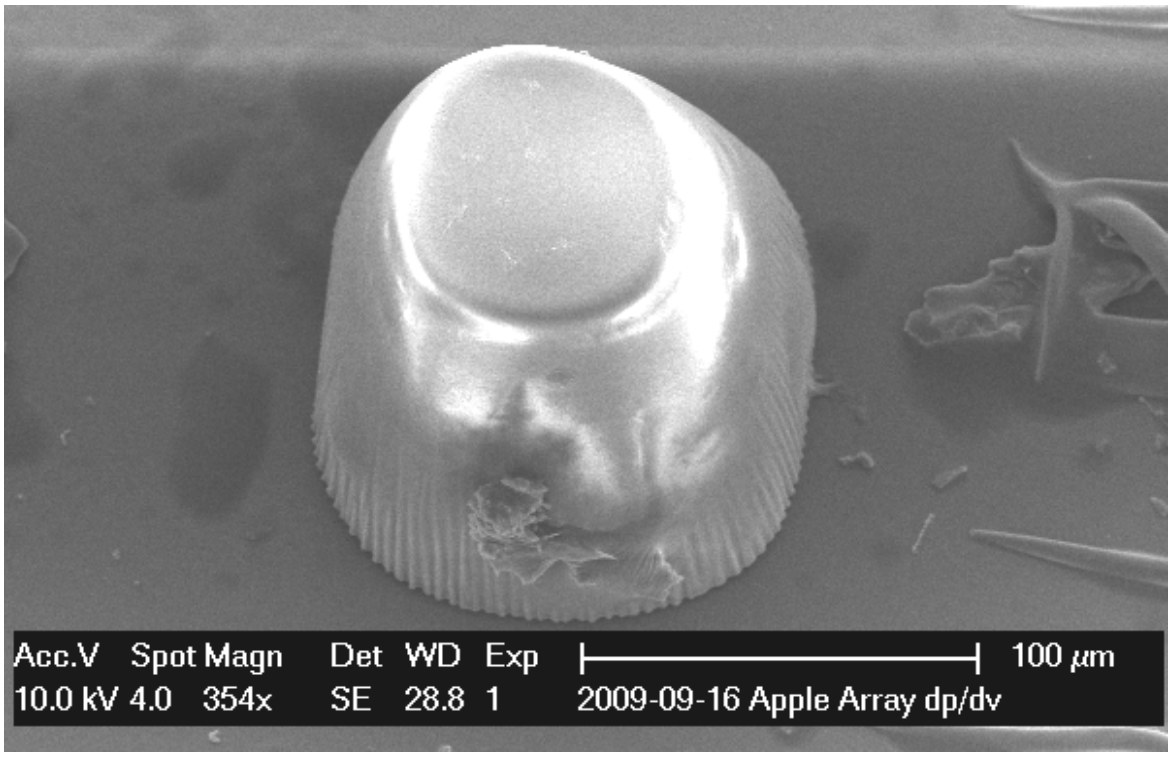

Figure 68: Half a CAD apple fabricated at 40mW, 250µm/s, Ormocer, 20x

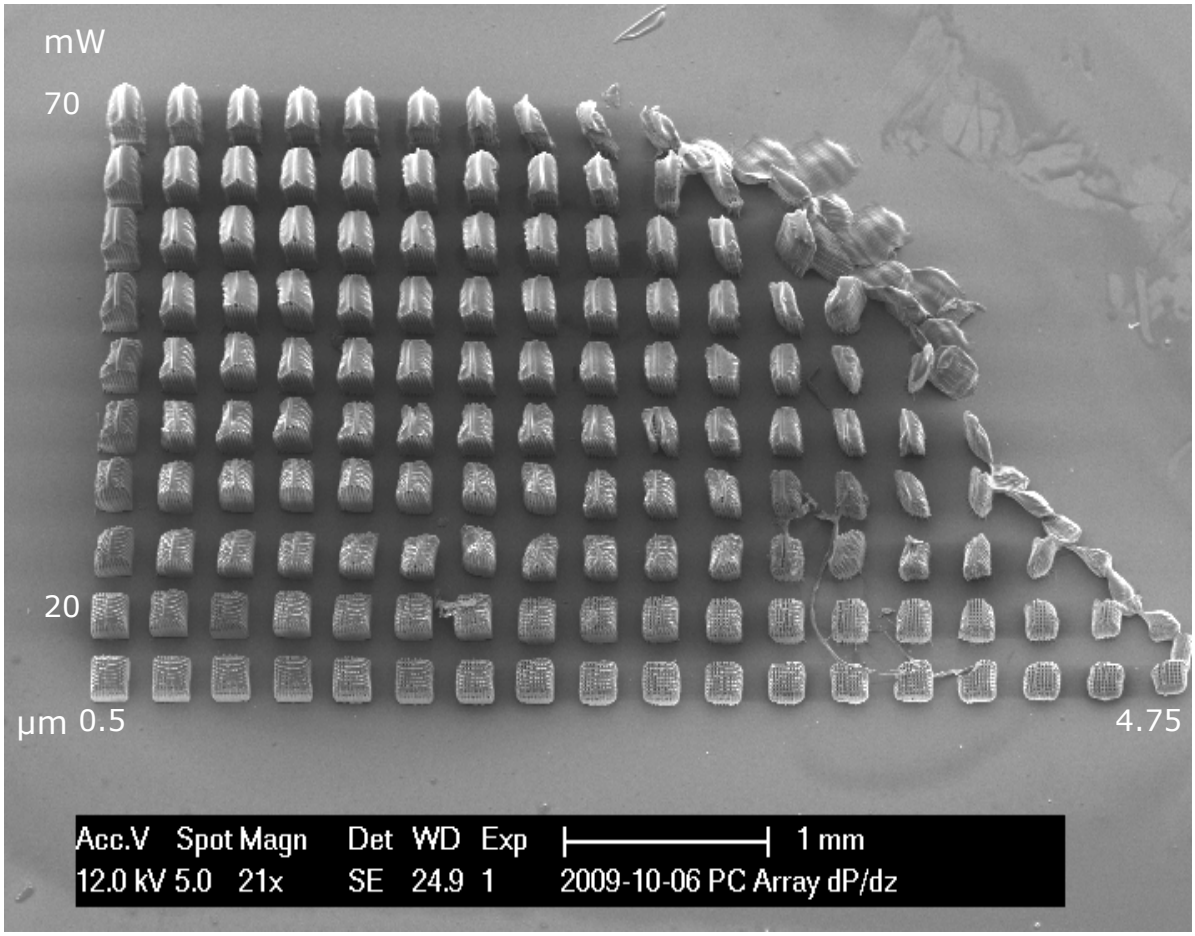

Figure 69: dP/dz Array of Scaffolds; 20x objective; Ormocer

The processing window for this resin was remarkably large as almost all structures were fully developed throughout nearly all process parameters. Neither thermal explosion nor insufficient development of the layers occurred. However, at high laser powers and larger distances between the layers, the structures did not stick to the surface of the slide. This might have had two reasons. As no triangulation was adjusted, the slide's position might not have been perfectly orthogonal to the interface between the resin and the slide. A clockwise tilt around an axis diagonal to the power and layer-distance axis (an imaginary axis drawn from the top left to the bottom right of Figure 69) could have been the reason for the insufficient adhesion of the structures at the top right. Another reason might have been the voxel size induced by the 20x magnification microscope objective with low NA.

This is in agreement with the already cited findings of Kuba and Nakayama (1998). Other researchers (Sun, Maeda, Takada, Chon, Gu, & Kawata, 2003) investigated the relation between NAs and voxel shapes (Sun, Maeda, Takada, Chon, Gu, & Kawata, 2003) did without changing the objective, rather altering NAs with a variable pinhole. Their 2PP setup comprised a 780nm wavelength, 80fs pulse-width and 80MHz repetition-rate laser focused to an unspecified photo-polymeriseable resin. The laser power was adjusted to the polymerisation threshold.

The experiments showed that the lateral voxel size decreases with the NA under identical exposure conditions. A lateral size of 350nm was achieved with a NA of 0.88, whereas the size increased to 460nm as the NA was set to 1.4. This is simply due to the laser power being distributed over a larger volume at low NAs. This leads to a solidified front *"demarcated by the threshold camber vertically expanded and laterally shrunken"* (Sun, Maeda, Takada, Chon, Gu, & Kawata, 2003, p. 821). Therefore a 2PP structuring process using low NA microscope objectives leads to a high and thin voxel. The length and width of the voxels differ as the exposure time is increased and NA is lowered (Figure 70).

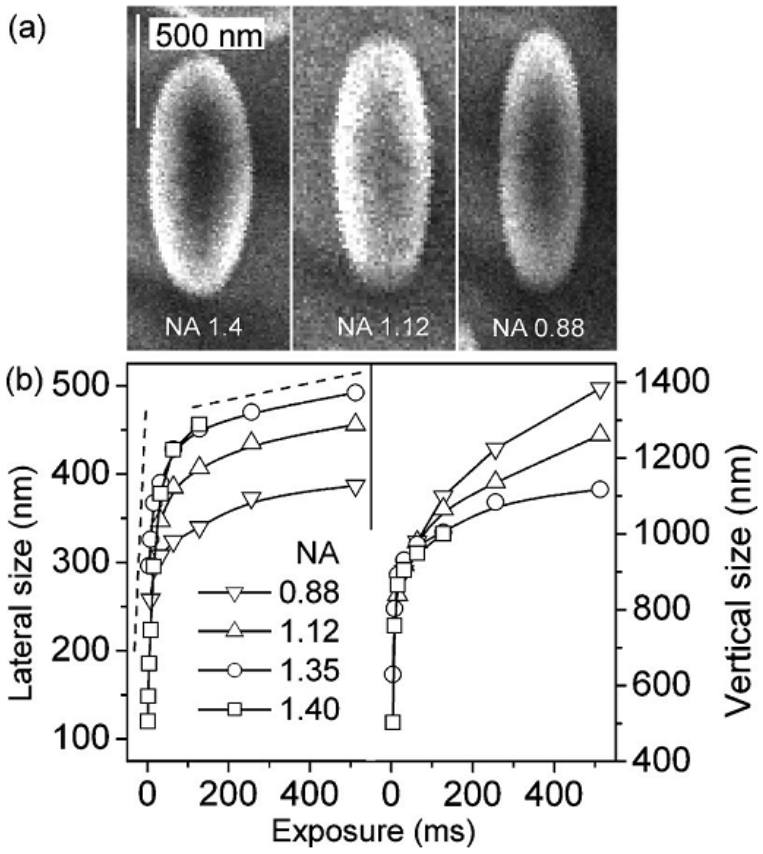

Figure 70: NA-dependent voxels; (a) SEM images of voxels formed with identical focal spot laser power (b) Exposure time-dependent voxel size in both lateral and longitudinal directions under different NAs (Sun, Maeda, Takada, Chon, Gu, & Kawata, 2003)

A closer look confirmed the findings. Figure 71 shows that none of the distances were large enough to fit the layer distance to the voxel size. The layers of the lowest scaffolds (0.5µm between the layers) stick together because of the height of the voxel. Picture number 1 shows structures written at maximum laser power (70mW) together with the lowest layer distance in this experiment. The scaffolds feature a kind of gabled roof. The desired height was considerably exceeded; Figure 71 shows that the top left scaffold set to 2.5µm height exceeded this by a factor 40[59].

The bottom right picture of Figure 71 shows flatter structures. These scaffolds, fabricated at 20, 25 and 30mW and 2.25, 2.5 and 2.75µm layer distance, did not form gabled roofs like the structures top right. Yet the single hatches were still not distinguishable, the structures were not flat and of exceeding height. An optical analysis showed that the close-up structure on the bottom right supposed to be 7.25 µm high was actually 45µm high.

A decrease in laser power to the polymerizing threshold of ORMOCER using the 20x objective (18mW) would in fact decrease the voxel length compared to its diameter. The voxel shape would not be sufficient for an adequate structuring process yet.

[59] Considering tilt of 45° and scale.

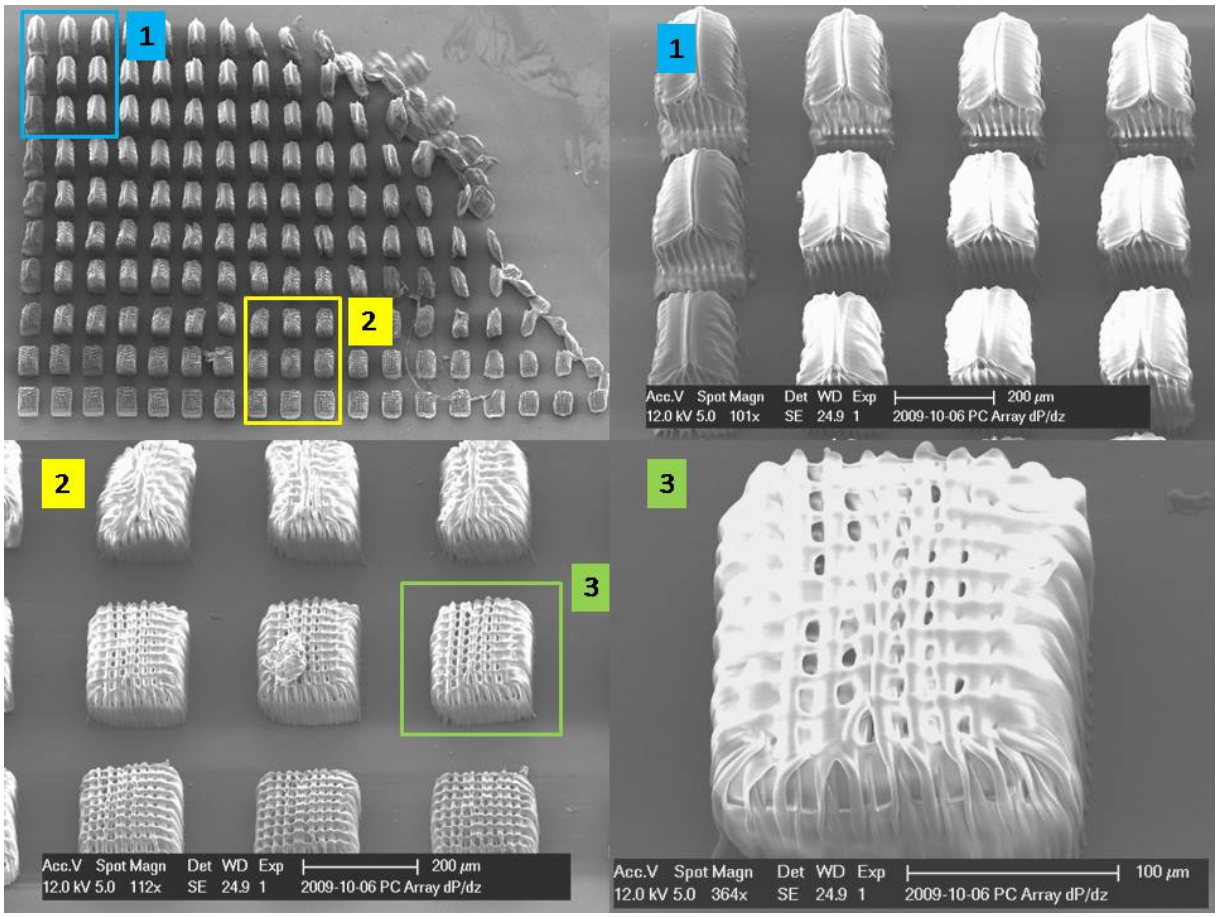

Figure 71: Close-ups of scaffold, dP/dz array; 20x objective; Ormocer

A further increase in the distance between the layers resulted in structures having irregular shape (Figure 72). Because of the thin and high voxel, the walls of the structure fabricated at 50mW and a layer distance of 8µm looked like weaving lines. The findings showed that high resolution structuring using the 20x objective without any aberration correction is simply not possible.

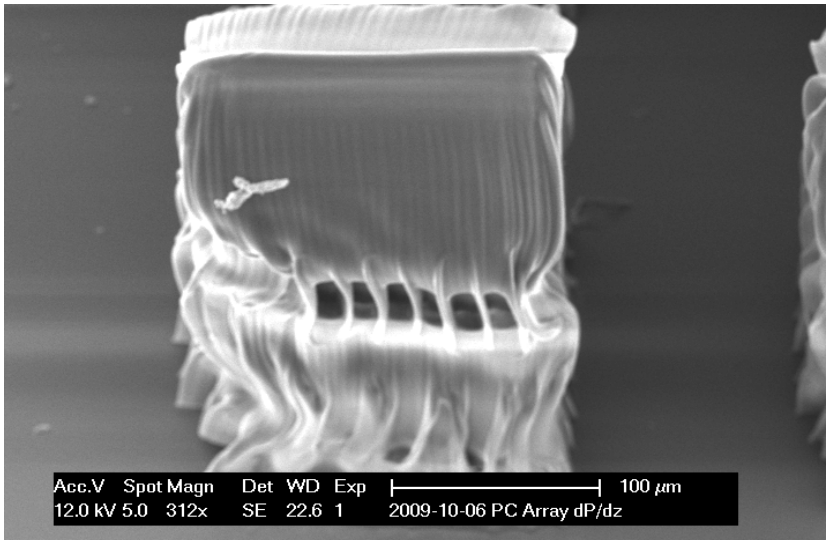

Figure 72: Scaffold fabricated at 50mW, layer distance 8µm; 20x objective; Ormocer

A "voxel test"[60] revealed a similar problem. The first step of the experiment was to investigate the threshold in laser power where the resin was just about to polymerise. Two parameters were considered. The "shot time" was defined as the time it took to polymerise the resin at a given laser intensity, whereas the "threshold power" was defined as the intensity of the beam the resin was exposed to for a a constant time. In either case, the value at which polymerisation first occurred was the desired result. Figure 73 shows the outcome of the experiment. The threshold is outlined as a function opposing "threshold power" (X) to "shot time" (Y).

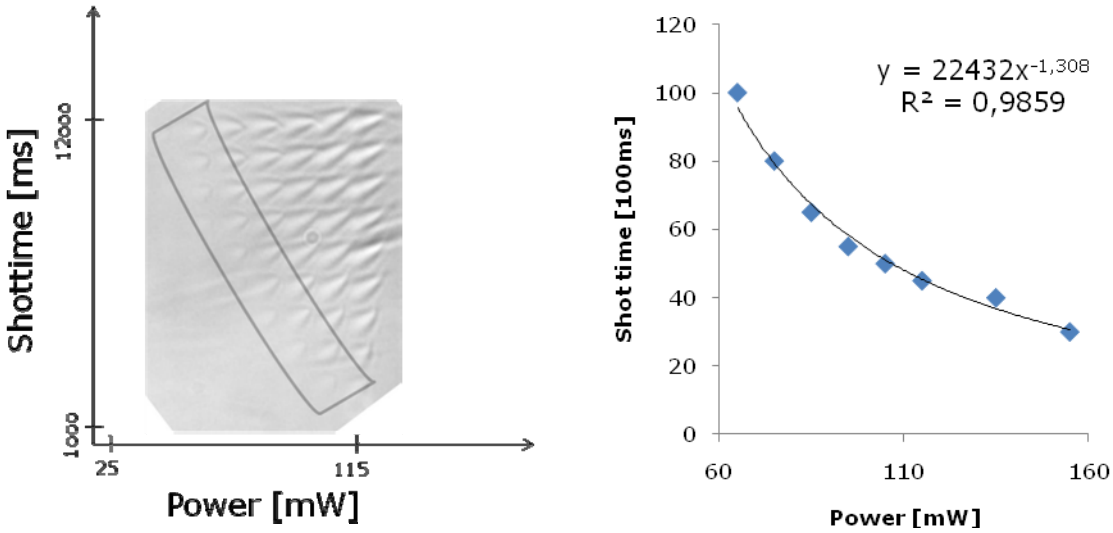

Figure 73: Investigation of the polymerisation threshold, Ormocer, 20x

To investigate the dimensions of the voxel at a specific laser power and "shot time", the focal point was placed completely in the body of the slide. Each voxel was fabricated at a laser power of 65mW and a "shot time" of 15000ms, indicating the polymerisation threshold. Each voxel in the Y-direction was placed an additional 0.5µm towards the centre of the resin. A row of 40 voxels was fabricated in the Y-direction. The columns consisted of 4 voxels each. Every voxel was kept 20µm off the slide towards the centre of the resin. The aim was to analyse the dimensions of the first voxel toppled. A schematic view of the experiment is shown in Figure 75. Figure 74 is a picture taken from the observation camera directly after the fabrication of the voxel array.

The described experiment is a common procedure to investigate the influence of numerous factors on the 2PP writing process. Passinger (2008) used voxel tests to benchmark different laser systems and resins together with associated writing speeds in order to achieve a quicker 2PP structuring process. Sun et al (2003) investigated the influence of the NA on voxel diameter and length. The elongation of voxels by the inclusion of an axicon lens in the laser beam line has

[60] More can be read in the chapter 8.10.1. "M3DL control software".

also been established by a voxel test[61] (Li, Winfield, O'Brien, & Crean, 2009). These examples show the broad applicability of this type of experiment. As the absorption cross-section of ORMOCERs have already been discussed (Houbertz, et al.), our particular objective was to investigate the influence of the 20x magnification Carl Zeiss with a low NA (0.4) and a large working distance (8.45mm without coverslip).

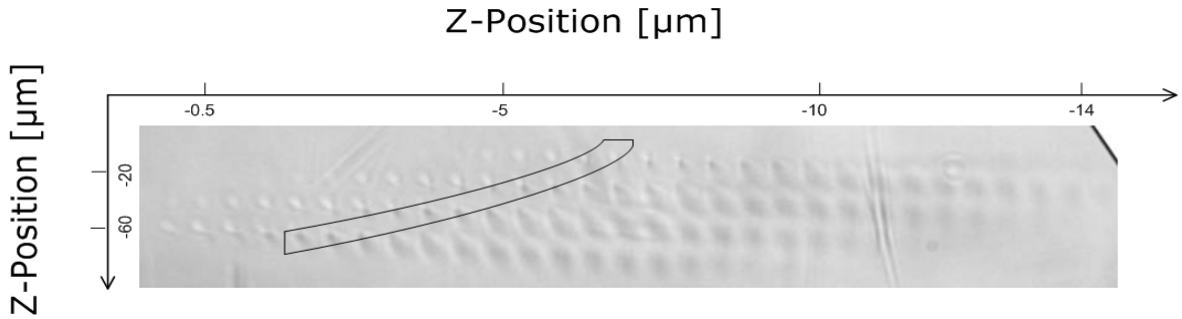

Figure 74: Investigation of voxel length, CCD Camera image, Ormocer, 20x

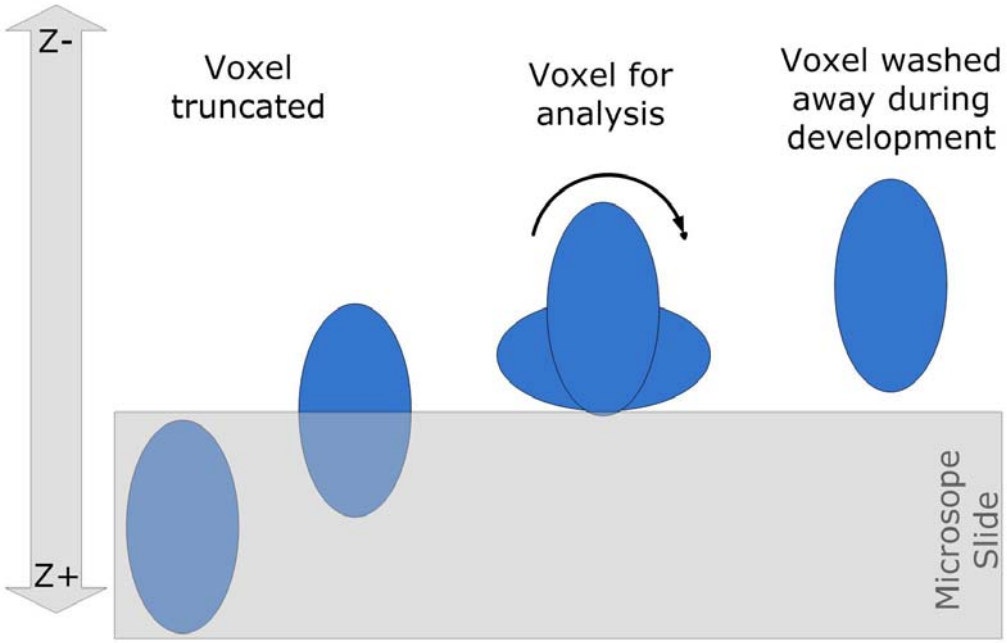

Figure 75: Investigation of voxel length, schematic picture of the procedure

Figure 76 shows voxels of such a length that every single one toppled. Most structures were not in their assigned position. Under the development the structures apparently connected to each other and lost their footing on the slide. Thus the gain of knowledge resulting from this experiment was very restricted

[61] Axicon lenses are also known as conical or rotationally symmetric prisms. An axicon can be used for a variety of optical applications: it can image a parallel beam into a ring; it can create a non-diffractive Bessel beam from a Gaussian beam or can focus a parallel beam into long focus depth (Del Mar Ventures, 2007).

due to insufficient measurement capabilities. Yet the structure displayed on the very left had fallen in another direction compared to the others. We assumed that this structure was the first voxel of the 4th row, so we believed that it was built as the laser beam focused 40µm closer to the centre of the resin relatively to the first structure of the first row. It might give us a rough idea of the length-to-width ratio of voxel dimensions in general. Considering the 45° tilt of the SEM clamp and the shape of the dropped structure, the length of the voxel amounted to approximately 35µm and the diameter to about 4µm, giving a length-to-width ratio of 8.75.

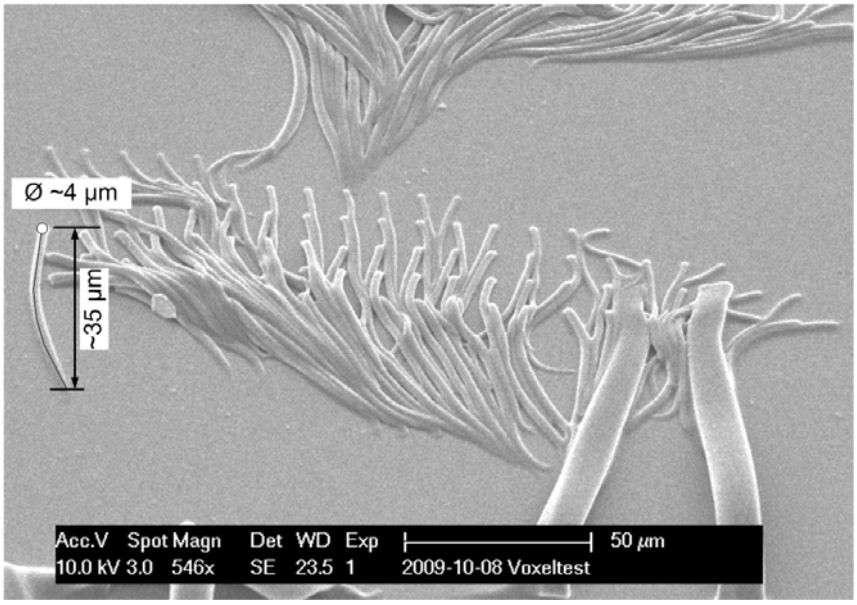

Figure 76: Voxel test, Ormocer, 20x

Sun et al (2003) show that a structuring process using an objective with a NA of 0.88 resulted in a length-to-width ratio maximum of 4 as their resin was exposed to a laser power of 5mW at an exposure time of 500ms. According to the authors, a structuring process with such a voxel shape leads to insufficient quality of the fabricated objects, at least for most 2PP applications. Looking at Figure 68 and Figure 69 we absolutely agree.

Nevertheless, the 20x objective offers a couple of constitutive advantages for the in-vivo-writing process. First, it favours the possibility to increase the part's dimensions at a comparably high level of structuring speed. The decreased feature size resolution is negligible since it is still substantially higher compared to a common 1PP process. The whole writing process is performed within a reasonably shorter period of time, which implies that the organism is exposed to the harmful resin for a shorter time, leading to a better chance of survival. In addition, the focal point of the objective is a lot larger, leading to decreased laser intensities per area and thus to a lower level of cellular stress within living tissue.

Moreover, the large working distance of this objective offers a lot more flexibility and three-dimensional capabilities of the 2PP system. Especially for the in-vivo-writing process, long working distances are essential as the structuring must

occur reasonably deep inside a volume. The latter is especially important as it is the aim to fabricate parts inside biological tissue. However, this leads us to the same problem again. High laser powers are necessary if the focal point is to move deep inside into a tissue.[62] Since high intensities cause a high length-to-width ratio of the voxel resulting in dimension incorrectness of the fabricated part, this problem needs to be resolved in the future. One possibility could be a technique based on astigmatic shaping of a femto-second writing beam (Cerullo, et al., 2002). The authors used the device to control the size and shape of optical waveguides with a diameter of 1.5µm. The apparatus allowed them to eliminate the asymmetry and to control the size of their fabricated structures. Their cylindrical lens setup is shown in Figure 77.

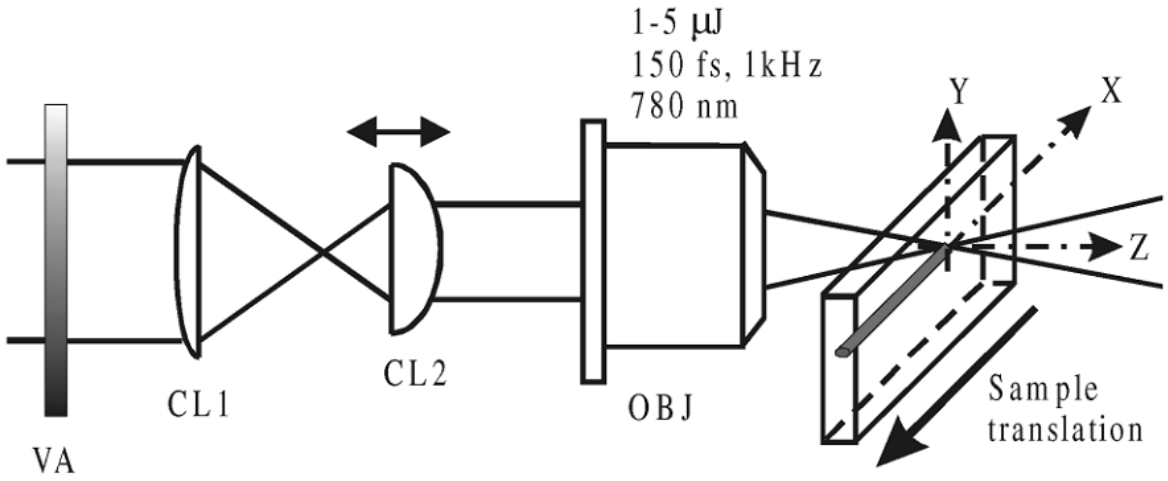

Figure 77: Setup for waveguide writing: VA, variable attenuator; CL1, CL2, cylindrical lenses; OBJ, microscope objective (Cerullo, et al., 2002)

Figure 78 outlines the influence of the spot size and the effect of the cylindrical telescope on the exit face of optical waveguides. Waveguide I was fabricated by a circularly symmetric beam focused to a waist of ω_0=3µm, waveguide II was written with a spot size of ω_0=1.3µm and waveguide number III was structured with the initial spot size of ω_0=3µm with the interconnected cylindrical telescope. A nearly symmetric waveguide with a surface area similar to the waveguide number I was manufactured by the authors. Picture (b) shows the corresponding simulation outlining the same results (Cerullo, et al., 2002).

[62] As already discussed in chapter 10 "Stress response in C. elegans caused by infrared laser".

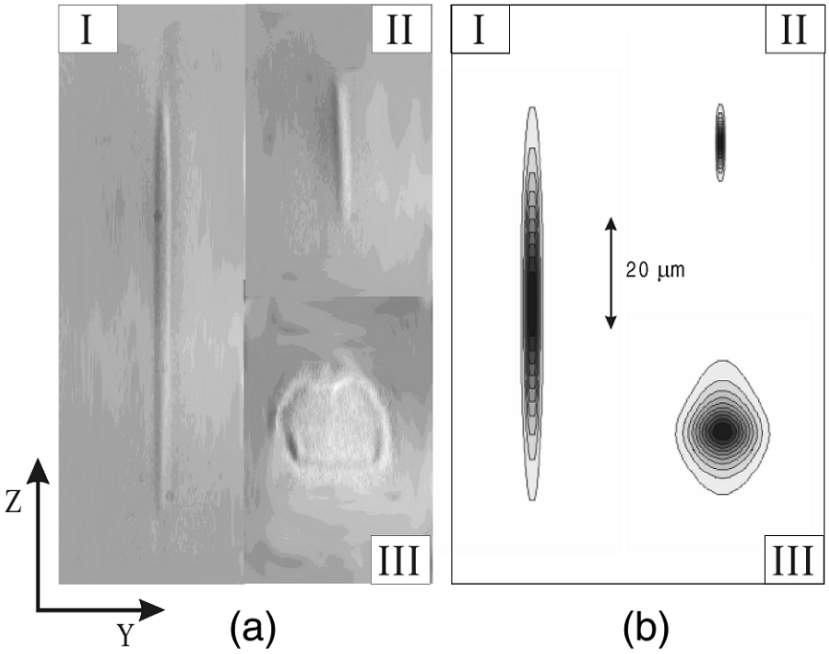

Figure 78: (a) microscope images of the end face of waveguides; (b) simulated density distributions (Cerullo, et al., 2002)

Currently, Dipl.-Ing. Klaus Stadlmann plans to implement an extended device based on the same principles. It will soon be integrated in the experimental 2PP setup of M3DL. Faster structuring speeds and greater dimensions of the parts at reasonably larger working distances will be available soon.

11. Toxicity of the resin

To manipulate single worms, two different tools were available. A hook was used to take single worms out of the NGM plates[63] and to transfer them to other NGM plates or to liquid drops of low viscosity. To get the worms out of these drops, an adhesion hinge was used. The worms were caught in a small droplet of the specific substance sticking to the tool, so the animals could be transferred from the liquid drop to NGM plates.

Since ORMOCER is water insoluble, the adhesion hinge could not be used to transfer the worms from a drop of M9 into the resin. The hook was neither appropriate since it was impossible to get a worm off the tool inside the resin. Therefore we posed a drop of M9 buffer on a microscope slide. A drop of ORMOCER was placed right next to the aqueous liquid. Using the hook it was possible to transfer a worm from the agar plate to the M9 drop. From there the animal could be slid into the resin. Due to the insolubility of ORMOCER in water, no impurities resulted. The whole procedure is graphically explained in Figure 79.

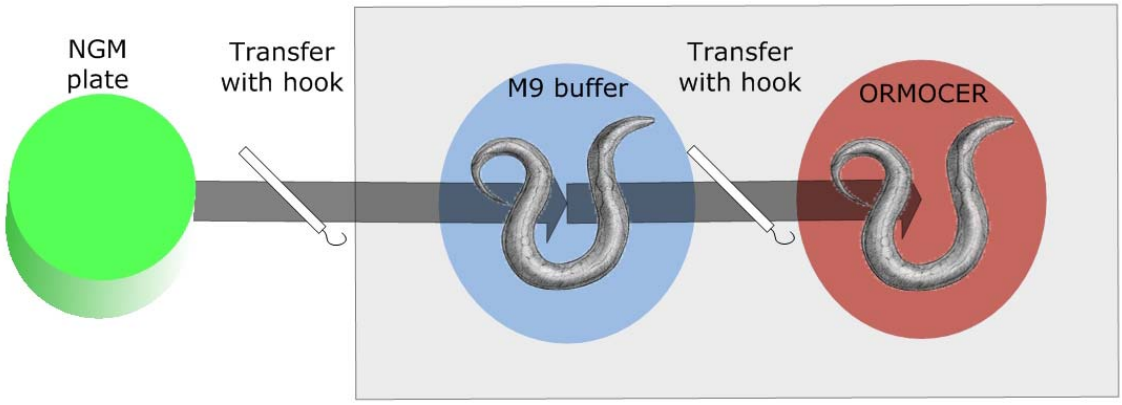

Figure 79: Transfer of the worm into an Ormocere drop, picture of C. elegans (Linden, 2008)

As an indicator for the life-death analysis of the worms we used pharyngeal pumping. It is a standard method used for toxicity studies at the Vienna Biocenter (Jantsch-Plunger, personal communication, June 2009).

Usually a population of C. elegans have to be bleached.[64] This results in animals of the same age. However, limited C. elegans maintenance knowledge and the lack of biological equipment at the University of Technology rendered this

[63] Nematode growth medium: In the laboratory, C. elegans are maintained on NGM petri dish. A dish has a lawn consisting of 3g NaCl, 2.5g Peptone and 17g agar per liter M9 medium (described later). This lawn is spread with E. coli as a food source. On such a petri dish, the animals can live and reproduce for several days (Stiernagle T. , 2005).

[64] Bleaching is a method to synchronies a population of C. elegans. Adult worms carrying eggs are treated with a solution of M9 buffer and 5% sodium hypochlorite as well as a drop of natrium hydroxide. The worms die but their eggs remain on a fresh NGM plate seeded with an Echerichia coli OP50 lawn.

procedure impossible. While our experiments using ORMOCER as a resin for the in-vivo-writing process stand for preliminary studies, bleaching will be necessary for a better reproducibility of future toxicity tests of more suitable resins.

50 worms were transferred into individual drops of ORMOCER. Two microscope slides carrying 3 worms each were prepared at the same time. The time of first exposure to the resin was noted. With a stop of the pharyngeal pumping, the worm was considered dead. The outcome of the toxicity study is shown in Figure 80. The survival times (displayed in 3min units) range from below 2min to over 71min.

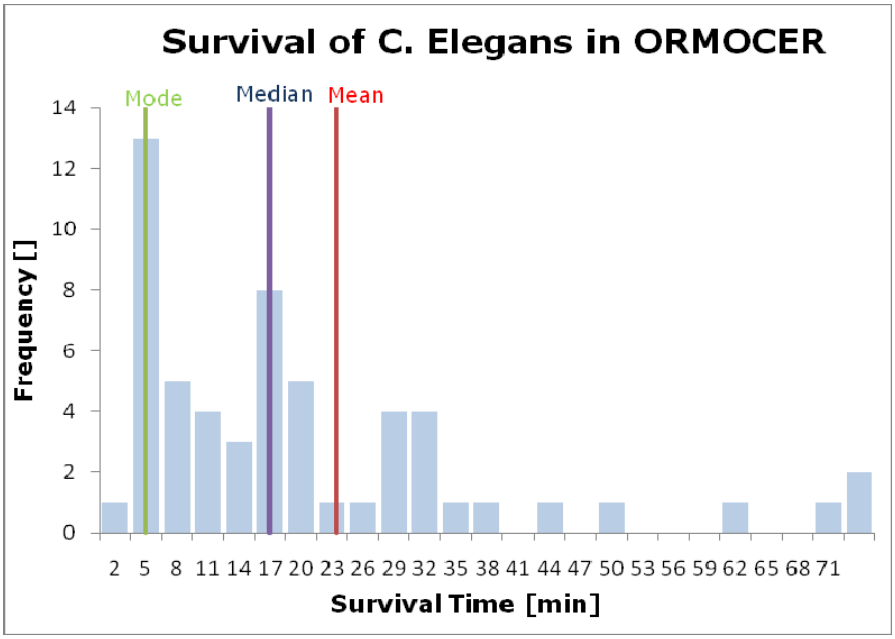

Figure 80: Survival of C. elegans in Ormocer

It is obvious that the numbers do not follow any classical probability distribution. Modal value, median and mean are far away from each other. Most worms stayed alive for about 5 minutes. A considerable number survived between 14 and 17min. Some of the animals survived for more than 70min, the most robust of them stayed alive for remarkable 135min.

The results are not very meaningful, though. We can only draw the conclusion that the survival time is solely dependent on the characteristics of the protective aqueous coat around the animal.[65] As soon as the cuticle came in direct contact with the resin, the worm died almost immediately. Reference animals in M9 buffer survived up to three hours. In our opinion, the fact that one specimen survived 135min mirrors the fact that hardly any compound of ORMOCER is soluble in water. The survival of the worm during the structuring process is, unfortunately, left to chance.

[65] For more information about the protective coat see chapter 11 "Structuring with ORMOCER"

12. The in-vivo-writing process

By now we gained knowledge of the stress inducing factors. Since the cellular impact of the beam's focal point as well as the toxicity of the resin was investigated, we can now look at polymerisation speed and time. We decided to manufacture a single scaffold with a base area of 300x300µm and a height of 80µm using the software tool "Photonic Crystals"[66]. Since ORMOCER is not soluble in water, the adhesion hinge described in the previous chapter could not be used to transfer the worm from a drop of M9 into the resin. Additionally the hook was not appropriate as it was impossible to get the worm off the tool inside the resin. Therefore we positioned a drop of M9 buffer on a microscope slide. A drop of ORMOCER was placed right next to the aqueous liquid. Using the hook it was possible to transfer the worm from the agar plate to the M9 drop. From there the animal could be slid into the resin. Due to the insolubility of ORMOCER in water, no impurities emerged. The whole procedure is graphically sketched in Figure 81.

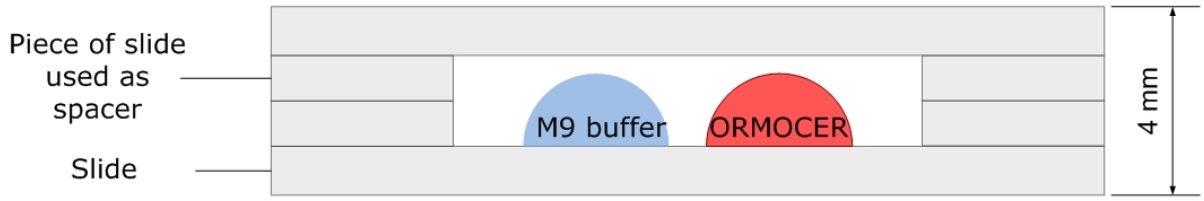

Figure 81: Preparation of the specimen for the in-vivo-writing process

As the animal sank to the bottom as soon it was placed inside the resin, we could not perform the usual upside-down structuring process. Moreover, the usual approach of compressing the resin to a thickness of 120µm by using tape as a spacer could not be used because the worms were either crushed or flushed away as the coverslip was placed on top (see Figure 36). Therefore a special sample holder had to be prepared. To make sure that the drops kept their shape, they must not touch the cover, so a 2mm spacer was placed in between the two slides (Figure 81). A slide cover was glued on top of the object holder after the animal was transferred to the resin.

After the preparation, the specimen could be mounted to the clamp in the usual way. We used the 20x magnification microscope objective as the special preparation of the specimen required a minimum working distance of more than 1mm, which excluded the use of the 100x objective. The toxicity of the resin limited the polymerisation time. In addition, it was much more difficult to establish the animal's exact position with a higher magnification. The pictures and videos made during the process were also more meaningful using the 20x objective as the animal's body dimensions rendered themselves better to this magnification.

[66] More information about this software tool can be read in chapter 8.10.1. "M3DL control software"

The settings were taken from the experiments discussed in chapter 10.2. Apart from the 300x300µm base area and the height of 80µm, the period was set to 30µm, resulting in 10 lines per layer. In total, 10 layers were fabricated with a distance of 8µm between them. The speed was set to 300µm/s, the power to a total of 35mW.

Figure 82 shows pictures taken during the live observation of the in-vivo-writing process. During the structuring of a single line, the laser was not turned off. Thus the focal point definitely hit inner organs and cells of the organism. As the animal showed no response to the exposure, we can agree to the propositions made by Leitz et al (2002). For future investigations we claim that laser power is not a limiting factor yet. However, another fact needs to be further investigated: the polymerisation temperature might affect the cuticle of C. elegans and might thus be a further cellular stress factor. Especially for the future fabrication of parts inside an animal, this has to be taken into account. Experiments as well as simulations determining the temperature distribution near the focal point in different resins will be important.

Limiting the movement of the model organism would be another improvement of the in-vivo-writing process. In this experiment, the animal's movement was decreased simply by the high viscosity of the resin. A slight movement was beneficial for taking a video, as it showed that the animal was alive. For the structuring of proper parts in high resolution, however, absolutely zero movement is necessary. Chemical immobilisation with levamisole (L[-]-2,3,5,6-tetrahydro-6-phenylimidazo{2,1-b}thiazole) or thermal immobilisation by cooling the specimen to 2-3°C, or a combination of both, could result in a complete suppression of movement without causing stress to the organism. This could also favour the application of less viscous resins.

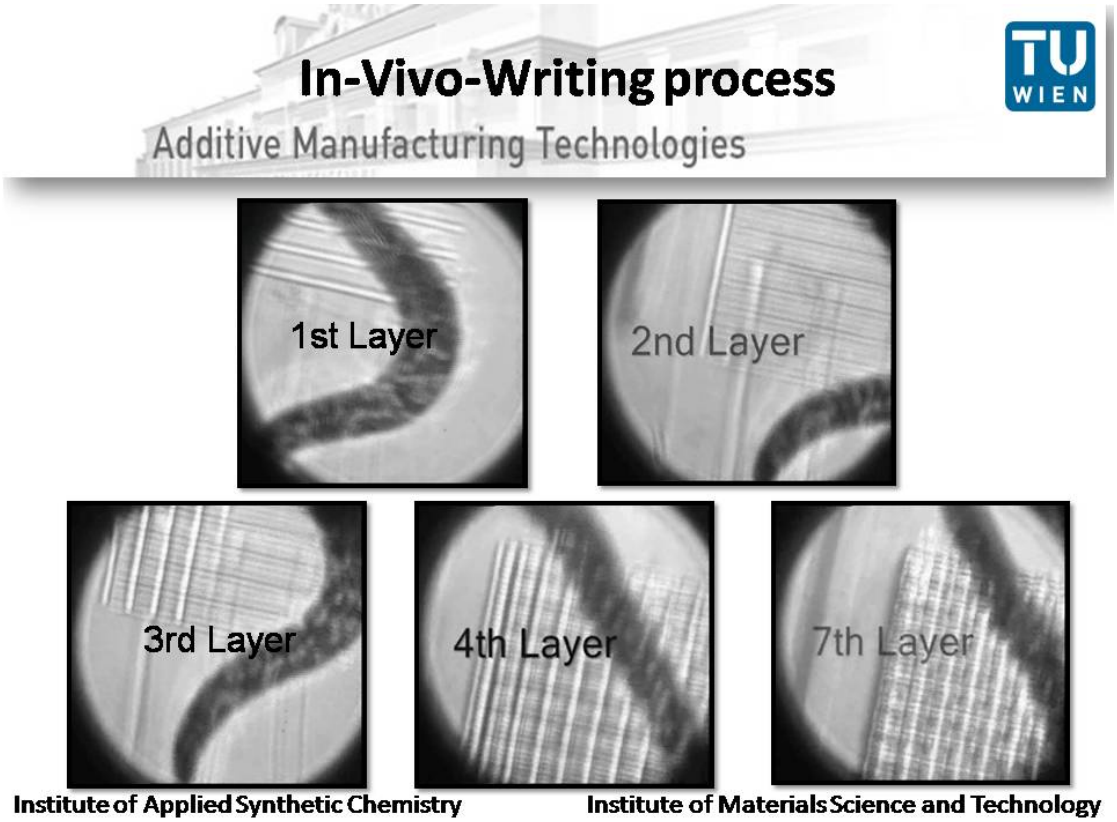

Figure 82: In-vivo-writing process, Ormocer, 20x

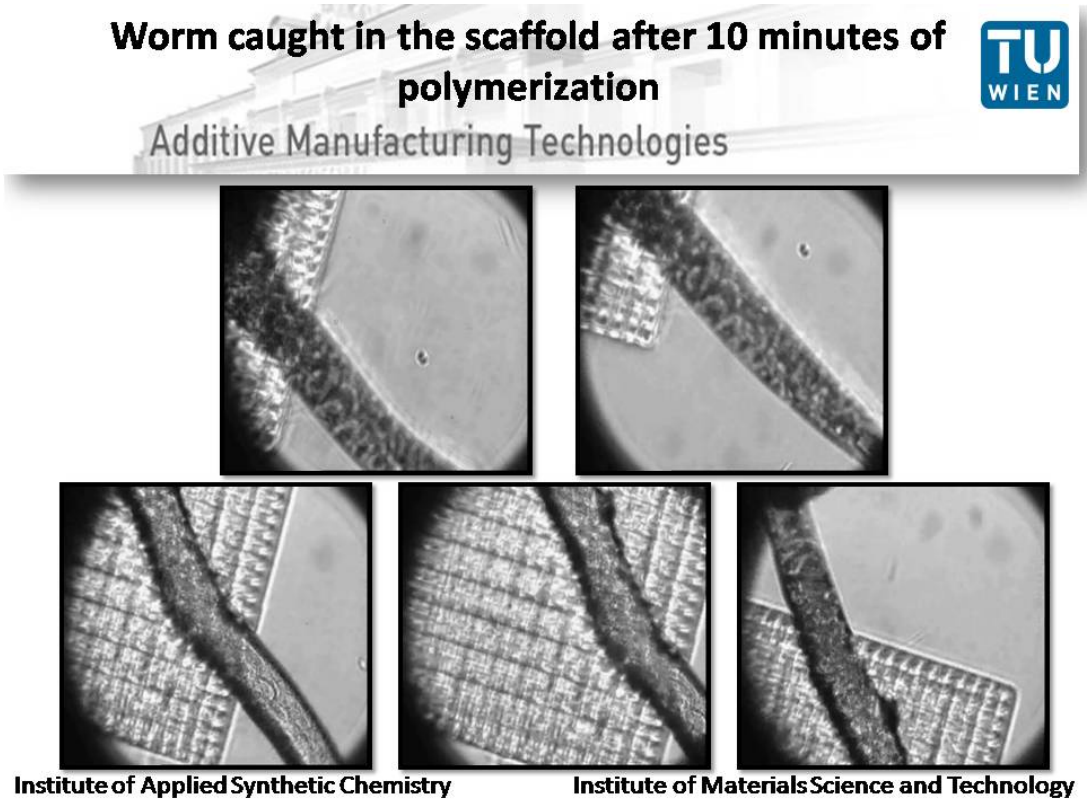

Figure 83: Worm caught in scaffold after 10 minutes of polymerisation, Ormocer, 20x

Figure 83 shows pictures taken after the successful fabrication of the scaffold. The worm was fully covered by the structure and could not flex inside the scaffold. However, it seemed as if the animal could move forward and backward suggesting that the lines of the fabricated part did not actually stick to the cuticle.[67] As a result we assume that resins with a higher viscosity might lead to a better chance of survival. In contrast, resins with lower viscosities, especially aqueous 2PP monomers, could favour the attachment of 2PP parts to living biological tissue. This will be subject to further research in this field.

Finally, Figure 84 provides the proof that the model organism survived the procedure. The sequence of pictures show that the tail of the worm actually moved up and down.

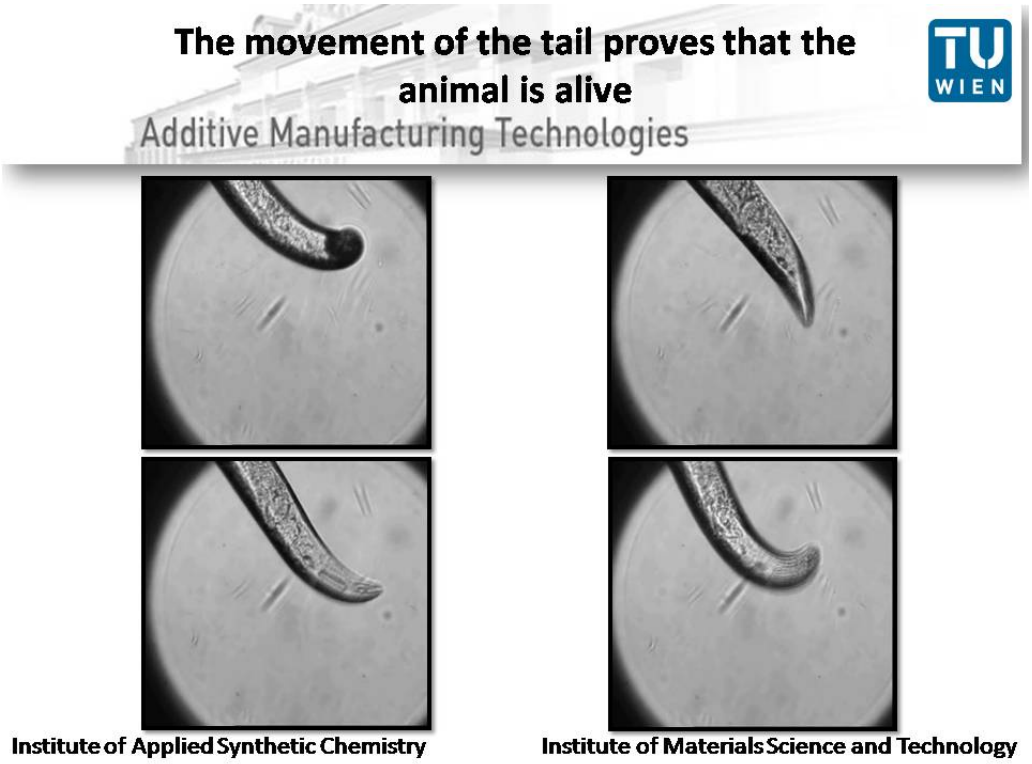

Figure 84: Prove of live after the structuring process, Ormocer, 20x

The necessary irritant solvents (isopropanol or isobuthylmethylether) for the development of the structures finally killed the animal. In the future, a resin soluble in water based solvents is therefore absolutely necessary. Not until then, a complete in-vivo-writing process, starting from the animal's exposure to the resin and ending in a proper development, doing away with all monomer residues while safeguarding the survival of the model organism will be possible. Figure 85 shows the SEM image of the specimen in this experiment. The structure does not look nicely shaped. This has two reasons. First, the structures fabricated using

[67] This is in line with the findings in chapter 10 "Structuring with ORMOCER" and 12 "Toxicity of the resin".

the 20x objective were unfeasible due to the shape of the voxel.[68] Secondly, the movement of the worm caused damage to the newly fabricated polymer lines. With the astigmatic beam focus proposed by Cerullo et al (2002), together with immobilization improvements, we expect nicely shaped structures. A summary of proposed modifications in the setup is shown in Figure 86.

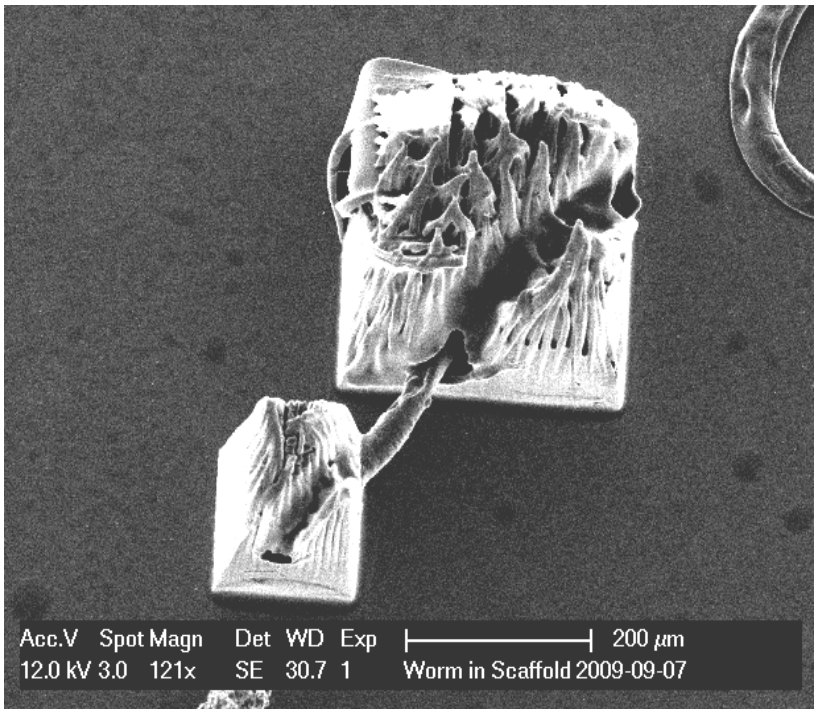

Figure 85: C. elegans caught in scaffold, Ormocer, 20x

[68] Voxel shapes are described in chapter 10.2 "Structuring Parameters with the 20x microscope objective".

13. Future modifications on the 2PP setup

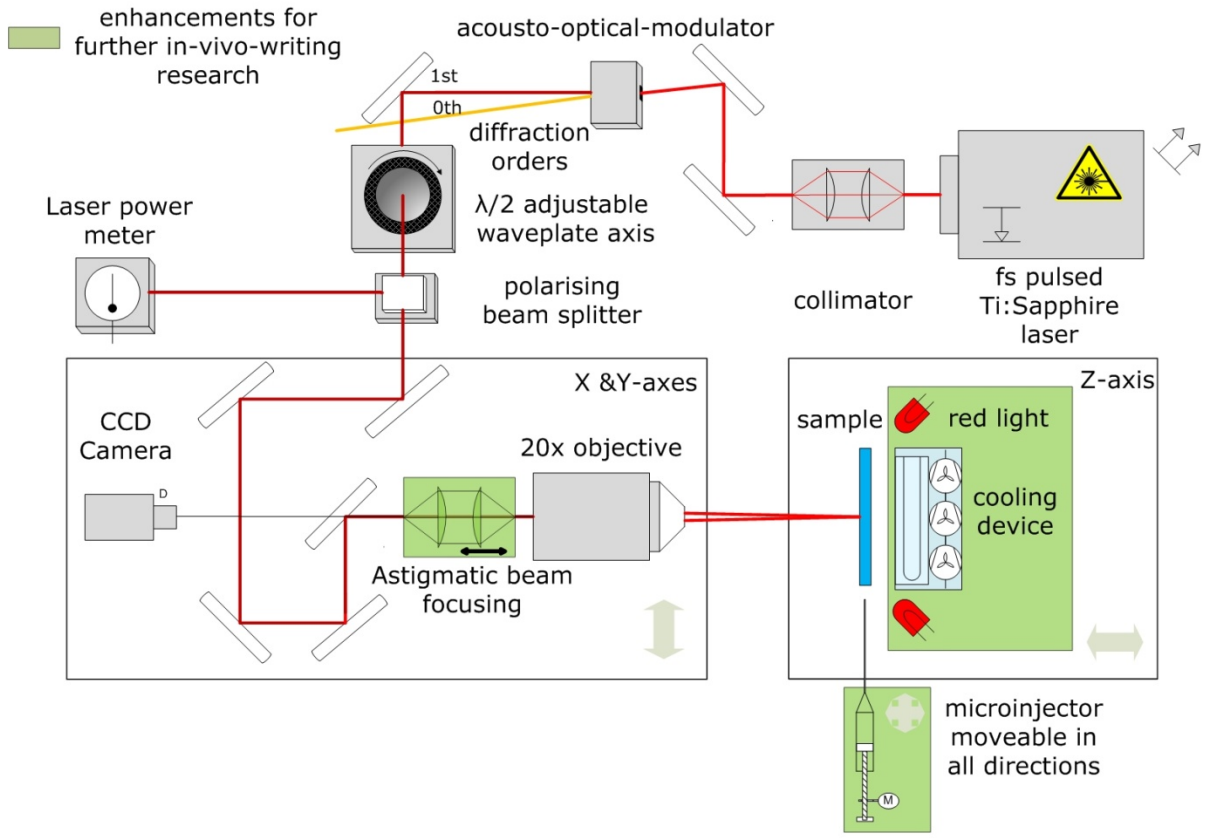

Figure 86: Modifications on M3DL for further research

This work shows that structuring of parts inside resins with living organisms embedded is possible. However, a method to literally "write in-vivo" –as the meaning of the title might imply- is not yet fully provided. In a future perspective, our objective will be to fabricate 2PP parts directly inside living biological tissues, i.e. laboratory organisms like the nematode C. elegans. Experiments in this field can be conducted with a modified setup as proposed in Figure 86.

- To be able to structure with higher intensities and higher speeds and, of course, to be able to use the 20x magnification microscope objective for a proper structuring process, we propose to use an astigmatic beam focusing device as described by Cerullo et al. (2002).
- A water cooling device, as described in the chapter 8 "Modifications on the setup" is necessary in order to limit the model organism's movement.
- A microinjector is necessary in order to inject the resin directly into the model organism.

14. Perspectives

As mentioned in several parts of this work, the long-range perspective is to fabricate parts inside living organisms. This could lead to potentially useful medical applications:

In surgery, for example, this method could help to cover and protect injured vessels without invading the patient. The injected monomer could be polymerised using the NIR laser through all biological tissues in between.

The 2PP method could also serve as a vector for osteoblasts. A way to encapsulate osteoblasts in a polyethylene glycol osteoconductive matrix was already described (Burdick & Anseth, 2002). This is a system providing an alternative to autograft procedures[69] using tissue engineering. The osteoconductive matrix may be designed to release osteoinductive factors or to deliver osteoprogenitor cells. The authors pointed out the advantage of in-situ forming scaffolds compared to the ex-vivo fabrication applied today. They claim that this method is not dependent on the complexity of the affected site. With 2PP both advantages could be combined. The complexity of the site could be taken in consideration as the parts would be fabricated in situ. Moreover, the fabrication of complex scaffolds would be possible. A developed 2PP process could play a role in the treatment of injuries and, especially in therapy of osteoporosis.

These examples show just a few ideas that came up during this work. Of course, we are far away from developing a commercial application using in-vivo-writing for operations or as a long-term treatment for patients with bone and/or tissue diseases. Nevertheless, our findings should provide a motivation for further research.

[69] In autograft procedures, a part of the bone is removed from one healthy area of the patient's skeleton and transplanted to another, injured one.

15. Summary

A method to fabricate three dimensional parts inside resins with embedded living organisms is presented. As we know from optical tweezer applications, the near-infrared laser beam does not harm experimental animals of the species Caenorhabditis elegans at the intensities used for structuring proper two-photon-lithography (2PP) parts. The main limitation of this process is therefore the toxicity of the resin. For the pre-experiments we used the already well developed and examined resin ORMOCER. In various experiments the process parameters of this resin are investigated, which are of particular importance in the in-vivo-writing process.

Structuring parameters with a Carl Zeiss Plan Appochromat 100x microscope objective with a Numerical Aperture (NA) of 1.4 as well as parameters with a Carl Zeiss LD Neofluar 20x microscope objective with a NA of 0.4 are described. Structuring with the 100x objective at low speeds (10-80µm/s) and low laser powers (10-20mW) allowed to fabricate nicely shaped parts. In contrast, no proper process window could be achieved with the 20x objective. Several scaffolds varying in their layer-to-layer distance revealed that the length-to-width ratio of the volumetric pixel (voxel) was much too high. The most satisfying scaffold could be fabricated 25mW of power at a writing speed of 250µm/s and a layer-to-layer distance of 2.75µm. Yet the height exceeded the desired one by approximately 37.5µm. A voxel test quantified exceeding length-to-width ratio of 8.75 at polymerisation threshold (power: 65mW, "shot time": 15000ms). Although, the 20x objective seems not appropriate for a satisfying structuring process, its large working distance is important for a proper in-vivo-writing process. Therefore, voxel shape correcting devices like axicon lenses have to be implemented.

Due to insolubility of ORMOCER in water, animals embedded in this substance could survive due to a protective aqueous coat surrounding their cuticula. As soon as the animals came in contact with the resin, they died almost immediately. Depending on the integrity of the aqueous coat and the movement of the animal, the survival time of the specimen differed to a great extend. Within a sample of 50 worms, the survival time ranged from 2min up to 130min.

A scaffold of 300x300µm base area and a height of 80µm was fabricated in a resin with an embedded living C. elegans. 10 lines per layer and a total of 10 layers were fabricated at a writing speed of 300µm/s and a laser power of 35mW. The whole process took 10min. The movement of the tail of the animal indicated its survival of the process. The body part caught in the scaffold was limited in its movement. The animal was prevented from lateral bending to either side and could not escape from the scaffold. This is the first time additive manufacturing was performed directly onto living tissue. With the development of water-based biocompatible and biodegradable hydrogels together with water

soluble, near-infrared initiators suitable for 2PP, this technique might play a role in a variety of medical applications like osteoporosis treatment.

16. Glossary

Amino acids: Molecules that contain an amine- (functional group of one base Nitrogen atom with a lone pair, a pair of valence electrons not shared with any other atom) and a carboxylic-acid (organic acids with the presence of a carboxyl group; usually -C(=O)OH) functional group.

Amphid: Invagination of the cuticle found in the anterior at the base of the lips. Amphids are

Caudal Papillae: Nipple-like structures in the back of the animal. They are often tactical receptors used in copulation. Caudal is another term for anterior and is often used with invertebrates.

Coelomocyte: Cells in the coelom of C.elegans which have been suggested to have immune, scavenging and hepatic functions (Greenwald & Fares, 2001). The adult C. Elegans has 6 coelomocytes.

Collagen: Collagen is the most abundant protein in humans, and it helps to maintain the integrity of many tissues via its interactions with cell surfaces, other extracellular matrix molecules, and growth and differentiation factors (Di Lullo, Sweeney, Körkkö, Ala-Kokko, & San Antonio, 2001).

Cuticulin: the outermost layer of the epicuticle

Depressor muscle: Muscle that stretches a body part.

Disproportionation: Happens if an element of a middle oxidation level passes partly into a low and partly into a negative one during a Redox-Reaction where it appears as oxidant and as reducer, respectively. The atoms get partly oxidized and partly reduced.

Escherichia coli: a bacterium that is found in the lower intestine of warm-blooded organisms.

Exoskeleton: is the skeleton which has contact to the exterior and protects the animal from external influences. This is in contrast to the skeleton of a human. The endoskeleton is an internal support structure.

Extra-cellular: the term extra-cellular refers to the area "outside" the cell. It is usually filled with fluid and affects the function of the cells.

Ganglion: A ganglion describes a biological tissue mass. In C. elegans several interconnected ganglions build up the nervous system.

Glycine: (NH_2CH_2COOH) is the smallest of the 20 amino acids. It is special at it can fit into hydrophobic and hydrophilic environments. It is not essential in the human's diet.

Glycoprotein: are proteins that contain oligosaccharide chains (a saccharide-polymer that conatins a compounds of sugar) connected to their polypeptide side-chains. Glyoproteins are often a compound of extracellular material as they play a role in cell-cell interactions (Berg, Tymoczko, Stryer, & Clarke, 2002).

Gonad: is an organ that produce gametes, the haploid cells used for sexual propagation (E.g. testes and ovaries).

Green fluorescent protein: a protein composed of 238 cells that exhibits bright green fluorescence when exposed to blue light. Usually refers to a protein first located in the jellyfish Aequorea victoria. It is used as a reporter of expression in different organisms (Prendergast & Mann, 1978) (Phillips, 2001).

Homolytic cleavage: is the dissociation (breaking) of a neutral molecule creating two free radicals. The two electrons which created the chemical (two-electron) bond remain one-by-one on each of the atoms.

Hypodermis: is the lowest layer of the integumentary system in vertebrates, the organ system that protects the body from damage.

Imino acid: Any molecule that contains imino (a functional group with a carbon-nitrogen double bound; >C=NH) and carboxyl (four atoms bonded together; –C(=O)-OH) functional groups. Sometimes amino acids, which contain a secondary amine group, are also sometimes called imino acids.

Keratinocytes: are a major constituent of the epidermis. On the one hand they prevent the entry of toxic substances from the environment; on the other hand they anticipate the loss of important compounds from the host. In progressing from the basal layer to the skin they start to differentiate. The normal turnover is around 30 days (American Academy of Dermatology, 2009)

Labial: referring to the lips

Lethargous: refers to lethargy or fatigue, which is a general state of reduced awareness, physical and/or mental.

Lumbar: referring to the abdominal (belly) part of the main part of the body (Describing humans lumbar refers to the body section between the bottom of the rip cage and the sacral bone)

Lumen: the inside space of a tubular structure

Mammals: are a class of vertebrate animals whose females have mammary glands (organs that produce milk for the young); both males and females have sweat glands (organs in the skin that are in charge of the temperature regulation), hair, three middle ear bones used in hearing and the neocortex (in history of development the youngest part of the brain).

Mus: the genus that contains the mouse

Oocyte: an immature ovum germ cell (cell that gives rise to the gametes of organisms that reproduce sexually) involved in reproduction.

Osmoregulation: is the regulation of the osmotic pressure (applied to a solution to prevent the inward flow of water across a semi-permeable membrane (Voet, Voet, & Pratt, 2001)) to maintain stable and constant conditions by altering the body's water content.

Pharynx: is the part of the animal that is situated immediately posterior (behind) the mouth and is part of the respiratory and digestive system (Stedman, 2009).

Photoimaging: is the formation of images by the use of light. In our case the image refers to one layer of the fabricated three-dimensional model built by additive manufacturing.

Polyaddition: Heterogeneous monomer molecules with a minimum of two different functional groups react together under the transference of protons. No separation of intermediate products takes place. An industrial usage of polyaddition is the production of polyurethane.

Polycondensation: The stepwise condensation-reaction of monomer molecules under the separation of easy built molecules (e.g.: water). Phenoplast and Polyester are two examples produced by Polykondensation.

Programmed Cell Death: any form of death of a cell mediated by an intercellular death-program (Engelberg-Kulka, Amitai, Ilana, & Hazan, 2006).

Prokaryotic cells: cells that lack of a nucleus (cell core) or any membrane bound cell organells (an organ in a cell that has a specific function e.g. mitochondria)

Protozoans: microorganisms classified as eukaryotes (animals that have eukaryotic cells) (Dorland's Medical Dictionary, 2009).

Pseudocoelom: a closed fluid-filled cavity that acts as a hydrostatic skeleton to maintain body shape, circulate nutrients, and hold the major organs in roundworms, rotifers, spiny-headed worms, and horsehair worms (National Oceanic Athmospheric Administration (NOAA), 2009)

Rectum: the final part of the intestine which leads to the anus.

RNA interference: a natural mechanism that alters the gene expression of particular cells of eukaryotic cells (cells with a core, a chromosome-organized DNA and a core cover around it). RNA is always the indicator molecule.

Seam Cell: is a hypodermal cell that lies along the apical (apex, tip) midline of the hypodermis

Sodium lauryl sulfate: ($C_{12}H_{25}SO_4Na$) is an anionic surfactant used in various cleaning products. Its amphiphilic properties (hydrophil and lipophil; i.e. it can solve water and fat) makes it a favored detergent (material that eases cleaning).

Sonication: describes the application of sound to a probe. In biology it is often used to disrupt or deactivate biological materials.

Stomodeum: A part of C. elegans digestive system. It contains the mouth, the lips and the pharynx (Albert Einstein College of Medicine, 2009).

Transfer Agent: transfers the rest of a chain to another chain or a polymer backbone or suchlike. The molecular weight of the polymer increases. In that case the transfer agent may be the monomer itself, the initiator, the solvent or any other deliberately added transfer agent (Matyjaszewski & Davis, 2002).

Tyrosine: (4-hydroxyphenylalanin) one of the 20 amino acids that are used by cells to synthesize proteins. It belongs to the non-essential amino acids which can be produced by the human body itself.

Uterus: the hollow muscular organ in female animals in which the developing embryo and fetus can be nourished (Merck & Co, Inc., 2002-2009).

Vertebrate: Animal with a backbone or spinal column (bony fish, sharks, rays, amphibians, reptile, mammals and birds) (Chen, Chen, & Dickson, 2004).

Xenopus: is an aquatic frog which lives in Sub-Saharan Africa, it is also known as African Clawed frog.

Yeast: eukaryotic cell organisms which belong to the Fungi. Yeast is the dominant fungal population of the ocean (Kurtzman & Fell, 2005).

17. List of figures

18. Bibliography

Abramowitz, M., Keller, E. H., Spring, K. R., Flynn, B. O., Long, J. C., Parry-Hill, J., et al. (2003, April 28). *Molecular Expressions*. Retrieved February 10, 2010, from Optical Microscopy Primer - The anatomy of the microscope: http://micro.magnet.fsu.edu/primer/anatomy/aberrationhome.html

Aerotech. (2009). Retrieved January 8, 2010, from http://www.aerotech.com/products/stages/agrspecs.html

Aerotech. (2009). Retrieved January 10, 2010, from http://www.aerotech.com/products/stages/art300specs.html

Aerotech. (2010). Retrieved January 14, 2010, from http://www.aerotech.com/PDFfiles/A3200.pdf

Albert Einstein College of Medicine. (2009). Retrieved October 02, 2009, from Wormatlas: http://www.wormatlas.org

American Academy of Dermatology. (2009). Retrieved November 9, 2009, from http://www.aad.org

Ashkin, J. (1997). Optical trapping and manipulation of neutral particles using lasers. *Proceedings of the National Academy of Sciences 94* , pp. 4853-4860.

Berg, J. M., Tymoczko, J. L., Stryer, L., & Clarke, N. D. (2002). *Biochemistry 5th Edition.* New York: W.H. Freeman and Company.

Bratton, D., Da, Y., Dai, J., & Ober, C. K. (2006, January 17). Recent progress in high resolution stereolithography. *Polymers for advanced technology, Volume 17, Issue 2* , pp. 94-103.

Burdick, J. A., & Anseth, K. S. (2002). Photoencapsulation of osteoblasts in injectable RGD-modified PEG hydrogels for bone tissue engineering. *Biomaterials 23* , pp. 4315-4323.

Burke, K. (2008, August 11). Retrieved November 19, 2009, from Andrew Computing Services: http://www.andrew.cmu.edu/user/kburke/Organic/

Burri, M., Tromvoukis, D., Bopp, G., & Noll, M. (1989, April 8). Conservation of the paired domain in metazoans and its structure in three isolated human genes. *EMBO Journal* , pp. 1183-1190.

Burt, J., Goarter, A., Hayden, C., Morris, D., Rizvi, N., & Talary, M. (2006). *Developments in the Microfabrication of Biochips Using Laser Micromachining*. Retrieved September 3, 2010, from The Industrial Laser User: http://www.lasermicromachining.com/downloads/AILU_Developments_In_The_Microfabrication_Of_Biochips_Using_Laser_Micromachining.pdf

Carl Zeiss. (2005-2006). Retrieved February 11, 2010, from Zeiss - LD Plan Neofluar 20x: http://www.zeiss.de/C12567BE0045ACF1/Contents-Frame/33AD4A39AD39593BC1256B61003128FA

Cerullo, G., Osellame, R., Marangoni, M., Polli, D., Ramponi, R., Laporta, P., et al. (2002, November 1). Femtosecond micromachining of symmetric waveguides at 1.5 μm by astigmatic beam focusing. *Optics Letters Volume 27 Number 21* , pp. 1938-1940.

Chapman, J. L., & Reiss, M. J. (1999). *Ecology - Principles and Applications 2nd Edition.* Cambridge: Cambridge University Press.

Chen, Z. K., Chen, S. Y., & Dickson, D. W. (2004). *Nematology: advances and perspectives, Volume 1.* China: Tsinghua University Press, CABI publishing.

Chichkov, B. (2007, May 7). *Biomedical Optics & Medical Imaging: Two-photon polymerization enhances rapid prototyping of medical devices*. Retrieved January 25, 2010, from SPIE Newsroom: http://spie.org/x13541.xml?ArticleID=x13541

Chichkov, B. (2002, November 26). *Femtosecond pulses generate microstructures*. Retrieved March 9, 2010, from Optics Analysis Articles: http://optics.org/cws/article/articles/16472

Chichkov, B., & Osianikov, A. (2008). Two-Photon Polymerization – High Resolution 3D Laser. In A. Korkin, & F. Rosei, *Nanoelectronics and Photonics: From Atoms to Materials, Devices and Architectures* (p. 453). Ottawa, Ontario, Canada: Springer Verlag.

Cobweb. (2009, December 01). Retrieved January 19, 2010, from http://cobweb.ecn.purdue.edu/~tmt/NervSys/Projects/Group01.pdf

Coherent. (2010, January). Retrieved January 7, 2010, from http://www.coherent.com/Lasers/index.cfm?fuseaction=show.page&ID=1024&loc=830&ShowMe=More

Cox, G. N., Kusch, M., & Edgar, R. S. (1981). Cuticle of Caenorhabditis elegans: Its isolation and partial characterization. *Journal of Cell Biology 90* , pp. 7-17.

Cummings, R. D., & Esko, J. D. (2009). *Essentials of Glycobiology 2nd Edition.* New York: Cold Spring Harbor.

Del Mar Ventures. (2007). *Sciner*. Retrieved March 05, 2010, from Opticsland: http://www.sciner.com/Opticsland/axicon.htm

Di Lullo, G. A., Sweeney, S. M., Körkkö, J., Ala-Kokko, L., & San Antonio, J. D. (2002, February 8). Mapping the Ligand-binding Sites and Disease-associated Mutations on the Most Abundant Proteins in the Humans, Type I Collagen. *The Journal of Biological Chemistry* , pp. 4223-4231.

Doraiswarny, A., Patz, T., Narayan, R., Chichkov, B., Osianikov, A., Houbertz, R., et al. (2004). Biocompatibility of CAD/CAM Ormocer Polymer Scaffold Structures. *Materials Research Society Proceedings 845* , Paper Number AA2.4.

Dorland's Medical Dictionary. (2009). Retrieved November 10, 2009, from Merck Source Health Information: http://www.mercksource.com/pp/us/cns/cns_hl_dorlands_split.jsp?pg=/ppdocs/us/common/dorlands/dorland/seven/000087548.htm

Edgar, R. S., Cox, G. N., Kusch, M., & Politz, J. C. (1982). The cuticle of C. elegans. *Journal of Nematology 14* , pp. 248-258.

Emmons, S. W., & Lipton, J. (2003, January). Genetic basis of male sexual behavior. *Journal of Neurobiology Volume 54* , pp. 93-110.

Engelberg-Kulka, H., Amitai, S., Ilana, K.-G., & Hazan, R. (2006, October 27). Bacterial Programmed Cell Death and Multicellular Behavior in Bacteria. *PLoS Genetics 2(10)* , p. e135.

Fällman, E., & Axner, O. (1997). Design for fully steerable dual-trap optical tweezers. *Applied Optics 36* , pp. 2107-2113.

Francis, G. R., & Watersen, R. H. (1985). Muscle Organization in C. elegans: Localiztaion of filament attachement in I-band organization. *Journal of Cell Biology 101* , pp. 1532-1549.

Global Spec. (2010, January 04). Retrieved February 10, 2010, from The Engineering Search Engine: http://www.globalspec.com/learnmore/optics_optical_components/optical_components/achromats

Göppert-Mayer, M. (1997). Über Elementarakte mit zwei Quantensprüngen. *Annalen der Physik vol. 401 Issue 3* , pp. 273-294.

Gray, N. F. (1988). Diseases of nematodes. In G. O. Poinar, & H. B. Jansson. Florida: CRC Press.

Greenwald, B., & Fares, H. (2001, September). Genetic analysis of endocytosis in Caenorhabditis elegans, Coelomocyte uptake defective mutants. *Genetics Vol. 159* , pp. 133-145.

Gruber, H. (2008). *Vorlesungsunterlagen Chemische Technologie organischer Stoffe - Radikalische Polymerisation.* Wien: Technische Universität.

Hahn, S., & Taton, A. (2006, July 31). Kinetic of free radical polymerisation of styrene. *University of Minnesota - Laboratory Reports* , pp. 1-4.

Harley, R. (2002, May 02). Retrieved January 14, 2010, from Monstercable: http://wsc.monstercable.com/emails/may02/article_hdtv_robertharley.html

Hodgkin, J., & Barnes, T. M. (1991). More is not better: Brood size and population growth in a self-fertilizing nematode. *Proceedings of the royal society Number 246* , pp. 19-24.

Hodgson, N., & Weber, H. (2005). *Laser Resonators and Beam Propagation - 2nd Edition.* New York, USA: Springer.

Houbertz, R., Schulz, J., Fröhlich, L., Domann, G., Popall, M., Serbin, J., et al. (2003). Inorganic-Organic Hybrid Materials for Real 3-D sub-µm Lithography. *Materials Reseach Society Volume 780* , Paper Number Y4.12.

Hull, C. W. (1986). *US Patent No. 4575330.*

Inführ, R., Stampfl, J., Krivec, S., Liska, R., Lichtenegger, H., Satzinger, V., et al. (2009). 3D-structuring of optical waverguides with two photon polymerization. *Material Research Society Symposium Volume 1179E* , Paper Number 1179-BB01-07, 7 pages.

Ionescu, E., Mera, G., & Toma, L. (2002). *TU Darmstadt Fachbereich Maschinenbau.* Retrieved January 25, 2010, from TU Darmstadt Fachbereich Maschinenbau: http://www1.tu-darmstadt.de/fb/ms/fg/phm/skripte/SolGel.pdf

Johnson, T. E., & Wood, W. B. (1982). Genetic Analysis of life-span in Caenorhabditis elegans. *Proceedings of National Academy of Sciences Number 79(21)* , pp. 6603-6607.

Kaiser, W., & Garett, C. (1961, Septmeber 15). Two-Photon Excitation in CaF2:Eu2+. *Physical Review Letters Volume 7, Issue 6* , pp. 229-231.

Kramer, J. (1997). Extracellular Matrix. In D. L. Riddle, T. Blumenthal, B. J. Meyer, & J. R. Priess, *C. elegans II* (Chapter 17). New York: Cold Spring Harbour Laboratory Press.

Kuba, K., & Nakayama, S. (1998). Two-photon laser-scanning microscopy: test of objective lenses and Ca2+ probes. *Neuroscience Research 32* , pp. 281-294.

Kurtzman, C., & Fell, J. (2005). Yeast systematics and phylogeny - implications of molecular identification methods for studies in ecology. In C. A. Rosa, & G. Peter, *The Yeast handbook* (pp. 11-30). Heidelberg, Berlin: Springer Verlag.

Leitz, G., Fällman, E., Tuck, S., & Axner, O. (2002, April). Stress Response in Caenorhabditis elegans Caused by Optical Tweezers: Wavelength, Power, and Time Dependence. *Biophysics Journal Volume 82* , pp. 2224-2231.

Lewis, E., Sebastiano, M., Nola, M., Zei, F., Lassandro, F., Ristoratore, F., et al. (1994). Cuticulin genes of nematodes. *Parasite 1* , pp. 57-58.

Li, X. F., Winfield, R. J., O'Brien, S., & Crean, G. M. (2009, March). Application of Bessel beams to 2D microfabrication. *Applied Surface Science Volume 255 Issue 10* , pp. 5146-5149.

Linden, D. J. (2008). *How brain evolution has given us love, memory, dreams and god*. Retrieved February 03, 2010, from The Accidental Mind: http://accidentalmind.org/notecards/c_elegans.html

Liu, K. S., & Sternberg, P. W. (1995, January 14). Sensory regulation of male behaviour in Caenorhabditis elegans. *Neuron (1)* , pp. 79-89.

Maizels, R. M., Blaxter, M. L., & Selkirk, M. E. (1993). Forms and functions of nematode surfaces. *Experimental Parasitology 77* , pp. 380-384.

Matrox. (2010, January 01). Retrieved January 14, 2010, from http://www.matrox.com/imaging/en/products/software/mil/

Matyjaszewski, K., & Davis, T. P. (2002). *Handbook of Polymerization.* New York: Wiley Interscience.

Merck & Co, Inc. (2002-2009). *Health Information*. Retrieved November 3, 2009, from Merck Source: http://www.mercksource.com/pp/us/cns/cns_home.jsp

Meyer, B. (1997). Sex Determination and X Chromosome Dosage Compensation. In D. L. Riddle, T. Blumenthal, B. J. Meyer, & J. R. Priess, *C. Elegans II* (Chapter 9). New York: Cold Spring Harbor Laboratory Press.

Micro resist technology GmbH. (2008). *EG-Sicherheitsdatenblatt gemäß Verordnung (EG) Nr. 1907/2006 - OrmoCore Materialnummer B419B5D.* Berlin, Deutschland: Micro Resist Technology GmbH.

Moffitt, J. R., Chemla, Y. R., Izhaky, D., & Bustamante, C. (2006, June 13). Differential detection of dual traps improves the spatial resolution of optical tweezers. *Proceedings of the Narional Academy of Science 103 (24)* , pp. 9006-9011.

Murray, P. R., Rosenthal, K. S., & Pfaller, M. A. (2005). *Medical Microbiology, 5th Edition.* United States: Elsevier Mosby.

National Oceanic Athmospheric Administration (NOAA). (2009, October 20). *Noaa's coral reef information system*. Retrieved November 3, 2009, from http://coris.noaa.gov/

Odian, G. G. (2004). *Principles of Polymerization 4th Edition.* New Jersey: Wiley-Interscience.

Ophart, C. E. (2003). *Virtual Chembook.* Elmhurst: Elmhurst College.

Park, S.-H., Yang, D.-Y., & Lee, K.-S. (2009). Two-photon stereolithography for realizing ultraprecise three-dimensional nano/microdevices. *Laser & Photonics Reviews No. 1-2* , pp. 1-11.

Paschotta, R. (2009, November 02). *Encyclopedia of Laser Physics and Technology*. Retrieved January 06, 2010, from http://www.rp-photonics.com/waveplates.html

Passinger, S. (2008). *Two-Photon Polymerization and application to Surface Plasmon Polaritons.* Hannover: Cuviller Verlag Göttingen.

Peatross, J. B., & Ware, M. (2009). *Physics of Light and Optics.* Provo, United States: Brigham Young University.

Phillips, G. J. (2001, Octobre 20). Green fluorescent protein- a bright idea for the study of bacterial protein localization. *FEMS Microbiology Letters 204(1)* , pp. 9-18.

Prendergast, F. G., & Mann, K. G. (1978, August). Chemical and physical properties of aequorin and the green fluorescent protein isolated from Aequorea forskalea. *Biochemistry 17* , pp. 3448-3453.

Rand, J. B., & Nonet, M. L. (1997). Synaptic Transmission. In D. L. Riddle, T. Blumenthal, & B. J. Meyer, *C. elegans II* (Chapter 22). New York: Cold Spring Harbor Laboratory Press.

Riddle, D. D., & Albert, P. (1997). Genetic and Environmental Regulation of Dauer Larva Development. In D. D. Riddle, T. Blumenthal, B. J. Meyer, & J. R. Priess, *C. elegans II.* New York: Cold Spring Harbor Laboratory Press.

Riddle, D. L., Blumenthal, T., Meyer, B. J., & Priess, J. R. (1997). *C. elegans II.* New York: Cold Spring Harbor Laboratory Press.

Roberts, L. S., & Janovy, J. J. (2009). *Foundations of Parasitology 8th Edition.* United States: McGraw-Hill.

RP Photonics Consulting GmbH. (2008, October). Retrieved February 11, 2010, from Encyclopedia of Laser Physics and Technology: http://www.rp-photonics.com/group_delay_dispersion.html

Schüngel, F. M. (2005). *Objektivkonstruktionen*. Retrieved February 10, 2010, from foto-net.de: http://www.foto-net.de/net/objektive/kostruktion.html

Singh, R. N., & Sulston, J. E. (1978). Some observations on molting in C. elegans. *Nematologica 24* , pp. 63-71.

Stampfl, J. (2006). RP- Einführung Vorlesungsunterlagen. Wien, Österreich.

Stedman. (2009). Retrieved November 3, 2009, from Stedman's medical dictionary: http://www.stedmans.com/

Stiernagle, T. (2005, May 07). *The online review of C. elegans biology*. Retrieved March 05, 2010, from WormBook: http://www.wormbook.org/chapters/www_strainmaintain/strainmaintain.html

Stiernagle, T. (2005, May 7). *Worm Book*. Retrieved February 8, 2010, from Maintenance of C. elegans: http://wormbook.sanger.ac.uk/chapters/www_strainmaintain/strainmaintain.html

Stringham, E. G., Dixon, D. K., Jones, D., & Candido, E. P. (1992). Temporal and spatial expression patterns of the small heat shock (hsp16) genes in transgenic Caenorhabditis elegans. *Molecular Biology of the Cell 3* , pp. 221-223.

Sun, H.-B., Maeda, M., Takada, K., Chon, J. W., Gu, M., & Kawata, S. (2003, August 4). Experimental investigation of single voxels for laser nanofabrication via two-photon photopolymerization. *Applied Physics Letters Volume 83 Number 5* , pp. 819-821.

Swainson, W. K. (1977). *US Patent No. 4041476.* Berkeley/California.

Thein, M. C., McCormack, G., Winter, A. D., Johnston, I. L., Shoemacker, C. B., & Page, A. P. (2003). Caenorhabditis' exoskeleton collagen COL-19: an adult-specific marker for collagen modification and assembly, and the analysis of organsimal morphology. *Developmental Dynamics 226* , pp. 523-539.

University of Arizona. (2005). Retrieved October 08, 2009, from Tree of Life web project: http://www.tolweb.org/tree

University of Berlin. (2001). *Herstellung von Kunststoffen*. Retrieved November 19, 2009, from Vorlesungsunterlagen: http://www.chemie.fu-berlin.de/chemistry/kunststoffe/polyradi.htm

University of Bern. (2002, November 2). Retrieved January 21, 2010, from Molekularbiologie Kurse: http://e-learning.studmed.unibe.ch/Gen_Kurs/GEN_KURS/DNA/ORG02.HTM

Verhoeven, J. W. (1996). Glossary of terms used in photochemistry. *Pure and Applied Chemistry Vol. 68 No. 12* , pp. 2223-2286.

Voet, D., Voet, J. G., & Pratt, C. W. (2001). *Fundamentals of Biochemistry.* New York: Wiley Interscience.

Vorobjev, I. A., Liang, H., Wright, W. H., & Berns, M. W. (2993). Optical trapping for chromosome manipulation: a wavelength dependence of induced chromosome bridges. *Biophysics Journal 64* , pp. 533-538.

Waksman. (2001/2002). Retrieved October 06, 2009, from Waksman Student Scholars: http://avery.rutger.edu/WSSP/StudentScholars/project/introduction.html

Watec. (2010, January 01). Retrieved January 14, 2010, from http://www.watec.com/english/bw_top.html

White, J., & Sulston, J. (1988). *The Nematode C. elagans.* New York: Cold Spring Harbour Laboratory Press.

Wisconsin Outreach Research Modules. (2004, January 22). Retrieved October 8, 2009, from W.O.R.M. initiative: http://www.loci.wic.edu/outreach/index.html

Wissenmedia GesmbH. (2000-2009). Retrieved November 11, 2009, from Wissen.de: http://www.wissen.de/wde/generator/wissen/ressorts/natur/naturwissenschaften/indexoffline,page=1215470.html

Wood, W. B. (1995). Basic culture methods. In W. B. Wood, *Caenorhabditis elegans - Modern Biological Analysis of an Organism.* New York: Academic Press.

Wood, W. B. (1988). *The Nematode Caenorhabditis elegans.* New York, USA: Cold Spring Habor Monograph Series 117.

Wu, S., Serbin, J., & Gu, M. (2006, April 18). Two-photon polymerisation for three- dimensional micro-fabrication. *Journal of Photochemistry and Photobiology A: Chemistry 181* , pp. 1-11.